Crystal surfaces in and out of equilibrium: A modern view

Chaouqi Misbah

Laboratoire de Spectrométrie Physique, Université Joseph Fourier Grenoble I, and CNRS, BP 87, F-38402 Saint Martin d'Hères, France

Olivier Pierre-Louis*

Laboratoire de Spectrométrie Physique, Université Joseph Fourier Grenoble I, and CNRS, BP 87, F-38402 Saint Martin d'Hères, France
and Rudolf Peierls Centre for Theoretical Physics, 1 Keble Road, Oxford OX1 3NP, United Kingdom

Yukio Saito

Department of Physics, Keio University, 3-14-1 Hiyoshi, Kohoku-ku, Yokohama 223-8522, Japan

(Published 26 March 2010)

The last two decades of progress in the theory of crystal surfaces in and out of equilibrium is reviewed. Various instabilities that occur during growth and sublimation, or that are caused by elasticity, electromigration, etc., are addressed. For several geometries and nonequilibrium circumstances, a systematic derivation provides various continuum nonlinear evolution equations for driven stepped (or vicinal) surfaces. The resulting equations are sometimes different from the phenomenological equations derived from symmetry arguments such as those of Kardar, Parisi, and Zhang. Some of the evolution equations are met in other nonlinear dissipative systems, while others remain unrevealed. The novel and original classes of equations are referred to as "nonstandard." This nonstandard form suggests nontrivial dynamics, where phenomenology and symmetries, often used to infer evolution equations, fail to produce the correct form. This review focuses on step meandering and bunching, which are the two main forms of instabilities encountered on vicinal surfaces. Standard and nonstandard evolution scenarios are presented using a combination of physical arguments, symmetries, and systematic analysis. Other features, such as kinematic waves, some aspect of nucleation, and results of kinetic Monte Carlo simulations are also presented. The current state of experiments and confrontation with theories are discussed. Challenging open issues raised by recent progress, which constitute essential future lines of inquiries, are outlined.

DOI: 10.1103/RevModPhys.82.981 PACS number(s): 68.55.−a, 68.35.Md, 68.35.Ct

CONTENTS

*Present address: Laboratoire de Physique de la Matière Condensée et des Nanostructures, Université Lyon 1, 43 Bd du 11 novembre, 69622 Villeurbane, France.

I. INTRODUCTION

A major goal of theories on nonequilibrium surface dynamics is to predict the continuum evolution of surfaces from knowledge of elementary microscopic processes. Growth is an open nonequilibrium dissipative process where matter is constantly brought into the growing solid from the surrounding environment; it is a prototype of problems where traditional statistical mechanics are difficult to apply. Principles such as maximum entropy, minimum free energy, etc., do not apply in general.

Growth embraces several disciplines such as metallurgy (solidification of alloys) (Tiller, 1991), microelectronics (growth of nanodevices) (Ritter *et al.*, 1998), biophysics (growth of proteins, cell and tumor growth, and cytoskeleton polymerization in the immune system) (Vekilov and Alexander, 2000), etc. While each system has its own specificities, the general hope is that progress achieved on one given problem may help shed light on problems with seemingly different underlying mechanisms.

For our problem of surface dynamics, the nature of crystalline surfaces is important. At the microscale, crystalline surfaces exhibit two distinct structures: (i) a rough surface and (ii) a smooth or atomically flat surface. At melting temperatures most metals and several organic components fall into the first category (Jackson, 2004). In this case, the surface fluctuates strongly and the notion of a crystalline plane is hard to define. In the second category, surface atoms (or molecules) are perfectly aligned in a smooth (atomically flat) plane. Semiconductors, some metals, and several organic materials belong to this category; in theory, they can become rough if the temperature is high enough (this temperature may be above sublimation temperature). The distinction between rough and smooth phases is precise. Indeed, crystalline surfaces are known to undergo a roughening transition of Kosterlitz-Thouless (Kosterlitz and Thouless, 1973) type at a critical temperature T_R given by

$$k_B T_R = 2a^2\alpha/\pi, \tag{1.1}$$

where k_B is the Boltzmann constant, a is the lattice spacing in the crystal, and α is a macroscopic surface free energy. In principle, by increasing the temperature, each smooth (or atomically flat) surface should undergo a

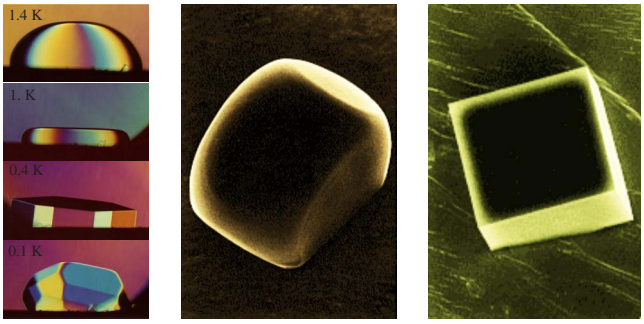

FIG. 1. (Color online) Roughening transition. (a) Facetting of ^{4}He crystal. From top to bottom, the temperatures are successively 1.4, 1, 0.4, and 0.1 K. The size of the facets is larger than on equilibrium shapes due to slow growth. From Balibar *et al.*, 2005. (b) and (c) NaCl crystal. From Heyraud and Métois, 1987. From (b) to (c), the temperature is decreased leading to the appearance of a facetted shape with an atomically flat surface.

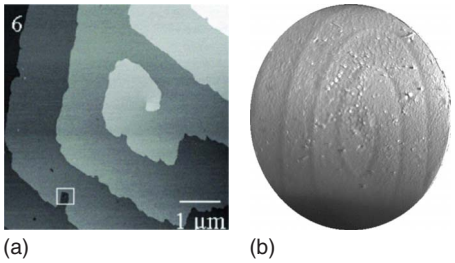

FIG. 2. (Color online) Screw dislocations. (a) Atomic force microscope picture of a screw dislocation during the growth of an insulin crystal (Yip *et al.*, 1998; Gliko *et al.*, 2003). (b) Low distortion reflection electron microscope (REM) image of a screw disclocation on Si(111) (Müller and Métois, 2005).

roughening transition. The temperatures at which materials are grown depend largely on the process of growth (melting temperature for solidification, an appropriate temperature for growth from the vapor phase, etc.). Given the "working temperature," the surface may be either rough or smooth at the microscale. There is, in general, a transfer of information from the microscale to the macroscale (Fig. 1): roughening is accompanied with the transition from facetted to rounded macroscopic shapes.

The physics of crystal growth largely depends on the microscopic nature of surfaces. For solids with rough surfaces (i), the addition of a new particle to the growing solid is quick since many unsatisfied bonds are available. In this case, growth is often limited by slow mass transport to the crystal. A typical transport process is diffusion from the bulk toward the surface. This is referred to as diffusion-limited growth. For solids with smooth (atomically flat) surfaces (ii), attachment sites are rare and the addition of particles to the surface is not an easy process. Growth may occur either via two-dimensional (2D) nucleation or via the attachment of atoms to the preexisting steps. Steps may be created during a preparation process, such as cutting a material with a miscut angle with respect to a closely packed plane. The resulting surface is called vicinal. Steps may also be occasional or produced by screw dislocations emerging at the surface of the solid (Burton *et al.*, 1951); see Fig. 2. The interface attachment kinetics are rather slow in this category. Here, besides diffusion, attachment kinetics and 2D nucleation play a (if not the) decisive role.

The first category (bulk diffusion-limited growth) usually leads to patterns in the form of dendrites or fractals. The velocity selection of the dendritic tip has been a problem, which shares some similarities with the width selection of a Saffman-Taylor finger (Saffman and Taylor, 1958) observed when a less viscous fluid (such as air) is injected into a more viscous fluid (such as oil) in a channel. Patterns such as fingers, dendriticlike structures, and fractal-like morphologies (or their formal analogs) have been identified in diffusion-limited growth. There has been a significant advance in both problems. Both situations have proved to be nontrivial and nonlinear selection problems, where surface tension plays the role of a singular perturbation. Furthermore, in the dentritic problem, the crystalline anisotropy has been shown to play a decisive role; for a review see Kessler *et al.* (1988).

We are interested in the second category of kinetics-controlled growth problems. Here the interface is flat on the microscale: terrace, individual steps, and individual atoms can be identified (Fig. 3). Adatoms have to diffuse on the terrace, meet with other building blocks (2D nucleation), or attach to preexisting defects (steps and islands). The difficulties encountered in this category are greater than in the first category of the dendrite problem because of the variety of microscopic processes involved. Materials in this category include semiconductors (used in everyday nanodevice manufacture), many organic components, and biological materials [such as protein crystals (Chernov, 2003)]. On the macroscale, growth forms are often facetted, while on mesoscales and nanoscales, they sometimes exhibit intricate patterns, the understanding of which requires precise identification of the microscopic growth process. In its general form, this problem continues to represent a formidable challenge.

Kinetics-controlled growth can be classified according to the mother phase into three prototypes: (i) growth

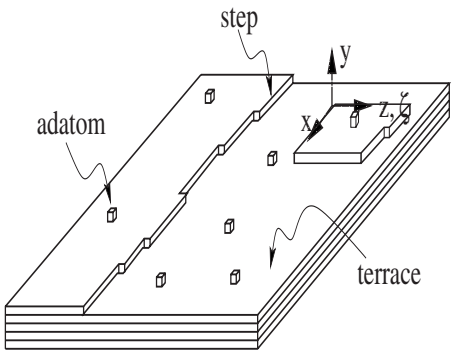

FIG. 3. Schematic view of the surface during 2D growth.

from a solution (this is the case for many organic materials, minerals, biological materials, etc.), where the elementary building blocks diffuse in the solution (Chernov and Nishinaga, 1987) along the surface (of the growing material) and execute various kinetics, as evoked above (e.g., nucleation, attachment to preexisting steps, etc.); (ii) growth from a vapor; and (iii) growth from a beam (Saito, 1996; Pimpinelli and Villain, 1998; Michely and Krug, 2004). In cases (ii) and (iii), the transport process in the mother phase is nonessential. We refer to the last two categories as *ballistic growth* or molecular beam epitaxy (MBE).

MBE growth, to which a significant part of this review is devoted, and other variants of vapor growth are used to produce materials with abrupt surfaces on the atomic scales (quantum wells, wires, dots, etc.). Such materials are used for optoelectronic and microelectronic devices. The task of producing a surface with an atomic control is often hampered by the presence of inherent instabilities and/or by the kinetic roughness associated with, for example, shot noise due to the deposition flux.

In principle, on a flat surface exposed to a flux in MBE (usual fluxes in MBE range from a fraction of a monolayer to a few monolayers per second), each deposited atom has ample time to diffuse and attach to a favorable site (e.g., a step) before a new atom is deposited. On the other hand, it is known that shot noise (a noise inherent to the deposition flux) is able to reinstitute itself and may cause kinetic roughening of the surface at different scales. The surface may develop stochastic roughness. Prominent examples of descriptions of this type of roughness are the Edwards-Wilkinson equation (Edwards and Wilkinson, 1982) and the Kardar-Parisi-Zhang (KPZ) equation (Kardar *et al.*, 1986). The latter is one of the earliest nonlinear evolution equations put forward in MBE growth literature and was derived from symmetries. In 1+1 dimensions, the KPZ equation reads

$$\partial_t h = \nu \partial_{xx} h + \lambda (\partial_x h)^2 + \eta(x,t), \tag{1.2}$$

where $h(x,t)$ is the surface height, x is the spatial coordinate along the front, $\eta(x,t)$ is a noise term, and ν and λ are two positive coefficients.

A major outcome of the KPZ equation is the determination of the static roughness exponent α (which describes the degree of the increase in roughness by increasing the size of the surface in the lateral direction L) in the saturation regime and the dynamical exponent z (which tells us how long it takes for a given surface with a linear scale L to reach the saturation regime). Roughness w obeys a scaling law

$$w \sim L^{\alpha} f(t/L^{z}). \tag{1.3}$$

This scaling law has been identified for many continuum models, as well as in Monte Carlo (MC) simulations (Barabàsi and Stanley, 1995). However, the KPZ equation raises several questions which are still a matter for debate. One particularly important point is to specify its range of applicability. More precisely, what are the length and time scales beyond which the KPZ scaling exponents describing surface roughness can be expected to appear? Let it suffice to say that if growth is produced without—or with only a small number of—defects (such as holes, usually called overhangs in numerical simulations) or if desorption of deposited atoms is unlikely on the time and length scale of interest (which is often the case in many MBE growth processes), then a description in terms of KPZ dynamics is not *a priori* justified. Other alternatives have been suggested [see Barabàsi and Stanley (1995) and Pimpinelli and Villain (1998)] to account for the absence of desorption and overhangs (or holes).

Besides the noise-driven roughness, there is now increasing evidence that surface roughness may result from a deterministic origin. Instabilities of deterministic origin are the rule in systems which are brought away from equilibrium. These instabilities may lead to patterns which may be either ordered or disordered, depending on specific nonequilibrium conditions. This review is mainly devoted to these questions of deterministic instabilities, albeit the effect of noise will be discussed at different places.

One of the main goals in materials science is to describe the surface evolution including relevant microscopic effects. This is a difficult task in general, from both an analytical and a numerical point of view. Proper analysis of the nucleation process represents a significant challenge. For example, how does one describe surface evolution including the nucleation process in a continuum theory? Several attempts have been made, but often the theories are based on *ad hoc* assumptions and, at best, only very qualitative features may be extracted.

Evoking symmetries for the effective evolution equations gives some hope for progress. However, in general, it is not always easy to get information on the functional dependence of the coefficients in the evolution equation on relevant material and growth parameters. In addition, there are several situations (where derivation from "microscopic" considerations becomes possible) where the evolution equation is nontrivial and cannot be easily inferred from symmetries or scaling arguments.

Progress in any complex field (such as the subject of this review) can be made only by a progressive refinement of concepts. This is why we focus on simplified geometries where derivations of evolution equations, their classification, and their outcomes become possible and unambiguous; they are vicinal surfaces (Fig. 4) comprising terraces and steps. The advantage of these surfaces is that atom nucleation on the terraces may be avoided (provided that the temperature is not too low, the interstep distance is not too large, and the deposition flux is not too high, so that deposited atoms reach a step before other new atoms land): deposited atoms or molecules wander along the terrace until they reach a terrace edge where preexisting steps act as a sink. Thus, surface growth occurs by the addition of particles at the steps; this growth mode is known as *step flow*. Figure 4 summarizes the basic growth processes. Vicinal surfaces are widely used as templates for the production of many surface nanoarchitectures. They present systems of both fundamental and technological importance.

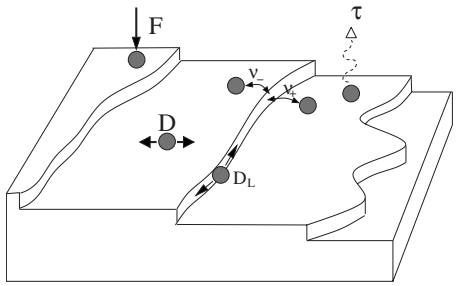

FIG. 4. Summary of various atomic processes on a vicinal surface. Deposition (with a flux F), diffusion (with D as the diffusion constant), desorption (with rate $1/\tau$), and step attachment or detachment (with rate $\nu_{\pm}$ from each side) is shown. D_L represents the line diffusion along the step.

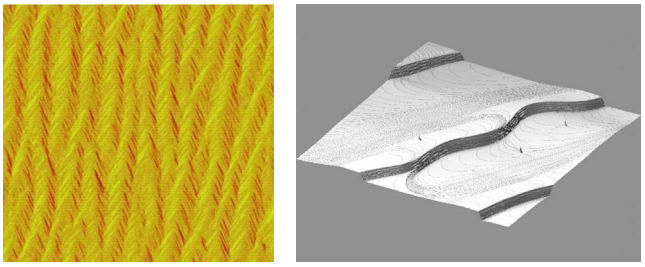

FIG. 5. (Color online) Instabilities on vicinal surfaces. (a) Meandering instability on Si(001). From Omi and Ogino, 2000. (b) Bunching instability with three macrosteps formed from bunching of many monatomic steps. From Thürmer *et al.*, 1999.

Since atoms only diffuse (some may regain the atmosphere via thermal agitation) and attach to the steps, the problem amounts to solving the diffusion problem with boundary conditions (such as conditions on the mass flux at the step). The definition of the growth problem in its simple version is therefore nonambiguous. On this basis, it is hoped to extract general prototypical evolution equations.

Within this simplified picture of growth on a vicinal surface, the problem remains complex on the absolute level. On the one hand, while diffusion is described by a linear equation, the fact that the step profiles (and thus the surface morphology) are *a priori* unknown makes the problem *highly nonlinear* and *nonlocal*. Even a numerical solution of the surface dynamics in detail on a reasonable sample size is still not completely feasible despite the progress of recent computing facilities. Furthermore, although a direct numerical solution may provide a full picture of dynamics and enables comparison of results with experiments, it would be highly desirable to dispose of analytical progress on surface evolution dynamics. This has recently become possible in several circumstances and constitutes a central issue of this review.

This review focuses on a significant achievement: we are now able to classify the type of dynamics on vicinal surfaces on the basis of general considerations. Various microscopic dynamics take place on a vicinal surface, as shown in Fig. 4: deposition, surface diffusion, desorption, and step attachment or detachment. There are other processes which require essential considerations. Atoms that are in the vicinity of the step are not automatically absorbed at their arrival sites: an atom may wander along the step for a certain period of time before it attaches to the step. Thus line diffusion may play an essential role. On the other hand, steps may interact via the elastic field because a step is a defect, and the elastic distortions lead to an effective interaction with other steps. We shall see that including or disregarding elasticity leads to a drastically different dynamics. Thus, we must identify the relevant physical processes in a given situation.

Different types of approaches have recently been published (Haselwandter and Vvedensky, 2008). These are based on the renormalization of stochastic lattice models leading to continuum surface equations. While this approach is appealing, scenarios like those leading to highly nonlinear equations are not captured. It will be an interesting task for future studies to conceive of approaches of this type in order to deal with more general scenarios.

A uniform vicinal surface is known to undergo two types of primary instabilities: (i) step meandering [Fig. 5(a)] and (ii) step bunching [Fig. 5(b)]. These instabilities occur during growth or sublimation and their basic microscopic sources are quite diverse. For example, mass diffusion with asymmetric attachment to a step may lead to these instabilities. Likewise, the drift of surface atoms due to a heating electric current (electromigration) or an elastic stress often appears as a decisive component causing instabilities (Jeong and Williams, 1999; Yagi *et al.*, 2001). We encounter both "smooth" (weakly nonlinear) and "strong" (highly nonlinear) instabilities. For example, we may have smooth step meandering in some cases, while in other cases step meandering may be so strong that the initial vicinal surface may be completely destroyed and look quite rough (Fig. 6).

The interesting feature lies in the fact that it is now feasible to describe these dynamics with the help of con-

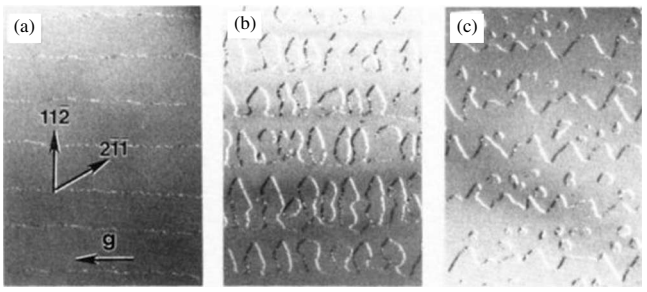

FIG. 6. Changes in the morphology of the Si(111) surface during the deposition of Si. The growth rate is 0.5 Å/s. (a) Before growth. (b) One monolayer deposited. (c) Two monolayers deposited. (Dark field transmission electron microscope images of a SiO_2 coated surface.) The surface is initially smooth and becomes rough after a meandering instability (Tung and Schrey, 1989).

tinuum evolution equations without *ad hoc* assumptions. In particular, the coefficients that enter the evolution equations can be expressed in terms of basic quantities (such as atom diffusion, desorption frequency, etc.). Broadly speaking, within the meandering and bunching instabilities, it is now possible to identify two types of dynamics: (i) smooth and (ii) strong (nonstandard form of equations). How and when each type prevails is becoming clearer. The continuum evolution equations derived from microscopic considerations reveal a variety of phenomena such as order or chaos, "diverging" amplitudes, freezing of wavelength or perpetual coarsening, etc. Interestingly enough, two equations that appear quite similar may exhibit significantly different dynamics. For example, in one case the wavelength is fixed (or at least an average length scale persists over time), while in the other case we may have coarsening (an increase in wavelength over time). Some general criteria on when coarsening is expected to occur are now beginning to emerge (Politi and Misbah, 2004, 2006).

The main objectives of this review are to present the current state of the art in this fast-moving field and to present a rational study of dynamics. Emphasis is put on the concepts and ideas rather than on technical details, although the review is largely self-contained. Comparisions with experiments are made whenever possible and a list of questions remaining to be answered by future investigations is presented.

Most of the review is devoted to the dynamics of vicinal surfaces. While the study of vicinal surfaces has now been basically rationalized, the questions related to high symmetry surfaces have been based on symmetry arguments and qualitative reasoning. It is hoped that the type of classification achieved on vicinal surfaces will shed light on more general problems. Some progress has been made on kinetic Monte Carlo (KMC) simulations, and this will be mentioned. Finally, some stress effects will be discussed in the context of vicinal surface dynamics only.

II. FLUCTUATIONS AND WAVES

While morphological instabilities constitute the central focus of the review, we first discuss fluctuations and waves on stable surfaces. The first sections are devoted to equilibrium fluctuations. The problem of kinetics at global equilibrium is then outlined. Finally, the occurrence of kinematic waves on vicinal surfaces is discussed.

A. Equilibrium roughness and static correlations

Studying equilibrium properties of a surface constitutes an important part of experimental investigations, allowing for the determination of thermodynamic (e.g., step energy) as well as kinetic (e.g., diffusion) properties by comparing observations with theoretical predictions. Furthermore, this enables us to determine, among a large manifold of possibilities, the prevailing mechanisms (such as diffusion or step attachment or detachment) for a given range of parameters (e.g., a specific range of temperatures). There are different levels of approach: microscopic, mesoscopic, and continuum approaches. Bridging between these three scales is, in general, a formidable task. The microscopic scale would be necessary in order to capture detailed microscopic dynamics (such as kinetics at the steps and anisotropic diffusion). This information could be injected into more mesoscopic or macroscopic theories. Having a systematic bridge for each particular system is a program of research that attracts a considerable amount of studies and is far from being fulfilled. The strategy in this review relies on a coarse-grained picture (of the step topography). It is thus hoped that a confrontation between mesoscale analysis with continuum (or semicontinuum; the step topography is treated as continuum, whereas the steps will often be treated as individual entities) predictions will shed light on this multiscale problem. For example, while scanning tunneling microscope (STM) imaging of a step (such as in Fig. 7) can be viewed as a microscopic probe for individual steps, the step topography (and hence statistical analysis of fluctuations) can be analyzed at a mesoscale. This way has provided satisfactory agreement in several instances (Giesen, 2001). It must be kept in mind, however, that while STM can have access to atomic resolution, obtaining reliable information on a micrometer scale requires the collection of many images for ensemble averaging. To our knowledge, such a task has not yet been systematically performed. Past reviews have been devoted to the experimental study of static and kinetic fluctuations at global equilibrium (Jeong and Williams, 1999; Giesen, 2001). Many of the experimental facts, as well as experimentally measured parameters used here, are extracted from these reviews.

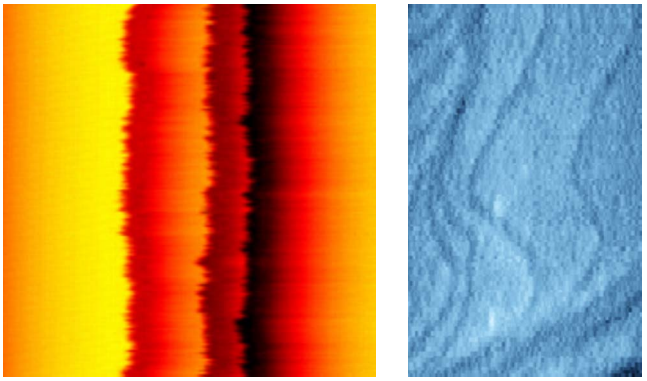

FIG. 7. (Color online) Atomic steps wandering at equilibrium: (a) STM image of steps on Cu(100) vicinal surface. The fuzziness accounts for the fast fluctuations (Giesen-Seibert *et al.*, 1993). (b) REM image of Si(111) steps. Courtesy of J.-J. Métois.

1. Isolated step

Vicinal surfaces are made of terraces separated by monatomic steps. A step is a one-dimensional entity for which it is known that fluctuations may be much stron-

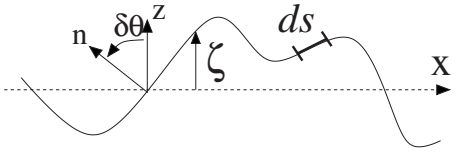

FIG. 8. Top view of a step of meander ζ. The average step tangent vector is along x and the average normal is along z. The arclength is denoted as s and $\delta\theta$ is the angle between z and the normal **n**.

ger than for a higher dimension entity, such as a surface. Figure 7 shows STM and REM pictures where a step can wander about its straight configuration; wandering may have a large amplitude in comparison with atomic length. This type of wandering can be analyzed and exploited to obtain interesting information. It must be remembered that step wandering is not mechanical, like bending, but materialized by mass transport (diffusion along the step, mass exchange with terraces, etc.).

We start our consideration systematically from an isolated step as shown in Fig. 8. x is the coordinate along the average orientation of the step, while ζ refers to the step position along the z direction. The local step deformation $\zeta(x)$ increases the length of a step segment from dx to $ds=dx\sqrt{1+(\partial_x\zeta)^2}$, and the step perimeter length increases. (Hereafter we use the abbreviated notation for the partial derivative $\partial/\partial x=\partial_x$.) Associated with this increase in step length (for a constant mass), there is a cost in free energy, which is simply the line free energy γ (we may also use the step free energy per length). For a crystal it is obvious that the free-energy cost γ depends on the step orientation θ with respect to the crystallographic symmetry $\gamma(\theta)$.

When the step deforms by $\zeta(x)$, orientation deviates from an average $\bar{\theta}$ by $\delta\theta$, as shown in Fig. 8. Of course, its average should vanish: $\langle\delta\theta\rangle=0$. ζ and $\delta\theta$ are related:

$$\partial_x\zeta=\tan\delta\theta\approx\delta\theta, \tag{2.1}$$

where the last approximation is valid for small deformations and $\delta\theta\ll1$. The total free-energy cost is expanded to quadratic order in the modulation $\zeta(x)$ or $\delta\theta$:

$$\mathcal{F}=\int dx[\gamma(\theta)\sqrt{1+(\partial_x\zeta)^2}-\gamma(\bar{\theta})]\approx\frac{1}{2}\tilde{\gamma}(\bar{\theta})\int dx(\partial_x\zeta)^2. \tag{2.2}$$

Here θ dependence of γ is also expanded and introduces the step edge stiffness $\tilde{\gamma}=\gamma+\partial_{\theta\theta}\gamma$ (Fisher *et al.*, 1982) at the average orientation $\bar{\theta}$.

For a step with a length L, the step deformation is decomposed in Fourier modes

$$\zeta(x)=\sum_k\zeta_k e^{ikx}. \tag{2.3}$$

With the assumption of a periodic boundary condition $\zeta(x+L)=\zeta(x)$, the wave number takes the value $k=2\pi m/L$, with $m=\pm1,\ldots,\pm\infty$. The step energy [Eq. (2.2)] is then written as

$$\mathcal{F}=L\sum_k\frac{1}{2}\tilde{\gamma}k^2|\zeta_k|^2, \tag{2.4}$$

and the probability of realizing the deformation $\{\zeta_k\}$ is given by the Boltzmann factor

$$P_{\rm eq}(\{\zeta_k\})\sim e^{-\mathcal{F}/k_BT}. \tag{2.5}$$

The interesting feature is that the energy in Fourier space is additive and thus the probability appears as a product. In other words, in Fourier space the modes are independent. Thus, for example, the equilibrium correlation is obtained from the equipartition law

$$\langle|\zeta_k|^2\rangle_{\rm eq}=k_BT/L\tilde{\gamma}k^2. \tag{2.6}$$

The correlation function of the step fluctuation at a distance x is defined by

$$w^2(x)\equiv\langle[\zeta(0)-\zeta(x)]^2\rangle, \tag{2.7}$$

and it grows linearly with the distance x (when $|x|\ll L$),[1]

$$w^2(x)=2\sum_k\langle|\zeta_k|^2\rangle_{\rm eq}(1-\cos kx)$$
$$=\frac{2k_BT}{\tilde{\gamma}}\frac{1}{L}\sum_k\frac{1-\cos kx}{k^2}=\frac{k_BT}{\tilde{\gamma}}|x|. \tag{2.8}$$

For a periodic step with a length L, the step width is defined and calculated by

$$w_{\rm eq}^2\equiv\frac{1}{L}\int_0^L\langle\zeta(x)^2\rangle_{\rm eq}dx=\sum_k\langle|\zeta_k|^2\rangle_{\rm eq}=\frac{k_BT}{12\tilde{\gamma}}L. \tag{2.9}$$

If both ends of the step are fixed, for example, by the pinning of impurities (Alfonso *et al.*, 1992), then the width of the step fluctuation increases like $w_{\rm eq}^2=k_BTL/6\tilde{\gamma}$. From this relation, the step stiffness can be extracted from the experimental measurement of $w_{\rm eq}^2$. For Si(111), Alfonso *et al.* (1992) found $\tilde{\gamma}=10^{-10}$ J/m. These type of data were extracted systematically from experimental pictures of steps in various systems (Jeong and Williams, 1999; Giesen, 2001). The characteristic feature is that the correlation function $w^2(x)$ and the equilibrium step width $w_{\rm eq}^2$ increase linearly in proportion to the distance x and the step length L, respectively. This diverging fluctuation is a manifestation of the rough character of a step. This problem is similar to that of random walking in which x plays the role of "time" and $w_{\rm eq}$ is the mean excursion of the random walker.

2. Train of steps

When the crystal surface is tilted from a singular surface [see Fig. 9(a)], it is called a vicinal surface. On it, the steps run parallel and the flat surface between two neighboring steps is called a terrace.

In general, steps cannot cross or overlap due to the large energy cost of overhangs. Steps also deform the

[1]The expression of the sum is obtained by integrating twice the relation $\partial_{xx}\Sigma_k(1-\cos kx)/k^2=\Sigma_k\cos kx=L\delta(x)$.

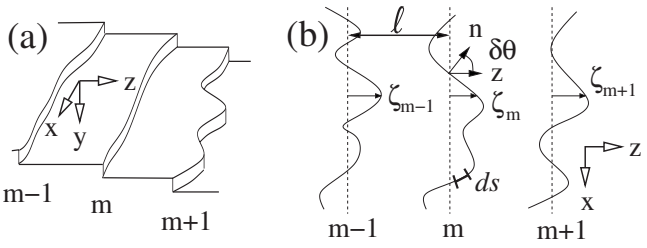

FIG. 9. A schematic view of (a) a vicinal surface inclined down in the z direction. Steps run parallel to the x direction on average. (b) A top view. The deviation of the mth step from its regular position is $\zeta_m(x)$.

underlying crystal and therefore interact elastically (Marchenko and Parshin, 1980; Jayaprakash *et al.*, 1984; Houchmandzadeh and Misbah, 1995; Müller and Saul, 2004). These interactions affect step fluctuation, and the measurement of step fluctuation provides information on the step-step interaction. We first discuss the harmonic approximation of the step interaction in order to see the general tendency of the interaction effects on step fluctuation, and then treat the noncrossing condition by a mapping to the fermion problem (Akutsu *et al.*, 1988, 1989; Saam, 1989; Joós *et al.*, 1991; Yamamoto *et al.*, 1994). The terrace width fluctuation and its probability distribution are discussed last.

a. Harmonic approximation

On a vicinal surface, steps run on average in the x direction with an average separation ℓ. The position of the mth step is defined as

$$z_m(x) = m\ell + \zeta_m(x), \tag{2.10}$$

where $\zeta_m(x)$ is the deviation from the average position (see Fig. 9 for notations).

When the step is formed on the substrate, it induces elastic deformation in the substrate and a force or force doublet field is created on the surface. Therefore, two straight steps interact with a certain potential $U(\ell)$. When the terraces on both sides are not identical [due, for example, to a surface reconstruction like on Si(001)] (Marchenko, 1981; Alerhand *et al.*, 1988, 1990), a force field on the step produces the interaction $U(\ell)=B\ln\ell$. When the two terraces on both sides of a step have identical properties, the step can be viewed from the elastic point of view as a location of a force doublet (Marchenko and Parshin, 1980; Jayaprakash *et al.*, 1984; Houchmandzadeh and Misbah, 1995). The force doublet yields the interaction

$$U(\ell) = \mathcal{A}/\ell^2. \tag{2.11}$$

The order of magnitude of $\mathcal{A}$ can be obtained from a simple dimensional analysis. Indeed, the relevant energy scale is controlled by the Young modulus E and an atomic length scale a. Therefore, one expects $\mathcal{A}\sim Ea^4$. Taking $E\sim 10^{10}$ Pa and $a\sim 1$ Å, one finds $\mathcal{A}\sim 10^{-30}$ J m. This is in the range of experimentally observed values for $\mathcal{A}=4.6\times 10^{-30}$ J m on Si(111) at 900 °C (Alfonso *et al.*, 1992; Jeong and Williams, 1999).

The single-step fluctuations and step-step interactions contribute to variations in total step energy of a vicinal surface[2]

$$\mathcal{F} = \sum_m \int dx \left[\frac{\tilde{\gamma}}{2}(\partial_x z_m)^2 + U[z_{m+1}(x) - z_m(x)] - U(\ell) \right]$$
$$\approx \sum_m \int dx \left[\frac{\tilde{\gamma}}{2}(\partial_x \zeta_m)^2 + \frac{U''(\ell)}{2}[\zeta_{m+1}(x) - \zeta_m(x)]^2 \right]. \tag{2.12}$$

By assuming a small deformation $\zeta_m(x)$, the harmonic approximation is performed in the second equality.

By allowing fluctuation of the mth step only, but freezing all other deformations, $\zeta_{m'}(x)=0$ for $m'\neq m$, the fluctuation of the mth step was calculated exactly by Bartelt *et al.* (1990). It remains finite,

$$w_h^2 = k_B T/\sqrt{8U''(\ell)\tilde{\gamma}}, \tag{2.13}$$

since it cannot escape from the harmonic potential whose minimum lies at $\zeta_m(x)=0$ for all values of x. Subscript h in w_h stands for harmonic.

If all steps are allowed to fluctuate, then steps can meander together, and fluctuations can diverge for an infinitely large system. We transform the step fluctuation in Fourier modes with wavelength k and phase ϕ (Pimpinelli *et al.*, 1994) to

$$\zeta_m(x) = \int_0^{2\pi} \frac{d\phi}{2\pi} \int_{-\infty}^{\infty} \frac{dk}{2\pi} \zeta_{k\phi} e^{i(kx+m\phi)}, \tag{2.14}$$

where $\zeta_{-k-\phi}=\zeta_{k\phi}^*$. We have assumed that the surface is very large, making k a continuous variable. The step energy is rewritten (Pierre-Louis and Misbah, 1998a)

$$\mathcal{F} = \int \frac{d\phi}{2\pi} \int \frac{dk}{2\pi} \left[\frac{1}{2}\tilde{\gamma}k^2 + U''(\ell)(1-\cos\phi) \right] |\zeta_{k\phi}|^2, \tag{2.15}$$

and the probability distribution to realize the configuration $\{\zeta_{k\phi}\}$ is given by the Boltzmann weight $P_{\rm eq}(\{\zeta_{k\phi}\}) \sim e^{-\mathcal{F}/k_BT}$. The equilibrium fluctuation of the mode (k,ϕ) is given by the equipartition law

$$\langle |\zeta_{k\phi}|^2 \rangle_{\rm eq} = k_B T/[\tilde{\gamma}k^2 + 2U''(\ell)(1-\cos\phi)]. \tag{2.16}$$

If all steps fluctuate in phase ($\phi=0$), the elastic effect disappears and the result is that of an isolated step [Eq. (2.6)]. If $\phi=\pi/2$, the effect from the two neighboring

[2]Here steps interact with their nearest neighbors only. This approximation is meaningful only if the sum of the interaction energies of one step with all others is a convergent quantity. This is the case in the presence of force doublets or for the alternated monopoles [as in the case of the 2×1 reconstructed Si(100) surface]. In the case of surfaces under stress in heteroepitaxy, the sum of all terms should be taken, as discussed in Sec. IV.F.

steps disappears and the result by Einstein *et al.* (Bartelt *et al.*, 1990) [Eq. (2.13)] is recovered [upon Fourier transform (FT)]. In general, all phase fluctuations ϕ must be considered. For a system with a large size L, the asymptotics of the step width $w_{\rm eq}^2$ can be evaluated in the harmonic approximation because the long wavelength provides the dominant contribution. By taking the lower cutoff $k_0=2\pi/L$ in the k integration, the width diverges logarithmically (Pierre-Louis and Misbah, 1996, 1998a; Ihle *et al.*, 1998),

$$w_{\rm eq}^2 \equiv \frac{1}{L}\int_0^L \frac{1}{N}\sum_{m=1}^{N} \langle[\zeta_m(x)]^2\rangle_{\rm eq} dx = \int \frac{d\phi}{2\pi}\int \frac{dk}{2\pi}\langle|\zeta_{k\phi}|^2\rangle \approx \frac{k_BT}{2\pi\sqrt{\tilde{\gamma}U''(\ell)}}\ln\left(\frac{L}{L_e}\right), \tag{2.17}$$

with the characteristic "elastic" length

$$L_e = \pi\sqrt{\tilde{\gamma}/U''(\ell)}. \tag{2.18}$$

Even when the elastic interaction is vanishingly small, the step is not completely free since it cannot cross the neighboring steps (Gruber and Mullins, 1967). Indeed, step crossing creates overhangs, which cost significant excess energy. We now consider the effect of this short-ranged hard-core repulsion on the step fluctuation. The prohibition of double occupancy of a single site by steps can be modeled by the fermion exclusion principle, and the statistical mechanics of the step system can be cast onto the quantum mechanics of the free fermion system (Villain and Bak, 1981; Jayaprakash *et al.*, 1984), where an exact solution is available. This result will be summarized next, but first we give a qualitative explanation of the result. For short length scales a step behaves as if isolated. When the distance x along the step increases, the thermal fluctuation enhances the step meandering $w(x)$ as given in Eq. (2.8). Along the step, at a distance of collision length

$$L_{\rm coll} = \tilde{\gamma}\ell^2/k_BT, \tag{2.19}$$

the meandering $w(L_{\rm coll})$ becomes as large as the step separation ℓ, and the neighboring steps collide and sense their noncrossing restriction (Fisher and Fisher, 1982). A step with a length L thus collides with its neighbors approximately $L/L_{\rm coll}$ times and loses entropy because further thermal fluctuation is blocked. The free energy of a step then increases by around k_BT on each collision. The step free energy per unit length thus increases in proportion to $k_BT/L_{\rm coll}$. A more precise calculation from the free fermion model gives the energy increase as

$$U_{\rm FF}(\ell) = (\pi k_BT)^2/6\tilde{\gamma}\ell^2, \tag{2.20}$$

which has the same ℓ^{-2} dependence on the step separation as the elastic interaction (2.11). Thus, for a train of free steps, an effective interaction $U_{\rm FF}$ is used. Equation (2.17) gives the asymptotics for the step width as

$$w_{\rm eq}^2 = (\ell^2/2\pi^2)\ln(L/L_{\rm coll}) \tag{2.21}$$

for a large system, in agreement with that of the free fermion model (Akutsu *et al.*, 1989; Bartelt, Einstein, and Williams, 1992; Saito, 1996).

b. Fermion model

Here we review a more precise treatment of the noncrossing condition by mapping the statistical mechanics of the step train system onto the quantum mechanics of the one-dimensional fermion system. On a vicinal surface of size $L\times L_z$ (L_z is the length along the vicinal surface), N steps run, on average, in the x direction (Fig. 9). The position of the mth step is described by $z_m(x)$, and the noncrossing condition is represented by

$$0 \le z_1(x) < z_2(x) < \cdots < z_N(x) \le L_z \tag{2.22}$$

for all values of x. First one disregards the elastic interaction between steps. Step deformation costs energy as follows:

$$\frac{1}{2}\sum_{m=1}^{N}\int_0^L \tilde{\gamma}[\partial_x z_m(x)]^2 dx, \tag{2.23}$$

and the partition function at temperature T is written as

$$Z_{\rm int} = \int \mathcal{D}z_1(x)\cdots\mathcal{D}z_N(x) \times \exp\left[-\sum_{m=1}^{N}\int_0^L \frac{\tilde{\gamma}}{2k_BT}[\partial_x z_m(x)]^2 dx\right]. \tag{2.24}$$

In the configuration sum $\mathcal{D}z_1(x)\cdots\mathcal{D}z_N(x)$ the noncrossing condition (2.22) must be considered. Interestingly, Eq. (2.24) has the form of the Feynman path integral representation (Feynman, 1972) for the partition function of a one-dimensional quantum mechanical system with N free particles. z_m represents the position of the mth quantum particle with a "mass" $\tilde{\gamma}/k_BT$ (the Planck constant is chosen to be $\hbar=1$), L^{-1} represents the fictitious "temperature" of the quantum system, and x represents the "path" from 0 to the "inverse temperature" L. The quantum mechanical Hamiltonian operator only contains a kinetic energy term (Yamamoto *et al.*, 1994)

$$\hat{\mathcal{H}} = -\sum_{m=1}^{N}\frac{k_BT}{2\tilde{\gamma}}\frac{\partial^2}{\partial z_m^2}. \tag{2.25}$$

For a one-dimensional system, the noncrossing condition (2.22) is satisfied when the particles are fermions. In this case, the traditional statistical mechanics of a step train system in two dimensions reduce to the quantum statistical mechanics of a one-dimensional free fermion system. The partition function is then written as

$$Z_{\rm int} = {\rm Tr}\, e^{-\hat{\mathcal{H}}L}, \tag{2.26}$$

where the trace is taken over the N fermion space. In the second quantization form, the Hamiltonian is written as

$$\hat{\mathcal{H}} = \frac{k_B T}{2\tilde{\gamma}} \sum k^2 \hat{a}_k^+ \hat{a}_k, \tag{2.27}$$

where $\hat{a}_k^+$ and $\hat{a}_k$ are the creation and annihilation operators of spinless fermions with the wave number $k = 2\pi n/L_z$, where $n = 0, \pm 1, \ldots$. The thermodynamic limit with a large L of a step system corresponds to the "zero-temperature" state in the fictitious quantum system, and the "ground-state" energy E_1 of $\hat{\mathcal{H}}$ determines the thermodynamic behavior of the step system,

$$E_1 = \frac{k_B T}{2\tilde{\gamma}} \sum_{|k| \le k_F} k^2 \to \frac{k_B T}{2\tilde{\gamma}} L_z \frac{\pi^2}{3\ell^3}, \tag{2.28}$$

where $k_F = \pi N/L_z = \pi/\ell$ is the Fermi wave number for N fermions in a one-dimensional system with a length L_z. In the last step, the thermodynamic limit is taken with $L_z \to \infty$ and $N \to \infty$ by keeping the step density $\rho = 1/\ell$ fixed. The contribution of the step correlation to the surface free energy density per area is thus obtained by

$$f_{\rm int} \equiv -\frac{k_B T}{L L_z} \ln Z_{\rm int} = \frac{k_B T}{L_z} E_1 = \frac{\pi^2 (k_B T)^2}{6\tilde{\gamma}(\theta)\ell^3} = \frac{\pi^2 (k_B T)^2}{6\tilde{\gamma}(\theta)} \rho^3, \tag{2.29}$$

where θ is the angle of the average step orientation, $\ell = L_z/N$ is the average step separation, and $\rho = 1/\ell$ is the step density. Since there are ρ steps in a unit area, each step makes a contribution to the free energy equal to $f_{\rm int}/\rho = U_{\rm FF}$, as previously described. The total surface free energy f also includes the constant contribution from the terrace f_0 and the contribution $\gamma(\theta)\rho$ from straight steps in addition to $f_{\rm int}$:

$$f = f_0 + \gamma(\theta)\rho + [\pi^2 (k_B T)^2/6\tilde{\gamma}(\theta)]\rho^3. \tag{2.30}$$

The step width can be evaluated exactly using fermion operators (Yamamoto *et al.*, 1994), while the asymptotic behavior of $w_{\rm eq}^2$ for a large system size L is correctly given by the harmonic approximation (2.21). The step noncrossing restriction affects the fluctuation of long-wavelength modes ($k \le 2\pi/L_{\rm coll}$) and gives rise to the effective step-step interaction for modes with long wavelengths. The asymptotic step width is determined by these long-wavelength modes, which can now be described by the harmonic approximation.

When the steps m and m' interact repulsively with an elastic interaction $\mathcal{A}/|z_m - z_{m'}|^2$, the quantum Hamiltonian (2.25) changes to

$$\hat{\mathcal{H}} = -\sum_{m=1}^{N} \frac{k_B T}{2\tilde{\gamma}} \frac{\partial^2}{\partial z_m^2} + \frac{\mathcal{A}}{k_B T} \sum_{m<m'} \frac{1}{|z_m - z_{m'}|^2} = \frac{k_B T}{2\tilde{\gamma}} \left[-\sum_{m=1}^{N} \frac{\partial^2}{\partial z_m^2} + g \sum_{m<m'} \frac{1}{|z_m - z_{m'}|^2} \right] \tag{2.31}$$

with the coupling constant $g = 2\tilde{\gamma}\mathcal{A}/(k_B T)^2$. This is simply the one-dimensional interacting fermion system solved exactly by Sutherland (1971). The ground-state energy is known exactly by

$$E_1(g) = E_1 \bar{\lambda}^2(g), \tag{2.32}$$

where E_1 is the ground-state energy of the free fermion system (2.28) and the function $\bar{\lambda}(g)$ is defined by

$$\bar{\lambda}(g) = \tfrac{1}{2}(1 + \sqrt{1 + 2g}). \tag{2.33}$$

The interactive part of the surface free energy density $f_{\rm int}$ in Eq. (2.29) is now modified by the elastic interaction g,

$$f_{\rm int}(g) = (\pi k_B T)^2 \bar{\lambda}^2(g)/6\tilde{\gamma}(\theta)\ell^3. \tag{2.34}$$

The actual step interaction with elastic and noncrossing conditions can now be written as

$$U_{\rm eff} = [(\pi k_B T)^2/6\tilde{\gamma}\ell^2]\bar{\lambda}^2(g). \tag{2.35}$$

The asymptotic divergence of the step width for a large system size L is determined by the long-wavelength fluctuation mode. For this macroscopic description, the harmonic approximation gives the correct asymptotics. Since the strength of the harmonic potential with elastic interaction and noncrossing condition is written as

$$U''_{\rm eff}(\ell) = [\pi k_B T \bar{\lambda}(g)]^2/\tilde{\gamma}\ell^4, \tag{2.36}$$

with step width asymptotics changing from Eq. (2.17) to

$$w_{\rm eq}^2 = [\ell^2/2\pi^2 \bar{\lambda}(g)] \ln[L\bar{\lambda}(g)/L_{\rm coll}]. \tag{2.37}$$

c. Terrace width distribution

To obtain the form and strength of the step-step interaction, the terrace width fluctuation

$$W_{\rm eq}^2 \equiv \langle [z_{m+1}(x) - z_m(x) - \ell]^2 \rangle = \langle [\zeta_{m+1}(x) - \zeta_m(x)]^2 \rangle \tag{2.38}$$

has been measured in various experiments (Rousset *et al.*, 1992; Barbier *et al.*, 1996; Giesen, 1997). In these works the terrace width probability distribution $P(s)$, where $s = (z_{m+1} - z_m)/\ell$ is the normalized terrace width, has been measured. A simple model (with noncrossing condition) for the terrace width was earlier introduced by Gruber and Mullins (1967), where a free step is trapped between two fixed walls separated by twice the mean terrace width ℓ. The terrace distribution function reads

$$P_{\rm GM}(s) = \sin^2(\pi s/2), \quad 0 \le s \le 2, \tag{2.39}$$

with the terrace width fluctuation

$$W_{\rm GM}^2 = \ell^2(\langle s^2 \rangle - 1) = \ell^2(\tfrac{1}{3} - 2/\pi^2). \tag{2.40}$$

A remarkable feature is that the result does not depend on temperature.

Several groups (Bartelt *et al.*, 1990; Wang *et al.*, 1990; Alfonso *et al.*, 1992) investigated cases of step elastic interaction in the harmonic approximation. Even though they fixed the positions of neighboring steps, the noncrossing condition was not taken into account. The ter-

race width fluctuation is the same as the step width w_h in Eq. (2.13) since the step $m+1$ is fixed $\zeta_{m+1}=0$:

$$W_h^2 = w_h^2 = k_B T/\sqrt{8U''(\ell)\tilde{\gamma}}. \tag{2.41}$$

For interactions which fall off as the inverse square of the step separation ℓ, we have $U''(\ell) \propto \ell^{-4}$, and the fluctuation of the terrace width W_h is proportional to the average width ℓ. The distribution function is shown to be Gaussian with a variance W_h (Bartelt, Goldberg, *et al.*, 1992),

$$P_h(s) = (\ell/\sqrt{2\pi}W_h)\exp[-(s-1)^2\ell^2/2W_h^2]. \tag{2.42}$$

The restriction to freeze all step configurations other than that under consideration seems rather artificial. If neighboring steps are allowed to fluctuate, the step width w_{eq}^2 diverges with L as shown previously, but the terrace width fluctuation W_{eq}^2 still remains finite and is proportional to the square of the average terrace width ℓ (Alfonso *et al.*, 1992; Ihle *et al.*, 1998):

$$W_{\mathrm{eq}}^2 = 2\int_0^{2\pi}\frac{d\phi}{2\pi}\int_{-\infty}^{\infty}\frac{dk}{2\pi}\langle|\zeta(k,\phi)|^2\rangle(1-\cos\phi)$$
$$= \frac{2}{\pi}\frac{k_B T}{\sqrt{U''(\ell)\tilde{\gamma}}} = \frac{4\sqrt{2}}{\pi}w_h^2. \tag{2.43}$$

As previously described, the step train system is equivalent to the one-dimensional interacting fermion system. Joós *et al.* (1991) showed that the terrace width distribution function is related to the fermion two-particle correlation function, whose form is known accurately for specific values of the coupling g: $g=1/2$, 1, and 2 (Sutherland, 1971). More generally, the correlation functions in these special cases can be evaluated using Dyson's quarternion-determinant technique for the random-matrix theory (Sutherland, 1971; Guhr *et al.*, 1998). Joós *et al.* (1991) used this equation to calculate the exact terrace distribution function numerically.

Recently, a more accurate expression has been proposed (Einstein and Pierre-Louis, 1999) for the equilibrium terrace width distribution function $P(s)$. In the random-matrix theory, the Wigner surmise[3] of the distribution is known for specific values of the coupling parameter g. The simplest interpolation for the general values of the coupling g is proposed as

$$P_{\bar{\lambda}(g)}(s) = as^{2\bar{\lambda}(g)}\exp(-bs^2), \tag{2.44}$$

where a and b are determined by the normalization of the probability P and the unit-mean condition $\langle s\rangle=1$, respectively, as

[3]Wigner proposed that fluctuations in the spacing of energy levels exhibit certain universal features as follows from random-matrix theory. It turns out that the terrace width distribution (in the fermion analogy) is equivalent to the distribution energy spacing which can be deduced exactly for specific values of g. The Wigner surmise states that the probability density function of the eigenvalue spacing of a random system follows the Rayleigh distribution.

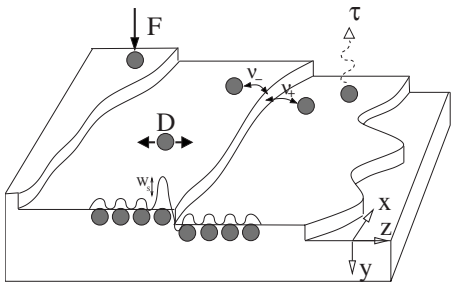

FIG. 10. Schematic view of a vicinal surface. D is the diffusion constant, F is the deposition flux, τ is the desorption time, and $\nu_\pm$ are step attachment coefficients from the lower and upper sides, respectively. The potential barrier to jump over the step is denoted as W_s.

$$a = \frac{2b^{\bar{\lambda}(g)+1/2}}{\Gamma(\bar{\lambda}(g)+1/2)}, \quad b = \left[\frac{\Gamma(\bar{\lambda}(g)+1)}{\Gamma(\bar{\lambda}(g)+1/2)}\right]^2. \tag{2.45}$$

Here $\Gamma(z)$ is the Gamma function defined by

$$\Gamma(z) = \int_0^{\infty} x^{z-1}e^{-x}dx. \tag{2.46}$$

The Wigner surmise corresponds to the probabilities at $\bar{\lambda}(g)=1/2$, 1, and 2 and reproduces the exact probability $P(s)$ quite well. From the interpolation formula (2.44), the terrace width fluctuation is obtained as

$$W_{\mathrm{eq}}^2/\ell^2 = \langle s^2\rangle - 1 = [\bar{\lambda}(g)+1/2]/b - 1, \tag{2.47}$$

which naturally reproduces the exact values at $\bar{\lambda}(g)=1/2$, 1, and 2. There is a plausible explanation for the probability (2.44) based on a simple averaging approximation in a Langevin model for step dynamics (Pimpinelli *et al.*, 2005). Finally, it would be interesting to extend the derivation of terrace width distribution to other laws of step-step interactions.

B. Fluctuation dynamics in equilibrium

The equilibrium step width contains information on the energetics of the system, such as step stiffness and elastic interaction, but is independent of kinetic processes. In order to obtain kinetic properties, dynamical quantities must be studied.

Various kinetic processes take place on a stepped surface, as shown in Fig. 10, and the small amplitude of the Fourier mode of Eq. (2.14) now depends on time $\zeta_{k\phi}(t)$ and relaxes generically via the linear Langevin equation

$$\partial_t\zeta_{k\phi}(t) = i\omega_{k\phi}\zeta_{k\phi}(t) + \eta_{k\phi}(t), \tag{2.48}$$

with the relaxation rate $i\omega_{k\phi}$ when step motion is slow and nonlinear effects are neglected (the origin of nonlinearities will be explained later). An equivalent approach bypassing Langevin formalism can be found in Flynn (2002). The correlation of the thermal noise $\eta_{k\phi}(t)$ is assumed to satisfy the fluctuation-dissipation theorem

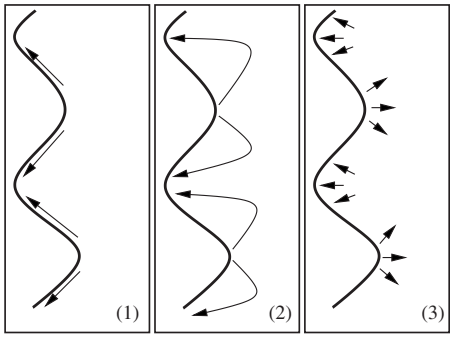

FIG. 11. Three basic mass transport mechanisms for an isolated step: (1) edge diffusion, (2) terrace diffusion (nonlocal mechanism), and (3) attachment-detachment (local mechanism).

$$\langle \eta_{k\phi}(t)\eta_{k'\phi'}(t')\rangle = -8\pi^2\langle|\zeta_{k\phi}|^2\rangle_{\rm eq} i\omega_{k\phi} \times \delta(k+k')\delta(\phi+\phi')\delta(t-t'). \tag{2.49}$$

Upon integration on time, the initially straight step relaxes to thermal equilibrium

$$\langle|\zeta_{k\phi}(t)|^2\rangle = \langle|\zeta_{k\phi}|^2\rangle_{\rm eq}(1-e^{2i\omega_{k\phi}t}). \tag{2.50}$$

The step fluctuation width is given as

$$w^2(t) = \langle\zeta_m(x,t)^2\rangle = \int_0^{2\pi}\frac{d\phi}{2\pi}\int_{-\infty}^{\infty}\frac{dk}{2\pi}\langle|\zeta_{k\phi}(t)|^2\rangle \tag{2.51}$$

and the terrace width fluctuation (Bartelt *et al.*, 1990; Alfonso *et al.*, 1992) as

$$W^2(t) = \langle[\zeta_m(x,t)-\zeta_{m+1}(x,t)]^2\rangle = \int_0^{2\pi}\frac{d\phi}{2\pi}\int_{-\infty}^{\infty}\frac{dk}{2\pi}\langle|\zeta_{k\phi}(t)|^2\rangle(1-\cos\phi). \tag{2.52}$$

The time correlation of the step fluctuation in equilibrium

$$G(t) = \langle[\zeta_m(x,t)-\zeta_m(x,0)]^2\rangle_{\rm eq} \tag{2.53}$$

is often obtained in experiments. This is, in fact, proportional to the step fluctuation width

$$G(t) = 2\int\frac{d\phi}{2\pi}\int\frac{dk}{2\pi}\langle|\zeta_{k\phi}|^2\rangle_{\rm eq}(1-e^{i\omega_{k\phi}t}) = 2w^2(t/2). \tag{2.54}$$

Therefore, the step width $w^2(t)$ gives the same information as the step correlation function $G(t)$.

1. Isolated step

In order for a step to change its conformation, various kinetic processes are involved, as shown in Fig. 10. The atoms composing the step have to change their positions. To do so, they can migrate along the step edge via a process called edge or line diffusion [see Fig. 11, (1)]. They can also detach from somewhere on the step or attach somewhere else [see Fig. 11, (3)]. Atoms detached from the step can still be adsorbed on the substrate surface—they are then called adatoms—or they can migrate on the terrace surface [surface or terrace diffusion, Fig. 11, (2)] and attach to the step again or desorb to the atmosphere. There is also a deposition flux of atoms from the gas phase. These different mass transport processes combine together to give rise to step motion.

The precise form of the relaxation rate $i\omega_{k\phi}$ depends on the step relaxation kinetics mechanism. When kinetics are limited by a single mass transport mechanism, a power-law form of the relaxation rate can often be assumed:

$$i\omega_{k\phi} = i\omega_k = -A_0|k|^n. \tag{2.55}$$

Furthermore, for an isolated step as well as for a step train in some specific regimes such as for short time correlations, the phase shift ϕ and elastic interaction are irrelevant. Thus, $\langle|\zeta_{k\phi}|^2\rangle_{\rm eq}$ in Eq. (2.50) can be replaced by an isolated step fluctuation: $\langle|\zeta_k|^2\rangle_{\rm eq}=k_BT/\tilde{\gamma}k^2$. The integration in Eq. (2.51) is then performed straightforwardly by partial integration, and changing the variable $2A_0t|k|^n=x$,

$$w^2(t) = \frac{G(2t)}{2} = \frac{k_BT}{2\pi\tilde{\gamma}}2\int_0^{\infty}\frac{dk}{k^2}(1-e^{-2A_0tk^n}) = \frac{k_BT}{\pi\tilde{\gamma}}n(2A_0t)\int_0^{\infty}dkk^{n-2}e^{-2A_0tk^n} = \frac{k_BT}{\pi\tilde{\gamma}}\Gamma\left(1-\frac{1}{n}\right)(2A_0t)^{1/n}, \tag{2.56}$$

where $\Gamma(z)$ is the Gamma function defined in Eq. (2.46) and $\Gamma(\frac{1}{2})=\sqrt{\pi}$, $\Gamma(\frac{2}{3})=1.351\,75\ldots$, and $\Gamma(\frac{3}{4})=1.225\,41\ldots$.

Thus, the study of fluctuations provides (i) qualitative information via the exponent n on the type of mass transport entering into play at the surface and (ii) quantitative information on the kinetic coefficients via the prefactor A_0. We now look at some specific regimes in more detail.

a. Attachment or detachment

The concentration c_+ or c_- of adatoms in front of or at the back of the step is generally different from the equilibrium concentration $c_{\rm eq}$. The difference drives the step motion as shown in Fig. 11, (3) at velocities

$$V_{\pm} = \Omega[J_{\pm}+\eta_{\pm}] = \Omega[\nu_{\pm}(c_{\pm}-c_{\rm eq})+\eta_{\pm}]. \tag{2.57}$$

Here the linear kinetics is assumed with the kinetic coefficient $\nu_{\pm}$, as shown in Fig. 10, and $J_{\pm}$ represents fluxes from both terraces to the step. The difference in the coefficients ν_+ and ν_- is due to the Ehrlich-Schwoebel (ES) effect (see Secs. II.B.2.b and IV.A for more details). Ω represents the specific area and $\eta_{\pm}$ is the thermal noise. The total step velocity V is given as a sum of the front and back contributions:

$$V = V_+ + V_-. \tag{2.58}$$

The equilibrium concentration c_{eq} depends on the step conformation. When the step forms a bump with a positive curvature

$$\kappa = -\partial_{xx}\zeta/[1+(\partial_x\zeta)^2]^{3/2} \approx -\partial_{xx}\zeta, \tag{2.59}$$

the line tension pushes the step back to the straight form by sublimating atoms from the step. Therefore a higher adatom concentration is required to keep the bump in equilibrium.

In general, the shift of an equilibrium concentration due to a new force can be written as

$$c_{eq} = c_{eq}^0 e^{\mu/k_BT} \approx c_{eq}^0[1+\mu/k_BT]. \tag{2.60}$$

Here μ is the chemical potential, including the contribution of the new force, and defined by the functional derivative as

$$\mu = \frac{\delta\mathcal{F}}{\delta\mathcal{N}} = \frac{\delta\mathcal{F}}{\delta\zeta}\frac{\delta\zeta}{\delta\mathcal{N}} = \Omega\frac{\delta\mathcal{F}}{\delta\zeta} \tag{2.61}$$

at a constant temperature, where $\mathcal{F}$ is the free energy and $\mathcal{N}$ is the number of particles. At the last equality, we used the fact that the area solidified due to a displacement ζ of the step is given by $\mathcal{N}\Omega = \int \zeta dx$ with a specific area Ω, so that $\delta\zeta/\delta\mathcal{N} = \Omega$. For $\mathcal{F}$ given by Eq. (2.2), $\delta\mathcal{F}/\delta\zeta = \tilde{\gamma}\kappa$. Therefore, for an isolated step, the curved step equilibrium concentration c_{eq} changes from the straight step c_{eq}^0 to

$$c_{eq}(x) = c_{eq}^0(1+\Gamma\kappa). \tag{2.62}$$

Here $\Gamma = \Omega\tilde{\gamma}/k_BT$ and it has a dimension of a length (Bales and Zangwill, 1990; Bena *et al.*, 1993).

Even if the step is initially straight in coexistence with the adatoms with concentration c_{eq}^0, thermal fluctuation η drives the step in motion. $c_\pm$ in Eq. (2.57) is set to c_{eq}^0. Combining Eqs. (2.57) and (2.62) in the linear approximation, the step motion is described (Bartelt, Einstein, and Williams, 1992) as

$$\partial_t\zeta = V_+ + V_- = (\nu_+ + \nu_-)\Omega c_{eq}^0\Gamma\partial_{xx}\zeta + (\eta_+ + \eta_-)\Omega. \tag{2.63}$$

The Fourier transformation gives the relaxation rate (Mullins, 1957, 1959, 1963) as

$$i\omega_k = -(\nu_+ + \nu_-)\Omega c_{eq}^0\Gamma k^2, \tag{2.64}$$

and the width is calculated from Eq. (2.56) with $n=2$ (Bartelt, Einstein, and Williams, 1992; Bartelt, Goldberg, *et al.*, 1992; Bartelt *et al.*, 1993),

$$w^2(t) = \frac{G(2t)}{2} = \frac{k_BT}{\pi\tilde{\gamma}}\Gamma\left(\frac{1}{2}\right)[2(\nu_+ + \nu_-)\Omega c_{eq}^0\Gamma t]^{1/2}. \tag{2.65}$$

b. Edge diffusion

When the step relaxes via edge diffusion, as shown in Fig. 11, (1), the normal step velocity is determined from the flux gradient by

$$V_n = -\Omega\partial_s J_L, \tag{2.66}$$

where s is the arclength along the step and $s=x$ in the linear approximation. The mass flux along the step J_L is proportional to the chemical potential gradient

$$J_L = -(M/\Omega)\partial_s\mu \tag{2.67}$$

with a mobility

$$M = aD_L/k_BT \tag{2.68}$$

along the edge, where D_L is the macroscopic edge-diffusion constant and a is the atomic length. Since the chemical potential is given by $\mu = \Omega\delta\mathcal{F}/\delta\zeta(x) = \Omega\tilde{\gamma}\kappa$, the step profile evolution

$$V_n = \partial_s[aD_L\partial_s(\Gamma\kappa)] \tag{2.69}$$

is obtained. Linearizing this equation, we find (Bartelt, Einstein, and Williams, 1992)

$$\partial_t\zeta = -aD_L\Gamma\partial_{xxxx}\zeta + \eta_e, \tag{2.70}$$

where η_e is the noise term. The subscript e refers to edge.[4] Equation (2.70) gives the relaxation rate (Mullins, 1957, 1963; Bartelt, Einstein, and Williams, 1992)

$$i\omega_k = -aD_L\Gamma k^4. \tag{2.71}$$

The width is then obtained from Eq. (2.56) with $n=4$ (Bartelt, Einstein, and Williams, 1992; Bartelt *et al.*, 1993),

$$w^2(t) = G(2t)/2 = (k_BT/\pi\tilde{\gamma})\Gamma(\tfrac{3}{4})(2aD_L\Gamma t)^{1/4}. \tag{2.72}$$

c. Terrace diffusion

Atoms detaching from the step can migrate on the terrace and then attach again to the same step in a different position [Fig. 11, (2)]. The adatom concentration $c(x,y,t)$ varies according to the diffusion law (Burton *et al.*, 1951)

$$\partial_t c = D\nabla^2 c + F - c/\tau = 0, \tag{2.73}$$

where D is the surface diffusion constant, F is the deposition rate, and τ is the lifetime before desorption (Fig. 10). Equilibrium is reached when $F = F_{eq} \equiv c_{eq}^0/\tau$. The second equality in Eq. (2.73) holds under the stationary approximation, where the step motion is sufficiently slow compared to the diffusional variation of the concentration field c. This quasisteady approximation holds for most practical purposes and will be adopted in this review. The material conservation at the step leads to the boundary condition

$$V_\pm = \pm\Omega D\partial_n c_\pm \approx \pm\Omega D\partial_z c_\pm, \tag{2.74}$$

where $\pm$ refers to the front and back of the step and $\partial_n \equiv \mathbf{n}\cdot\boldsymbol{\nabla}$ represents the derivative in the normal direction

[4]This noise is conserved, but instead of using this property explicitly, we use the fluctuation-dissipation theorem (2.49).

$$\mathbf{n} = (-\partial_x\zeta, 1)/\sqrt{1+(\partial_x\zeta)^2} \approx (-\partial_x\zeta, 1). \tag{2.75}$$

For a small deformation ζ the normal derivative ∂_n can be replaced by the derivative ∂_z in direction z in the linear approximation. If the attachment-detachment kinetics is fast enough compared to the diffusional relaxation of the step, the local equilibrium approximation $c_\pm = c_{\rm eq}$ obtained at the limit $\nu_\pm \to \infty$ in Eq. (2.57) may be used. Furthermore, we assume that deposition and desorption effects are insignificant and can be ignored ($F = \tau^{-1} = 0$). Step fluctuation $\zeta(x,t) = \zeta_k(t)\exp[ikx]$ thus induces the density fluctuation c of the same wavelength k in the x direction. The concentration obeys

$$(\partial_{zz} - k^2)c = 0 \tag{2.76}$$

and decays in the z direction at a decay rate $|k|$:

$$\begin{aligned} c(x, z>0, t) &= c_{\rm eq}^0[1 + \Gamma k^2 \zeta_k(t) e^{ikx-|k|z}], \\ c(x, z<0, t) &= c_{\rm eq}^0[1 + \Gamma k^2 \zeta_k(t) e^{ikx+|k|z}]. \end{aligned} \tag{2.77}$$

The conservation law at the step [Eq. (2.74)] determines step relaxation at the following rate (Mullins, 1957, 1963; Bales and Zangwill, 1990; Pimpinelli *et al.*, 1993, 1994):

$$i\omega_k = -2D_S\Gamma|k|^3, \tag{2.78}$$

where $D_S = D\Omega c_{\rm eq}^0$. Experimental evidence of the diffusive regime with $i\omega_k \sim k^3$ has been reported recently by means of low energy electron microscope diffraction (Ondrejcek *et al.*, 2005, 2006). The step width can be calculated from Eq. (2.56) with $n=3$ (Bartelt *et al.*, 1994),

$$w^2(t) = G(2t)/2 = (k_BT/\pi\tilde{\gamma})\Gamma(\tfrac{2}{3})(4D_S\Gamma t)^{1/3}. \tag{2.79}$$

2. Step train

We now consider a step train where the steps are close together with an average separation ℓ. We have focused on two situations where the dynamics differ qualitatively from the isolated step situation.

a. Instantaneous kinetics

Steps interact via the diffusion field of adatoms. If the local equilibrium assumption holds ($\nu_+ = \nu_- = \infty$), modulation of the mth step in the form $\zeta_m(x,t) = \zeta_{k\phi}(t)\exp[i(kx + m\phi)]$ leads to the concentration variation between the mth and $(m+1)$th steps:

$$\begin{aligned} c(x,y,t) - c_{\rm eq}^0 = c_{\rm eq}^0\Gamma k^2\zeta_{k\phi}(t)\frac{e^{i(kx+m\phi)}}{\sinh k\ell} \\ \times \{\sinh k[(m+1)\ell - z] \\ - e^{i\phi}\sinh k(m\ell - z)\}. \end{aligned} \tag{2.80}$$

Details of the calculation may be found in Pimpinelli *et al.* (1994). The conservation law [Eq. (2.74)] determines the relaxation rate (Pimpinelli *et al.*, 1993, 1994),

$$i\omega_{k\phi} = -2D_S\Gamma k^3(\cosh k\ell - \cos\phi)/\sinh k\ell. \tag{2.81}$$

The rate depends explicitly on the phase ϕ because a step can incorporate adatoms emitted from another step. After a long time when the long-wavelength mode ($k\ell \ll 1$) dominates the dynamics, those modes with phases $\pi/2 \geq \phi \geq 3\pi/2$ give the dominant contribution to the ϕ integration (Ihle *et al.*, 1998). This means we cannot use Eq. (2.56) (based on the fact that the phase shift is irrelevant at a sufficiently short time), and careful calculation yields the result (Pimpinelli *et al.*, 1993; Ihle *et al.*, 1998)

$$w^2(t) = G(2t)/2 \approx \frac{k_BT}{\pi\tilde{\gamma}}\Gamma\left(\frac{1}{2}\right)\frac{4}{\pi}\left(\frac{8D_S\Gamma}{\ell}t\right)^{1/2}. \tag{2.82}$$

b. Ehrlich-Schwoebel effect

So far we have not explained that adatoms can be incorporated in the step from the upper and lower terraces either symmetrically ($\nu_+ = \nu_-$) or asymmetrically ($\nu_+ \neq \nu_-$). For certain materials and temperature conditions asymmetry is observed in ν_+ and ν_-. When an adatom diffusing on the upper terrace jumps over the step, it has to pass a configuration where an adatom finds fewer substrate atom neighbors. Jumping over the step therefore requires high activation energy W_s (see Fig. 10), and incorporation into the step from the upper terrace is hampered, leading to a lower kinetic coefficient on the upper side of the step $\nu_- < \nu_+$ (Schwoebel and Shipley, 1966; Schwoebel, 1969). As an extreme limit, we consider the one-sided model where mass exchange between a step and the upper terrace is forbidden ($\nu_- = 0$). For mathematical simplicity, we also assume infinitely fast kinetics from the lower terrace ($\nu_+ = \infty$) such that local equilibrium is reached: $c_+ = c_{\rm eq}$. The concentration between the mth and $(m+1)$th steps is thus obtained by

$$\begin{aligned} c(x,y,t) = c_{\rm eq}^0\Bigg[1 + \Gamma k^2\zeta_{k\phi}(t) \\ \times e^{i(kx+m\phi)}\frac{\cosh k[(m+1)\ell - z]}{\cosh k\ell}\Bigg]. \end{aligned} \tag{2.83}$$

Details of the calculation can be found in Pimpinelli *et al.* (1994). The relaxation rate (Bales and Zangwill, 1990; Pimpinelli *et al.*, 1993, 1994) is

$$i\omega_{k\phi} = -D_S\Gamma k^3 \tanh k\ell, \tag{2.84}$$

which is independent of the phase ϕ of a step train. This is a direct and obvious consequence of the one-sided model. It does not matter how the neighboring steps move if one is only interested in leading order since adjacent terraces ignore each other because there is no terrace mass exchange (strong ES effect). The adatoms emitted from a step are reflected back by another step and can only be incorporated in the original step. Therefore the phase difference of neighboring steps only makes a second-order contribution to the step relaxation. In the long-wavelength limit $k\ell \ll 1$, the step width is calculated from Eq. (2.56) with $n=4$ (Pimpinelli *et al.*, 1993; Pierre-Louis and Misbah, 1996),

$$w^2(t) = G(2t)/2 \approx (k_B T/\pi\tilde{\gamma})\Gamma\left(\tfrac{3}{4}\right)(2\ell D_S \Gamma t)^{1/4}. \quad (2.85)$$

Since adatoms detached from the step are confined to the terrace in front and eventually recaptured by the original step, the step width w shows the same time dependence as that of the edge-diffusion process discussed in Sec. II.B.1.b, but the coefficient contains the terrace width information ℓ. Here the step mobility is

$$M = D_S \ell / k_B T \quad (2.86)$$

instead of Eq. (2.68) for the case of edge diffusion.

3. Desorption

We include the desorption process via a desorption time τ. The concentration then obeys Eq. (2.73) (recall that we consider here the case with $F=0$). Desorption means that the adatoms cannot diffuse on the substrate over a distance much longer than desorption length

$$x_s = (D\tau)^{1/2}. \quad (2.87)$$

This length scale therefore acts as a cutoff length in the diffusion field. The density fluctuation in Eq. (2.77) is then modified and the decay rate $|k|$ in the z direction is replaced by $\Lambda = (k^2 + x_s^{-2})^{1/2}$. The relaxation rate of an isolated step for a one-sided model with desorption is given by $i\omega_k = -D_S \Gamma k^2 \Lambda$. In a step train with an average terrace width ℓ, the diffusion field is shared by neighboring steps and the rate is reduced (Bales and Zangwill, 1990; Pimpinelli *et al.*, 1994), thus

$$i\omega_{k\phi} = -D_S \Gamma k^2 \Lambda \tanh \Lambda\ell \to -D_S \Gamma k^2 x_s^{-1} \tanh(\ell/x_s) \quad \text{for } k x_s \ll 1. \quad (2.88)$$

For an isolated step or $\ell \gg x_s$, Eq. (2.56) with $n=2$ gives

$$w^2(t) = G(2t)/2 \approx \frac{k_B T}{\pi\tilde{\gamma}}\Gamma\left(\frac{1}{2}\right)\left(\frac{2D_S\Gamma}{x_s}t\right)^{1/2}. \quad (2.89)$$

Inversely, for coupled steps on a vicinal surface, $\ell \ll x_s$ and

$$w^2(t) = G(2t)/2 \approx \frac{k_B T}{\pi\tilde{\gamma}}\Gamma\left(\frac{1}{2}\right)\left(\frac{2D_S\Gamma\ell}{x_s^2}t\right)^{1/2}. \quad (2.90)$$

In both cases, the step width shows the same time dependence as the kinetics-controlled relaxation (2.65), but here the exchange of adatoms with the ambient vapor phase governs the relaxation.

4. Crossover behavior

Previously we considered the elementary kinetic processes separately to clarify different time dependences of the step width w. Actually, for a given system, all these effects coexist and complicate the time evolution of w. The most general expression of $i\omega_{k\phi}$ is given by (Ihle *et al.*, 1998)

$$i\omega_{k\phi} = -b\Lambda(k^2 + \ell_{\text{eff}}^{-2}) \times \left[\frac{2(\text{ch} - \cos\phi) + \Lambda(d_+ + d_-)\text{sh}}{(d_+ + d_-)\Lambda\,\text{ch} + (1 + d_+ d_- \Lambda^2)\text{sh}} + \ell_\parallel \frac{k^2}{\Lambda}\right], \quad (2.91)$$

where $b = D_S\Gamma$ and new characteristic lengths are kinetic attachment lengths $d_\pm = D/\nu_\pm$, $\ell_\parallel = aD_L/D_S$, $\ell_c = \sqrt{\tilde{\gamma}/2U''(\ell)}$, $\ell_{\text{eff}} = \ell_c(1-\cos\phi)^{-1/2}$, and abbreviated notations $\text{sh} = \sinh(\Lambda\ell)$ and $\text{ch} = \cosh(\Lambda\ell)$.

When the Schwoebel effect is weak and the length scales are well separated as for $\ell_\parallel, d_+, d_- \ll \ell \ll \ell_c \ll x_s$, we can introduce characteristic time scales such as $t_1 = \max(\ell_\parallel d_\pm^2/b, \ell_\parallel^3/b)$, $t_2 = \max(d_\pm^3/b, \ell_\parallel^3/b)$, $t_3 = \ell^3/b$, and $t_4 = \ell\ell_c^2/b$. These time scales are well separated as $t_1 \ll t_2 \ll t_3 \ll t_4$, and the width behaves as (Ihle *et al.*, 1998)

$$w^2(t) = G(2t)/2 = k_B T/\pi\tilde{\gamma} \times \begin{cases} \Gamma(\frac{3}{4})(2b\ell_\parallel)^{1/4} t^{1/4} & \text{for } t \ll t_1 \\ \Gamma(\frac{1}{2})\{2b(1/d_+ + 1/d_-)\}^{1/2} t^{1/2} & \text{for } t_1 \ll t \ll t_2 \\ \Gamma(\frac{2}{3})(4b)^{1/3} t^{1/3} & \text{for } t_2 \ll t \ll t_3 \\ \Gamma(\frac{1}{2})\frac{4}{\pi}[2b/(\ell + d_+ + d_-)]^{1/2} t^{1/2} & \text{for } t_3 \ll t \ll t_4 \\ \text{no power law} & \text{for } t_4 \ll t. \end{cases} \quad (2.92)$$

Initially, edge diffusion governs step deformation, followed by attachment-detachment kinetics and terrace diffusion. Up to time t_3, the step fluctuation is small and each step behaves independently. After t_3, the steps sense their neighbors (as signaled by the presence of the interstep distance ℓ). After t_4 when the elastic effect becomes dominant, the step width ceases to exhibit a power-law behavior. Actually, in this regime, the evolution is logarithmic over time before saturation (full equilibration) is reached (Saito, 1999).

For a one-sided model with a strong ES effect ($d_- = \infty$), t_1 and t_2 are determined by d_+ and $\ell_\parallel$. Furthermore, new time scales $t_5 = \min(x_s^4/b\ell, \ell_c^4/b\ell)$ and $t_6 = \min(x_s^2\ell_c^2/b\ell, \ell_c^4/b\ell)$ are introduced. When the length scales are well separated as $\ell_\parallel, d_+ \ll \ell \ll x_s, \ell_c$, the time scales are also well separated as $t_1 \ll t_2 \ll t_3 \ll t_5 \ll t_6$, and the step width increases, thus

$$w^2(t) = G(2t)/2 = k_B T/\pi\tilde{\gamma} \times \begin{cases} \Gamma(\frac{3}{4})(2b\ell_\parallel)^{1/4} t^{1/4} & \text{for } t \ll t_1 \\ \Gamma(\frac{1}{2})(2b/d_+)^{1/2} t^{1/2} & \text{for } t_1 \ll t \ll t_2 \\ \Gamma(\frac{2}{3})(2b)^{1/3} t^{1/3} & \text{for } t_2 \ll t \ll t_3 \\ \Gamma(\frac{3}{4})(2b\ell)^{1/4} t^{1/4} & \text{for } t_3 \ll t \ll t_5 \\ \Gamma(\frac{1}{2})(2b\ell/x_s^2)^{1/2} t^{1/2} & \text{for } t_5 \ll t \ll t_6 \\ \text{no power law} & \text{for } t_6 \ll t. \end{cases} \quad (2.93)$$

Up to time t_3, the step width behaves essentially as before since the step is isolated from the others. After t_3,

the Schwoebel effect leads to effective edge diffusion until the adatom desorption breaks the conservation and yields effective kinetics-controlled behavior. Eventually, the elastic effect induces non-power-law behavior in the time dependence of the step width. Such scaling behavior [Eqs. (2.92) and (2.93)] and crossover in the intermediate time scales are observed in the numerical integration of Eq. (2.72) using the most general $i\omega_{k\phi}$ of Eq. (2.91) (Ihle *et al.*, 1998).

5. Low-temperature step relaxation and island diffusion

On several fcc metal surfaces, such as Cu(100) at room temperature, mass transport is dominated by diffusion along the steps (Giesen, 2001). Within this limit, the steps are described by an equation having a conservation form [Eq. (2.69)] (Mullins, 1957). As seen in Sec. II.B.1.b the step autocorrelation function must scale as $t^{1/4}$ in this situation. Nevertheless, low-temperature deviations toward the $t^{1/2}$ law were observed in temporal correlations of the steps on Cu(100) vicinal surfaces (Giesen, 2001). Such deviations were also observed for the diffusion of single-layer islands. Assume that an atom diffuses along a rough step of atomic distance a on a time scale t_m. If an island has a radius R, the resulting displacement of the center of mass of the island is $b_{\mathrm{CM}} \sim a^3/R^2$. At equilibrium, there is a concentration c_s of mobile atoms along the step; their total number is $N \sim Rc_s$. Assuming that the motion of these atoms is uncorrelated, the diffusion constant of the cluster reads

$$D_c \sim N(b_{\mathrm{CM}}^2/t_m), \tag{2.94}$$

so that $D_c \sim 1/R^3$. A model based on Eq. (2.69) and augmented with Langevin forces to account for fluctuations confirms this result (Khare *et al.*, 1995; Khare and Einstein, 1996). However, observation of small islands on Cu(100) (Pai *et al.*, 1997), in agreement with kinetic Monte Carlo simulations (Bogicevic *et al.*, 1998; Combe and Larralde, 2000), reveals that $D_c \sim R^{-\alpha}$, where α varies from $\alpha=3$ for large islands and high temperatures to $\alpha=1$ for small islands and low temperatures.

The observed deviations occur at low temperatures where the distance between thermal kinks L_k is relatively large. [Using the experimental results of Giesen (2001) on Cu(100), we find $L_k \sim 10^2$ at room temperature.] When the typical distance between thermal kinks is larger than the island size, we do not expect Eq. (2.69) to be valid, and the time scale for the motion of a mobile atom along the step is essentially limited by the probability of thermal kink presence. Therefore $t_m \sim L_k/R$. The number of mobile atoms along the step is now $N \sim 1$, and the distance along which the atom moves is approximately the size of the island, leading to a displacement of the center of mass $b_{\mathrm{CM}} \sim a/R$. From Eq. (2.94), we now find that $D_c \sim 1/R$. Using Markov chains describing atomic motion, this result has been analyzed by Combe and Larralde (2000).

Since the low-temperature deviations come from jumps of atoms between kinks that are far apart, it may be possible to incorporate this regime into a continuum model by introducing an additional mobile atom concentration field along the step, as shown in Fig. 12. Starting from a phenomenological free energy, a variational derivation (Pierre-Louis, 2001) leads to the following dynamical model for step position ζ and concentration c:

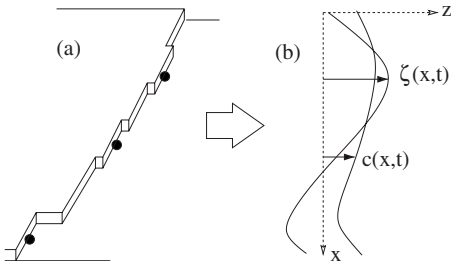

FIG. 12. Low temperature step relaxation. (a) Atomistic picture is coarse-grained to (b) a model with a continuous step profile and a continuous concentration of atoms along the step.

$$\Omega^{-1}\partial_t \zeta = \nu(c - c_{\mathrm{eq}}) + \eta, \tag{2.95}$$

$$\partial_t c = \partial_x[B\partial_x c - q] - \nu(c - c_{\mathrm{eq}}) - \eta, \tag{2.96}$$

where $c_{\mathrm{eq}} = c_{\mathrm{eq}}^0(1+\Gamma\kappa)$ and the correlations of the Langevin forces, η and q, are found within a local thermodynamic equilibrium approximation:

$$\begin{aligned} \langle \eta(x,t)\eta(x',t')\rangle &= 2\nu c(x,t)\delta(x-x')\delta(t-t'), \\ \langle q(x,t)q(x',t')\rangle &= 2Bc(x,t)\delta(x-x')\delta(t-t'). \end{aligned} \tag{2.97}$$

The kinetic coefficient ν is the relaxation frequency for the concentration. It is therefore simply the inverse of the time for one adatom to jump from one kink to another, separated by a distance L_k:

$$\nu = D_s/L_k(L_k + d_{k+} + d_{k-}), \tag{2.98}$$

where we have defined the diffusion constant of mobile edge atoms between kinks D_s and the kink kinetic attachment lengths $d_{k\pm} = a[\exp(E_\pm/k_BT) - 1]$, with $E_\pm$ the additional energy barriers (with respect to diffusion) for atoms to stick to a kink from both sides. Furthermore, the macroscopic diffusion constant B results from the global diffusion process with jumps from kink to kink, so that

$$B \approx \nu L_k^2. \tag{2.99}$$

This model predicts the low-temperature deviations for long observation time scales when long-wavelength fluctuations $\lambda \gg L_k$ dominate and

$$G_{\mathrm{long}}(t) = [a^2\Gamma(3/4)/\pi](b_0^2)^{3/4}(Bc_{\mathrm{eq}}^0)^{1/4}t^{1/4}, \tag{2.100}$$

where $b_0^2 = ak_BT/\tilde{\gamma}$ is step diffusivity. This expression corresponds to that given by Bartelt, Goldberg, *et al.* (1992) and Bartelt *et al.* (1993) starting from the Mullins model [Eq. (2.69)], with $D_L = aBc_{\mathrm{eq}}^0$ as expected from Mullins (1957, 1959). Note that this also provides an expression for the diffusion constant in the long scale limit (Pierre-Louis, 2001): $D_L = ac_{\mathrm{eq}}^0 D_s/[1+(d_{k+}+d_{k-})N_k]$, where $N_k = 1/L_k$ is the kink density. This expression for

D_L was confirmed by Monte Carlo simulations (Kallunki *et al.*, 2002). For short observation time scales, only short wavelengths ($\lambda \ll L_k$) contribute to G, and

$$G_{\text{short}}(t) = (a^{3/2}/\sqrt{\pi})(\nu c_{\text{eq}}^0 b_0^2)^{1/2} t^{1/2}. \tag{2.101}$$

Using Eq. (2.98) and $b_0^2 \sim N_k$, valid at low T, the crossover between the two regimes is found to correspond to $G(t) \sim a^2$. This result was found by Giesen-Seibert *et al.* (1995) by means of a discrete random kink model and MC simulations. From $G(t^*) \sim a^2$, the crossover time between the two regimes is found to be

$$t^* \sim (N_k^3 a^2 B c_{\text{eq}}^0)^{-1}. \tag{2.102}$$

The numerical values for Cu(11n) vicinal surfaces given by Giesen-Seibert *et al.* (1995) give $t^* \sim 10^{-19} \exp(14\,870/T)$ s, where T is in Kelvin. With observation times $t^* \sim 1$ s (Giesen-Seibert *et al.*, 1995), the crossover is found for $T \approx 340$ K, in quantitative agreement with experiments (Giesen-Seibert *et al.*, 1995). Also, in an isotropic circular model, correct scaling of the diffusion constant of a two-dimensional island with a radius R_0 is found:

$$D_c = \frac{\langle \mathbf{r}_{\text{CM}}^2(t) \rangle}{4t} = \frac{a^4 c_{\text{eq}}^0}{\pi R_0} \frac{1}{R_0^2/B + 1/\nu}, \tag{2.103}$$

where $\mathbf{r}_{\text{CM}}$ indicates the position of the center of mass of the cluster. However, such a simple model does not explain the sintering of two-dimensional islands studied by Liu and Evans (2002), which involves far-from-equilibrium concave shapes. Finally, similar deviations from the macroscopic theories occur in the rate of detachment of atoms from 2D clusters, as shown by Shao *et al.* (1996).

C. Kinematic bunching and introduction to instabilities

We have so far dealt with systems which are globally at equilibrium. When the surface is driven out of equilibrium, there are two major instabilities: (i) step meandering and (ii) step bunching. We may also have coexistence between bunching and meandering. In addition, bunching may cause meandering (despite the fact the step would be stable with respect to meandering if the interstep distance were to be kept constant) (Kandel and Weeks, 1995). The reverse situation is also possible: meandering may cause steps to bunch. More generally, dynamics may be quite complex, and we approach these notions in a progressive manner. Bunching can also take place not as a result of an instability but rather as a kinematic wave. Bunching and meandering occurring as a result of instabilities are the subject of Secs. III and IV. Here we present the traditional view of step bunching in terms of a shock in a kinematic wave (Frank, 1958; Bennema and Gilmer, 1973). It must be emphasized that there is a clear distinction between a shock wave and a morphological instability.

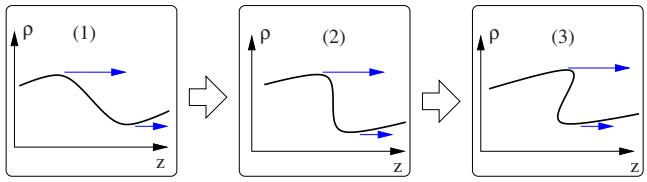

FIG. 13. (Color online) Formation of a shock when the velocity Q' increases with the density ρ, i.e., $Q'' > 0$. The plots (1)–(3) are in chronological order.

1. Shock waves

We start with a description of shocks in kinematic wave theory and their relation to step bunching. Since the total number of steps on a vicinal surface is conserved, the local step density ρ evolves within the continuum limit,

$$\partial_t \rho = -\partial_z Q = -Q'(\rho) \partial_z \rho. \tag{2.104}$$

In kinematic wave theory, the flux (say, step flux) Q is assumed to depend only on the local density ρ. Here we can view $Q' = dQ/d\rho$ as the local wave speed [local in the sense that it depends on the actual density $\rho(z,t)$]. Since Q is a flux, we can write it in the usual form $Q = V\rho$, with the step velocity V, which generally depends on ρ. Supposing first that V is constant, $\partial_t \rho = -V \partial_z \rho$. This equation has the general solution $\rho = f(z - Vt)$, meaning that if we start with an initial form of the wave packet, this will move in a shape-preserving manner. The situation is quite different if V is not constant or if Q is a nonlinear function of ρ. In these cases, local speeds differ at different densities, and the wave packet will be destroyed over time, as shown in Fig. 13. Shock fronts or shock waves will occur in a way which is similar to the breaking of waves on the seashore. Many systems are known to exhibit shocks, including traffic flow, flood waves, glaciers, chemical exchange processes, and sedimentation in rivers [see Whitham (1976) for examples and applications to many real systems].

In the case of vicinal surfaces, these shocks lead to rapid variations in step density. If $Q'' > 0$, step bunches are "convex," and if $Q'' < 0$, step bunches are "concave," as explained in Fig. 14. This figure shows that since a shock corresponds to the location of an abrupt variation of the density (say, the passage from high density to low density on a very short length scale), the shocks are not

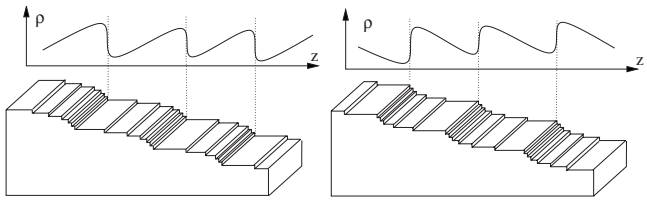

FIG. 14. Schematic view of the evolution of the bunches. Top panel: $Q'' > 0$, the bunches are convex. Bottom panel: $Q'' < 0$, the bunches are concave.

the actual bunches, but correspond to their edges. By conserving the number of steps through a shock, the shock velocity reads

$$V_{\text{shock}} = (Q_+ - Q_-)/(\rho_+ - \rho_-), \tag{2.105}$$

where the indices ± refer to quantities evaluated immediately to the left or right of the shock.

In a simple model such that the step velocity depends linearly on step density, $V_{\text{step}}=V_0(1+k_0\rho)$, the flux of steps is $Q=\rho V_{\text{step}}$, and $Q''=2k_0V_0$. We find from Eq. (2.105) that

$$V_{\text{shock}} = V_0[1 + k_0(\rho_+ + \rho_-)]. \tag{2.106}$$

Therefore, during growth, sublimation, or etching, we expect the formation of shocks that move faster than the average step motion $\sim V_0[1+k_0(\rho_++\rho_-)/2]$ if $k_0>0$ and slower if $k_0<0$.

In order to analyze the density profile in the shock region, we include the flux contributions due to a spatial variation of density. Thus, we cease to assume that Q depends on ρ only. In a long-wavelength expansion, the first expected term is $\partial_z\rho$. Including linear terms, as well as the first nonlinear term, in ρ, together with the contribution from $\partial_z\rho$, we obtain (an expansion around a given density ρ_0) $-Q\approx -Q_0+\delta\rho Q_1+\delta\rho^2Q_2/2+D\partial_z\delta\rho$, where $\delta\rho=\rho-\rho_0$ and Q_i's are constants. Using Eq. (2.104), we find the Burgers equation (Burgers, 1974)

$$\partial_t\delta\rho = D\partial_{zz}\delta\rho + Q_2\delta\rho\partial_z\delta\rho, \tag{2.107}$$

where D represents the analog of viscosity (and is thus assumed to be positive). The term containing Q_1 has been absorbed in the time derivative by a Galilean transformation. The Burgers equation is known to lead to shocks which coalesce due to the fact that shocks of different sizes move with different velocities. The average number of shocks per unit length is known to decrease with time (Burgers, 1974) $t^{-2/3}$. It can also be demonstrated (Burgers, 1974) that the density profile gets smoother over time, namely, that $\langle\delta\rho^2\rangle^{1/2}\sim t^{-1/3}$. Bunching is thus only transient and asymptotically vicinal surfaces should recover smoothness according to kinematic wave theory. Note that upon adding a noise term to the Burgers equation, we obtain the KPZ equation for ζ, having set $\partial_z\zeta=\delta\rho$.

Apart from the viscositylike effect, we may have the first contribution coming from higher-order derivatives [instead of a second derivative as in Eq. (2.107)], as in the study of gravity waves on the surface of a liquid. The third derivative[5] first appears in the gravity-wave equation (Whitham, 1976), and the density equation takes the form

$$\partial_t\delta\rho = -\partial_{zzz}\delta\rho + \delta\rho\partial_z\delta\rho, \tag{2.108}$$

where we have set $Q_2=1$ (this is always possible by appropriate rescaling). The sign in front of ∂_{zzz} is irrelevant since it can be changed by the transformation $(z,\delta\rho)\rightarrow(-z,-\delta\rho)$. This is known as the Korteweg–de Vries (KdV) equation (Whitham, 1976). It arises, in particular, in the study of gravity waves on shallow water. The KdV equation admits a steady-state solution in the form of a soliton moving steadily in a shape-preserving manner. More precisely, a solution of the KdV equation exists which reads $\delta\rho(z,t)=U(z-ct)$, where c is the soliton speed and U is given by (Whitham, 1976)

$$U = -3c\,\text{sech}^2[\sqrt{c}(z-ct)/2]. \tag{2.109}$$

This is a family of solutions parametrized by the soliton speed c. This means that this solution exists with an arbitrary speed. Note that the maximum amplitude is $-3c$, so the deeper the trough, the faster the soliton moves and the narrower it is. We see later that the KdV equation arises naturally, within certain limits, when studying step bunching under microscopic considerations.

2. Growth

It may be noticed that if the step velocity is taken to be proportional to the local terrace width, as expected during growth with a deposition flux F but without adatom desorption, then $Q=\Omega F$ (and $V_{\text{step}}=\Omega F/\rho$). Since $Q=\Omega F$ does not depend on density, no kinematic waves in the form of shocks are to be expected. We see later that, in fact, the bunching formation in this case follows from an intrinsic instability, which will be indicated by a negative constant D in Eq. (2.107). This differs significantly from shocks following from the Burgers equation. However, it does not rule out the possibility that kinematic bunching may occur. Examples may be encountered under etching.

3. Etching

Recent studies have pointed out that step bunching during etching of Si(111) surfaces in KOH solutions is of kinematic origin (Garcia *et al.*, 2004). An STM image of the bunches is shown in Fig. 15. The nonlinear dependence on ρ of the etching rate was checked experimentally. They showed that $k_0>0$ [see Eq. (2.105)]. Even with $Q''=2k_0V_0$ being negative since $V_0<0$, bunches observed in experiments and the results of kinetic Monte Carlo simulations are neither concave nor convex, as expected from kinematic wave theory. This dilemma needs further investigation.

III. STEP MEANDERING

Instabilities are ubiquitous under nonequilibrium conditions. Here we analyze the morphological instabilities and the underlying mechanisms which trigger them.

A typical out-of-equilibrium situation is one where the surface is exposed to an external flux F with desorption time τ as shown in Fig. 10. If the flux exceeds the equilibrium value $F_{\text{eq}}=c_{\text{eq}}^0/\tau$ for which adsorption exactly compensates desorption from the terraces, the crystal will grow. This is a prototype of a nonequilibrium

[5]In fact, at the scale of gravity waves, viscous effects together with surface tension play a minor role.

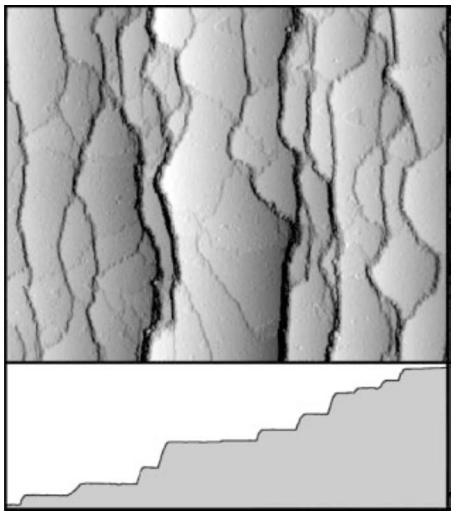

FIG. 15. STM image and cross section of vicinal Si(111) surface etched for 5 min at room temperature with KOH. From Garcia *et al.*, 2004.

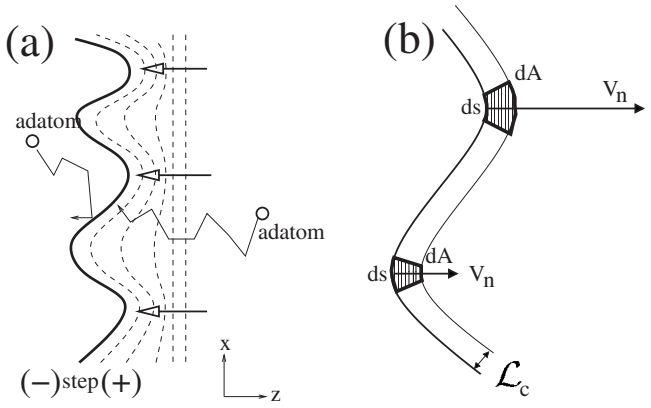

FIG. 16. Two schematic descriptions of the meandering instability mechanism in the presence of an Ehrlich-Schwoebel effect. (a) Point effect. The higher density of isoconcentration lines at the tip of protuberances indicates a larger attachment mass flux, leading to faster growth, thus amplifying the perturbation. (b) A strip of width $\mathcal{L}_c$ feeds the step. The area feeding a small step element of length ds depends on the local curvature.

problem where the surface grows by particle addition. We see that a vicinal surface suffers morphological instabilities caused by adatom diffusion. Two types of instabilities are generically encountered: *step meandering*, which is treated here, and *step bunching*, which is treated in the next section.

Meandering is the one-dimensional analog of the Mullins-Sekerka (1964) instability and was first studied in the linear regime by Bales and Zangwill (1990). Once the instability threshold is reached, nonlinear terms must be taken into account. In the form of nonlinear equations, we encounter two types of nonlinear regimes: the standard regime where an expansion in terms of leading powers of the nonlinearity is legitimate and a nonstandard regime where the validity of the expansion breaks down.

A. The strip model

During growth, steps are unstable with respect to meandering in the presence of front-back asymmetry at the step. This instability is known as the Bales-Zangwill instability (Bales and Zangwill, 1990). One common idea which is often evoked is the Erhlich-Schwoebel barrier: as discussed in Sec. II.B.2.b, an atom usually attaches more easily when coming from the lower terrace than from the upper one. Here we present a simple model based on the strip-mediated growth [Fig. 16(b)] scenario and on the equilibrium relaxation laws of Sec. II.B. For simplicity, we consider the one-sided attachment model. Moreover, we assume isotropic step properties. A cutoff length $\mathcal{L}_c$ related to diffusion on terraces accounts either for the desorption length x_s, defined in Eq. (2.87), or for the presence of other steps at a separation distance ℓ. The instability is a consequence of the increase of the strip area in positively curved regions, leading to a local increase of the growth rate. A protuberance is amplified, hence instability sets in.

We quantify the argument that leads to such instability, which is driven by mass transport in a strip of width $\mathcal{L}_c$. If all atoms landing on this strip attach to the step, the attachment rate to a straight step per unit length is $F\mathcal{L}_c$. Due to a step meander, the area feeding a step element of length ds varies. This can be shown by a simple calculation. Consider a strip of width $\mathcal{L}_c$ around a circle of radius R. The area of the strip is $A=\pi(R+\mathcal{L}_c)^2-\pi R^2=\pi\mathcal{L}_c(2R+\mathcal{L}_c)$. If $L=2\pi R$ is the length of the circle, $A/L=\mathcal{L}_c(1+\mathcal{L}_c/2R)$. This relation also holds for a fraction of the circle with a small angle $d\theta$. The length of a fraction of the circle is $dL=Ld\theta/2\pi$, and the corresponding area $dA=Ad\theta/2\pi$ obeys $dA/dL=\mathcal{L}_c(1+\mathcal{L}_c/2R)$. Since the step is always locally tangent to a circle of radius $R=1/\kappa$, where κ is the local curvature, the following results:

$$dA \approx ds\mathcal{L}_c(1+\kappa\mathcal{L}_c/2), \tag{3.1}$$

where κ can be positive or negative. The number of atoms attaching to the step element of length ds is then $FdA=V_n^A ds/\Omega$, where V_n^A is the contribution to the step normal velocity due to atom attachment. We therefore find

$$V_n^A=\Omega F\mathcal{L}_c(1+\kappa\mathcal{L}_c/2). \tag{3.2}$$

From the Gibbs-Thomson relation (2.62), the equilibrium concentration in the vicinity of a step is $c_{\rm eq}=c_{\rm eq}^0(1+\Gamma\kappa)$. We assume that atoms detach from the step to the strip, where they have a desorption rate of $1/\tau$. The number of atoms detaching from the step element ds per unit time is then $V_n^D ds/\Omega=-c_{\rm eq}dA/\tau$. Hence,

$$V_n^D=-\Omega\mathcal{L}_c(c_{\rm eq}^0/\tau)(1+\Gamma\kappa)(1+\kappa\mathcal{L}_c/2). \tag{3.3}$$

Previously we saw that edge diffusion is more efficient than attachment-detachment kinetics with regard to short-wavelength mode stabilization. We therefore add a

term related to diffusion along the strip, which is formally analogous to edge diffusion and which will stabilize short-wavelength modes. From Eq. (2.69), this strip-diffusion contribution reads

$$V_n^{\mathrm{SD}} = a_{\mathrm{eff}} D_{L\ \mathrm{eff}} \Gamma \partial_{ss} \kappa. \tag{3.4}$$

It is then natural to assume that $a_{\mathrm{eff}} = \mathcal{L}_c$ and $D_{L\ \mathrm{eff}} = D\Omega c_{\mathrm{eq}}^0$ (only mobile atoms whose fraction is given by Ωc_{eq}^0 contribute). Finally, adding the three contributions $V_n = V_n^A + V_n^D + V_n^{\mathrm{SD}}$, we find

$$V_n = \Omega \mathcal{L}_c [F - F_{\mathrm{eq}}(1 + \Gamma\kappa)](1 + \kappa\mathcal{L}_c/2) + \mathcal{L}_c D \Omega c_{\mathrm{eq}}^0 \Gamma \partial_{ss} \kappa \tag{3.5}$$

with the equilibrium flux $F_{\mathrm{eq}} = c_{\mathrm{eq}}^0/\tau$.

The velocity of a straight step ($\kappa = 0$) is then

$$\bar{V} = \Omega \mathcal{L}_c (F - F_{\mathrm{eq}}). \tag{3.6}$$

Linearizing Eq. (3.5) for small perturbations $\zeta(x,t)$ around the moving straight step yields

$$\partial_t \zeta = -\tfrac{1}{2}\Omega(F - F_c)\mathcal{L}_c^2 \partial_{xx}\zeta - \mathcal{L}_c D \Omega c_{\mathrm{eq}}^0 \Gamma \partial_{xxxx}\zeta, \tag{3.7}$$

where the critical flux is defined as

$$F_c = F_{\mathrm{eq}}[1 + 2\Gamma/\mathcal{L}_c]. \tag{3.8}$$

The Fourier transform of this relation (following the definition in Sec. II.B) gives the growth rate of the perturbations as a function of the wave vector k. We seek perturbations in the form $e^{i\omega t}$. Instability is thus indicated by a positive real part of $i\omega$. We find here

$$i\omega = \tfrac{1}{2}\Omega(F - F_c)\mathcal{L}_c^2 k^2 - \mathcal{L}_c D \Omega c_{\mathrm{eq}}^0 \Gamma k^4. \tag{3.9}$$

Although the geometrical strip model is not exact, it incorporates the main features of the instability: (i) the instability occurs when the incoming flux exceeds a critical value $F > F_c$; (ii) sufficiently small-wavelength modes are stable, and (iii) the most unstable wavelength k_m^{-1} with the largest $i\omega$ diverges as $(F - F_c)^{-1/2}$ when F becomes closer to the instability threshold F_c. The dispersion relation shows that the typical time for the appearance of the instability is $\sim(F - F_c)^{-2}$. Since the instability corresponds to long-wavelength modes, our long-wavelength assumption—on which the geometrical model is based—is self-consistent in the vicinity of the instability threshold.[6]

In the following sections we see that Eqs. (3.8) and (3.9) are in agreement with the stability analysis of the full step model at long wavelength up to some numerical prefactors. More specifically, provided the length scales are well separated, the threshold (3.8) agrees with the exact result, with the cutoff length written as[7]

$$\mathcal{L}_c = \min[x_s, \ell], \tag{3.10}$$

where $\mathcal{L}_c$ is the shortest cutoff length. The dispersion relation (3.9) with $\mathcal{L}_c = x_s$ corresponds to that obtained for a one-sided isolated step with strong desorption. The dispersion with $\mathcal{L}_c = \ell$ is obtained for a train of steps with weak desorption or $\tau \to \infty$. In this case $F_{\mathrm{eq}} = c_{\mathrm{eq}}/\tau \to 0$ and thus $F_c \to 0$: the step is always unstable during growth. While the weak and strong desorption limits are quite similar in the linear regime (regarding the form [Eq. (3.9)] of the dispersion relation), drastic differences will be encountered in the nonlinear regime.

B. Nonlinear evolution with desorption

1. An isolated step: The Kuramoto-Sivashinsky equation

In order to deal with the case of desorption, Eq. (2.73), which includes both deposition and desorption, must be solved. First consider an isolated step in the one-sided limit (only atoms coming from the lower terrace may be incorporated onto the step). At a large enough distance ahead of the step, the adatom concentration is given by the number of atoms deposited F (per unit surface and unit time) divided by the desorption frequency τ^{-1},

$$c(z = \infty) = \tau F. \tag{3.11}$$

At the step if there is no barrier for attachment and if the temperature is high enough so that kink density is sufficiently large, then the concentration c_+ in the immediate vicinity of the step is

$$c_{\mathrm{eq}}^0 \equiv \tau F_{\mathrm{eq}}. \tag{3.12}$$

In reality, the equilibrium concentration at the step is modified by curvature effects (the Gibbs-Thomson condition) and Eq. (3.12) must, according to Eq. (2.62), be written as

$$c_+ = c_{\mathrm{eq}} = \tau F_{\mathrm{eq}}(1 + \Gamma\kappa), \tag{3.13}$$

where κ is the step curvature defined by Eq. (2.59). We define curvature as being positive if the step profile is convex (i.e., it is positive for a sphere). Note that the line tension effect Γ has a dimension of a length (see Sec. II.B.1.a where Γ was first introduced). Therefore, the curvature effect is important only for protuberances such that the step curvature is approximately or larger than $1/\Gamma$.

[6] Hence, it is justified to neglect higher-order contributions $\sim\partial_{ss}\kappa$ coming from V_n^A and V_n^D which would provide terms $\sim k^4$. Indeed, these terms are proportional to $F - F_c$.

[7] A more general relation could be defined, which is valid for a finite Ehrlich-Schwoebel effect: $\mathcal{L}_c = \min[x_s, \ell, d_-]$, where the kinetic attachment length $d_- = D/\nu_-$. The kinetic coefficient ν_- is defined in Sec. II.B and $\nu_+ \to \infty$. In the case $\mathcal{L}_c = d_-$, the expression of the stability threshold given by Eq. (3.8) is valid, but the form of the dispersion relation (3.9) changes.

The normal velocity of the step is proportional to the normal gradient of the concentration ahead of the step according to Eq. (2.74). Since attachment from the upper terrace is not allowed, this reduces to

$$V_n = \Omega D \partial_n c_+. \tag{3.14}$$

Below we consider the case of growth where $F > F_{\rm eq}$. We use a reference frame moving at the constant speed $\bar{V}$ of a straight step, so that the straight step is positioned at $z=0$. The quantity $\zeta(x,t)$ will designate the deviation of the profile from the straight step motion, so that $c_+ = c[z=\zeta(x,t)]$ in Eqs. (3.13) and (3.14).

For a straight step, the solution $c_0(z)$ of Eq. (2.73) for $z>0$ takes the form $c_0 = \tau F + B_0 e^{-z/x_s}$, which approaches $c_\infty = \tau F$ asymptotically. We have used condition (3.11) in this expression. Condition $c(z=0)=c_{\rm eq}^0$ for $\kappa=0$ implies $B_0 = \tau(F_{\rm eq}-F)$, and the use of Eq. (3.14) yields the velocity $\bar{V}$ of the straight step in the form of Eq. (3.6) with the cutoff length $\mathcal{L}_c$ replaced by a desorption length x_s.

Diffusion generally induces morphological instabilities in moving interfaces (Mullins and Sekerka, 1964). In the presence of desorption, adatoms may regain the atmosphere before reaching the step, and only the adatoms within desorption length x_s of the step matter to stability. Due to this spatial limitation, a straight step remains stable up to a critical flux F_c, beyond which the step becomes unstable. The linear stability analysis can be performed (Bena *et al.*, 1993). Since line tension is known to stabilize a straight step at short length scales, we consider step stability of only a long-wavelength modulation with a wave number k such that $kx_s \ll 1$. Close to the instability threshold, the result is (Bena *et al.*, 1993)

$$i\omega = \tfrac{1}{2}\Omega(F-F_c)x_s^2 k^2 - \tfrac{3}{4}\Omega F_{\rm eq}\Gamma x_s^3 k^4 \tag{3.15}$$

with F_c given by Eq. (3.8) and $\mathcal{L}_c = x_s$. The dispersion relation is similar to that of the strip model in Eq. (3.9). Strong desorption is taken to mean that desorption is significant on the length scales of interest (i.e., the desorption length x_s is short in comparison to the length scale of interest). This means here that $kx_s \ll 1$ and $x_s < \ell$ (the separation of steps in a train of steps). The first term in Eq. (3.15) is only positive if the flux is greater than the critical value F_c. Sufficiently close to the critical point $F \approx F_c$, the amplification rate $i\omega$ is positive for small wave numbers below a critical value k_c, obtained by setting $i\omega=0$. It scales as

$$x_s k_c \simeq \sqrt{(F-F_c)/(F_c-F_{\rm eq})}. \tag{3.16}$$

This means that sufficiently close to the instability threshold F_c only modes with small enough wave numbers will be active. Thus in real space we expect only the leading spatial derivatives to be important (this is also usually known as the "hydrodynamic limit"). By inverting back to real space, Eq. (3.15) yields the linear part of the temporal evolution of the profile

$$\partial_t \zeta = -a\partial_{xx}\zeta - b\partial_{xxxx}\zeta, \tag{3.17}$$

where $a = \frac{1}{2}\Omega(F-F_c)x_s^2$ and $b = \frac{3}{4}\Omega F_{\rm eq} x_s^3 \Gamma$.

We may now ask which nonlinear terms are permissible *a priori*. If we assume that the meander ζ is small, the largest nonlinearity is quadratic. For example, it may be tempting to introduce ζ^2, while, e.g., cubic terms such as ζ^3 would remain smaller. However, since step position is undetermined up to an additive constant, this nonlinearity is not allowed. Indeed, if the z coordinate is transformed to $z' = z + C$ where C is constant, then the new step position would be given by $\zeta' = \zeta + C$. The equation should remain invariant under such a transformation, which would not be the case if ζ^2 was present. Thus, only terms which contain derivatives with respect to x (and which respect the $x \to -x$ symmetry) are permitted. The simplest term of this sort is $(\partial_x \zeta)^2$. This term breaks another symmetry, $\zeta \to -\zeta$, but this is possible since we assume that atoms can attach predominantly from the lower terrace. Other nonlinearities [e.g., $(\partial_{xx}\zeta)^2$] would be *a priori* possible. However, as seen above, since the unstable modes have small wave vectors in the vicinity of the instability threshold, $(\partial_{xx}\zeta)^2$ is negligible in comparison to $(\partial_x \zeta)^2$ and is therefore disregarded. The above considerations are based on symmetries. A nonlinear analysis was performed starting from the Burton-Cabrera-Frank (BCF) model and led to the same conclusion. The resulting evolution equation is (Bena *et al.*, 1993)

$$\partial_t \zeta = -a\partial_{xx}\zeta - b\partial_{xxxx}\zeta + \bar{V}(\partial_x \zeta)^2/2. \tag{3.18}$$

Note that the coefficient of the nonlinear term is simply $\bar{V}/2$, half of the straight step velocity [see Eq. (3.6)]. There is another edifying way to extract the nonlinear term. Indeed, the step equation can be written, without restriction, as follows:

$$V_n = \bar{V} + J(\partial_x \zeta, \partial_{xx}\zeta, \dots). \tag{3.19}$$

J is a flux which is a function of the step deformation (actually only of its derivatives due to translational invariance along the step in the uniform configuration). $J=0$ if $\zeta=0$, so that V_n reduces to $\bar{V}$, the velocity of a straight step. The normal velocity V_n is related to $\partial_t \zeta$ (in the laboratory frame) by $V_n = (\bar{V} + \partial_t \zeta)/\sqrt{1+(\partial_x \zeta)^2}$. Inserting this into Eq. (3.19) and expanding for small ζ, we obtain the first nonlinear contribution

$$\partial_t \zeta = \bar{V}(\partial_x \zeta)^2/2 + J_{\rm lin} + \text{higher-order terms}. \tag{3.20}$$

We have kept only the leading linear term in J, denoted as $J_{\rm lin}$ (already determined in the linear regime). The first nonlinearity is thus $(\bar{V}/2)(\partial_x \zeta)^2$, and, by combining the linear order calculation and the above argument, the nonlinear evolution equation is fixed to leading order. We insist on the fact that the above is the leading nonlinearity. The truncation at leading order is valid, in principle, close enough to the instability threshold. We now introduce the following small parameter:

$$\epsilon = (F - F_c)/F_c. \tag{3.21}$$

The critical wave number k_c [Eq. (3.16)] scales as $\sqrt{\epsilon}x_s^{-1}$. This means that the pattern associated with step modulation varies slowly in comparison to the desorption length. In real space this means that it is only after a distance of $\sim x_s/\sqrt{\epsilon}$ that a noticeable variation takes place. It is customary to introduce a slow spatial scale X related to the original scale x by

$$X = x\sqrt{\epsilon}. \tag{3.22}$$

The advantage in adopting a slow variable lies in the fact that the small perturbative parameter ϵ is explicitly present in the equations. The dispersion relation (3.15) shows that for the range of wave numbers $\sqrt{\epsilon}$ the growth rate $i\omega$ scales as ϵ^2. We introduce a slow temporal variable T related to time t by

$$T = \epsilon^2 t. \tag{3.23}$$

This means that dynamics are slow close to the critical point (this is the usual so-called critical slowing down). The introduction of the slow variable T means that dynamics evolve on a scale of order 1 in this variable. Introducing the slow variables X and T and omitting the factors which do not depend on ϵ, Eq. (3.18) can be rewritten as

$$\epsilon^2 \partial_T \zeta = -\epsilon^2 \partial_{XX}\zeta - \epsilon^2 \partial_{XXXX}\zeta + \epsilon(\partial_X \zeta)^2. \tag{3.24}$$

The nonlinear term is therefore of the same order as the linear terms provided $\zeta \sim \epsilon$. Imposing this condition guarantees the uniformity of the ϵ expansion, where a leading nonlinearity counterbalances the linear terms. Introduction of

$$\zeta(x,t) = \epsilon Z(X,T), \tag{3.25}$$

meaning that Z is of order unity, means that the small parameter scales out from Eq. (3.24) and reduces to the form

$$\partial_T Z = -\partial_{XX}Z - \partial_{XXXX}Z + (\partial_X Z)^2. \tag{3.26}$$

This is a canonical form of the step evolution equation. It is described in detail by Bena *et al.* (1993) as an expansion in powers of ϵ of the concentration field and the step position. Note that a similar type of evolution equation can always be written in the form of Eq. (3.26) with all coefficients order unity. Indeed, if we had an equation like $\partial_T Z = -a\partial_{XX}Z - b\partial_{XXXX}Z + c(\partial_X Z)^2$, then upon transformations $X' = X\sqrt{a/b}$, $T' = a^2 T/b$, and $Z' = cZ/a$ would produce a universal form of Eq. (3.26) (an equation which is free of parameters).

Equation (3.18) is known as the Kuramoto-Sivashinsky (KS) equation (Kuramoto and Tsuzuki, 1976; Sivashinsky, 1977) [which seems to have appeared earlier in the literature (Nepomnyashchii, 1974)]. It often arises as a generic nonlinear equation in dissipative systems (Misbah and Valance, 1994). The nonlinear term in Eq. (3.18) only enters out of equilibrium. Indeed, this term precludes one from writing the equation as a functional derivative of some quantity, which is typical of nonequilibrium situations. If the dynamics were written as a functional derivative of some functional, the system should have relaxed to the final equilibrium state determined by the minimization or maximization principle of this functional. In this case, the complex dynamic behaviors could not be expected.

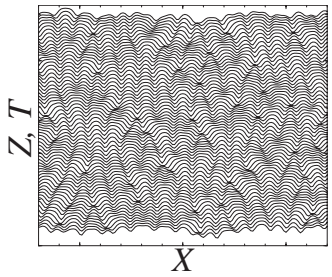

FIG. 17. A typical time evolution of the KS equation (3.26).

For $F < F_c$, the first term with a negative a in Eq. (3.18) is stabilizing, thus there is no need to introduce the fourth derivative as a stabilizing factor. Moreover, if noise is introduced in this formulation, this results (Karma and Misbah, 1993; Pierre-Louis and Misbah, 1996) in an additional stochastic term in Eq. (3.18). We then obtain the KPZ equation (Kardar *et al.*, 1986) which has been introduced phenomenologically as a plausible candidate to describe kinetic roughening. For $F > F_c$, a is positive, and the nonlinear equation (3.18) is the KS equation and is known to lead to spatiotemporal chaos. We thus expect the step to behave chaotically in both space and time. Figure 17 shows a typical snapshot of chaotic KS dynamics. The step develops a meander with a cellularlike structure (i.e., periodic array of protuberances). Then, as time elapses, each cell splits erratically or collides with others, while on average the structure maintains an intrinsic length scale. For example, the average structure factor $S_k \equiv \langle |\zeta_k|^2 \rangle$ (where the sample average is introduced) as a function of k is found to exhibit a peak at a value $k \approx k_m = k_c/\sqrt{2}$, which is the wave number corresponding to the fastest growing mode in the linear regime (Karma and Misbah, 1993).

The above analysis has focused on dynamics at leading order in the nonlinear term. The full lattice gas simulation of Saito and Uwaha (1994) and the phase-field simulation of dynamics by Pierre-Louis (2003b) both revealed chaotic dynamics similar to the dynamics resulting from the KS equation.

By including the anisotropy of surface tension, a term proportional to $(\partial_X Z)^2 \partial_{XX} Z$ is added to the step equation (3.26) (Saito and Uwaha, 1996). The equation then interpolates between the chaotic KS equation and the Cahn-Hilliard equation with periodic structure and slow coarsening (Politi and Misbah, 2004, 2006).

2. Noise and morphological instabilities: Competition between the KS and KPZ equations

Visually, in the chaotic regime, it is tempting to say that a rough step looks stochastic, owing to the apparent erratic motion due to deterministic chaos. Chaos, how-

ever, still preserves a length scale resulting from the instability, which corresponds (at least approximately) to the fastest growing mode obtained from linear theory (Karma and Misbah, 1993). A question then naturally arises: When and under what precise conditions would step dynamics be due to noise or to deterministic chaos? This question was addressed by Karma and Misbah (1993). If noise is added to Eq. (3.18) then a subtle interplay between noise and deterministic chaos takes place. For $F<F_c$, noise dominates and dynamics is rather of the KPZ type. For $F>F_c$, deterministic chaos prevails. In the intermediate regime $F\sim F_c$, competition develops between noise and determinism. With noise, Eq. (3.18) takes the form

$$\partial_t\zeta = -\lambda_1\partial_{xx}\zeta - \lambda_2\partial_{xxxx}\zeta + \lambda_3(\partial_x\zeta)^2 + \eta \tag{3.27}$$

with the noise correlations

$$\langle \eta(x,t)\,\eta(x',t')\rangle = \eta_0\delta(x-x')\,\delta(t-t'). \tag{3.28}$$

Here $\lambda_1\sim(F-F_c)$, λ_2 is a positive coefficient, and $\lambda_3=\bar{V}/2$ with $\bar{V}$ the velocity of the straight step. A systematic analysis (Karma and Misbah, 1993; Pierre-Louis and Misbah, 1998b) allowed the determination of a criterion to specify the condition where deterministic chaos competes with noise. From a power counting argument (Pierre-Louis and Misbah, 1998b), the width of the region around the critical point where noise competes with chaos (this is a nonequilibrium generalization of the Ginzburg criterion known in phase transitions) can be determined.[8] Indeed, by rescaling space, time, and ζ in Eq. (3.27) so that the linear and nonlinear terms take the form (3.26), a rescaled amplitude is obtained for noise, $A_{\text{noise}}\sim\eta_0\lambda_3^2\lambda_2^{1/2}\lambda_1^{-7/2}$. The region around the critical point where noise competes with chaos corresponds to the condition $A_{\text{noise}}\sim 1$ and leads to

$$\lambda_1 \sim |F-F_c| \sim \eta_0^{2/7}\lambda_2^{1/7}\lambda_3^{4/7}. \tag{3.29}$$

If noise is important (close to or below the threshold), the length scale picture disappears progressively and only fluctuations (at the atomic scale) without a dominant scale persist: purely noisy KPZ dynamics are achieved (Karma and Misbah, 1993).

3. Train of steps: Coupled advected KS equations

On a vicinal surface, steps interact with each other via several kinds of interactions. The best known are entropic, elastic, or electric. Out of equilibrium steps also interact in addition via the diffusion field (Pierre-Louis and Misbah, 1996). Indeed, steps compete for the same diffusion field since a step that absorbs adatoms creates a depletion which is felt by neighboring steps. It turns out that this interaction prevails over all others provided that (i) the deposition flux is not too small [about 0.1 monolayer/s at least in the case of Si(111) at usual growth temperatures $T\sim 600\,^\circ$C] and (ii) the interstep distance is long enough (longer than a few atomic distances). Inclusion of step-step interactions (of diffusive and elastic nature) (Pierre-Louis and Misbah, 1996) produces a generalization of Eq. (3.26) to the mth step among N (to leading order),

$$\begin{aligned}\partial_T Z_m = &(\eta_0\epsilon^{-2} - \eta_2\epsilon^{-1}\partial_{XX})(Z_{m+1}-Z_{m-1})\\ &+ \alpha\epsilon^{-2}(Z_{m+1}+Z_{m-1}-2Z_m)\\ &- \partial_{XX}Z_m - \partial_{XXXX}Z_m + (\partial_X Z_m)^2.\end{aligned} \tag{3.30}$$

The parameters η_0, η_2, α, and ϵ are functions of physical quantities [see Pierre-Louis and Misbah (1998a, 1998b) for more details]. The last three terms correspond to an isolated step treated in the last section [Eq. (3.26)]. The other terms represent interaction with neighboring steps $m+1$ and $m-1$. Here a finite ES effect is assumed, so that the effect of the step behind the reference step is felt.

Numerical solutions of Eq. (3.30) reveal (Pierre-Louis and Misbah, 1996, 1998b) that the steps behave chaotically on the vicinal surface, as for isolated steps, while executing their motion in a synchronized fashion.

4. Surface continuum limit: The advected anisotropic KS equation

In many circumstances surface problems (e.g., roughening transitions) are treated by resorting to a full continuum description. Previously the step was treated in a continuum limit along itself, but in the orthogonal direction the steps maintain their identity. It is sometimes useful to study the situation where the surface can be treated as a continuum object, disregarding the discrete nature due to individual steps. This has been done starting from Eq. (3.30) (Pierre-Louis and Misbah, 1998a, 1998b). The result is a new anisotropic equation for surface height $\Upsilon(X,Z,T)$ which is a function of appropriate dimensionless spatial and temporal variables. The equation takes the form

$$\partial_T\Upsilon = \tilde{\eta}_2\partial_{ZXX}\Upsilon + \partial_{ZZ}\Upsilon - \partial_{XX}\Upsilon - \partial_{XXXX}\Upsilon + (\partial_X\Upsilon)^2, \tag{3.31}$$

where $\tilde{\eta}_2$ is a coefficient dependent on various parameters [see Pierre-Louis and Misbah (1998b)].

An equation which shares some similarities with Eq. (3.31) was derived phenomenologically by Rost and Krug (1995). Their equation lacks the term $\partial_{ZXX}\Upsilon$, which arises naturally in the derivation of Eq. (3.31) (Pierre-Louis and Misbah, 1998b). Rost and Krug found different regimes ranging from chaos to a coarsening of rippled domains. To the best of our knowledge, the far-reaching consequences of Eq. (3.31) have not yet been studied. It would be interesting for future investigations to analyze dynamical roughening for this equation in its stable version (with a positive sign in front of $\partial_{XX}\Upsilon$). The first numerical solution of the above equation revealed (Pierre-Louis and Misbah, 1998b) several interesting features. Of particular interest is the fact that the striplike solution (the solution corresponding to an in-phase me-

[8] Interestingly, these scalings are changed in the case of a vicinal surface (Karma and Misbah, 1993; Pierre-Louis and Misbah, 1998b).

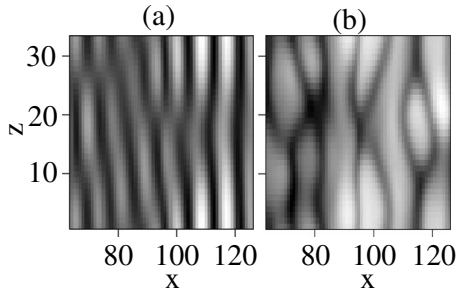

FIG. 18. A typical pattern obtained from a 2D numerical solution of Eq. (3.31): (a) first, ripples form from the linear meandering instability; (b) then, chaos takes place.

ander) may be strongly destroyed in that the stripe pattern emits chaotic spots where the notion of a vicinal surface seems to lose its meaning (Fig. 18).

C. Nonlinear dynamics with weak desorption: Nonstandard nonlinear equations

We now consider the most frequent situation (at least in MBE when the species are simple atoms) where desorption of atoms is negligible on the scales of interest (typically the terrace width $\ell \ll x_s$) so that most of the landing atoms have ample time to reach the surrounding steps. We focus on a train of steps in a parameter range where the distance between steps is small enough (or diffusion is fast enough) that atoms reach an attachment site at the steps quickly and nucleation is absent or may be considered very rare. As shown in Sec. III.A by the strip model, a uniform train corresponds to the situation where each step moves at a constant velocity given by $F\ell\Omega$. The question now arises of whether the nonlinear equation for the step meander may be inferred from simple arguments. Due to conservation (all landing atoms remain within the growing solid) and if no defects (such as holes) are created, then a nonlinearity of the KS or KPZ type is not permissible. A plausible candidate would be $\partial_{xx}[\partial_x\zeta]^2$ (the conserved form of the KS or KPZ nonlinearity). We see using the minimal model of BCF that the result came as a surprise (Pierre-Louis, 1997; Pierre-Louis *et al.*, 1998; Gillet *et al.*, 2000).

We first focus on the situation where the train is synchronized, giving collective uniform motion to the train, i.e., $\zeta(x,t)$ is the same for all steps. We also assume that $x_s \to \infty$ and $k\ell \ll 1$ (small wave-number assumption, as for the case with desorption). The linear dispersion relation for small $k\ell$ takes the form [see, e.g., Pimpinelli *et al.* (1994)]

$$i\omega = \tfrac{1}{2}\Omega F\ell^2 k^2 - (\tfrac{1}{8}F\Omega\ell^4 + D_S\Gamma\ell)k^4 \equiv ak^2 - bk^4, \tag{3.32}$$

where a and b are positive coefficients. The above dispersion relation has a form of Eq. (3.9) with $F_c=0$. By inverting back to real space, we find

$$\partial_t\zeta = \bar{V} - a\partial_{xx}\zeta - b\partial_{xxxx}\zeta, \tag{3.33}$$

where we have added the uniform train velocity $\bar{V} = F\Omega\ell$ since $\zeta(x,t)$ is measured in the laboratory frame. The linear evolution has the same form as in the case when allowance was made for desorption [Eq. (3.17)]. However, a nonlinearity of the KPZ type proportional to $(\partial_x\zeta)^2$ is forbidden here because there is no desorption. Indeed, if the full equation consists of Eq. (3.33) supplemented with a KPZ nonlinearity with a coefficient c, its average along the step on a length L, longer than any lengths of interest, would be

$$\langle\partial_t\zeta\rangle = \bar{V} - a\langle\partial_{xx}\zeta\rangle - b\langle\partial_{xxxx}\zeta\rangle + c\langle(\partial_x\zeta)^2\rangle, \tag{3.34}$$

where $\langle\cdots\rangle \equiv (1/L)\int_0^L\cdots dx$. Since on average there should be no difference between two points at $x=0$ and L, so that $\langle\partial_{xx}\zeta\rangle=0$ and $\langle\partial_{xxxx}\zeta\rangle=0$. This means that

$$\langle\partial_t\zeta\rangle = \bar{V} + c\langle(\partial_x\zeta)^2\rangle. \tag{3.35}$$

The result is that the average step velocity is not equal to $\bar{V}=\Omega F\ell$, as it should be due to mass conservation.[9] This implies that the KPZ nonlinearity must vanish, $c=0$. The general equation of motion must have a conservation form

$$\partial_t\zeta = \Omega F\ell - \partial_x J(\partial_x\zeta, \dots) \tag{3.36}$$

with the current J. Averaging the above equation always implies that $\langle\partial_t\zeta\rangle=\Omega F\ell$. The main task is to determine J, which in the linear regime is given by

$$J = a\partial_x\zeta + b\partial_{xxx}\zeta. \tag{3.37}$$

It may be argued that the first natural nonlinearity in the current would be $\partial_x[(\partial_x\zeta)^2]$ (due to symmetry if x is changed to $-x$ then the current must also change sign) or $(\partial_x\zeta)^3$; these are the first simplest nonlinearities which are compatible with symmetry. Later we see that this naive picture does not hold. This is one example where primary intuition fails to produce the correct result. A systematic investigation of the evolution equation is required before a general picture can be drawn of the class of equations in which dynamics falls. An expansion in powers series led us to discover that the above-mentioned nonlinearities are inadequate. A surprising feature is that the evolution equation is highly nonlinear (Pierre-Louis, 1997; Pierre-Louis *et al.*, 1998; Gillet *et al.*, 2000) and could not be inferred from simple dimensional or symmetry arguments. This strongly contrasts with traditional studies in nonlinear science where close enough to an instability threshold, and in the long-wavelength

[9] If defects such as holes are allowed then $\langle\partial_t\zeta\rangle \neq V_0$. It is sometimes stated that the KPZ nonlinearity accounts for "overhangs," meaning holes that are left behind the front. This is why the ballistic deposition algorithm where each atom sticks to a neighboring column whenever it meets a column along its trajectory—once it sticks it leaves holes below—is believed to simulate the KPZ nonlinearity [see Barabàsi and Stanley (1995)].

limit, weakly nonlinear equations are the rule. Recently (Gillet *et al.*, 2000) a general reason for the origin of this behavior has been given. Below we present a simplified version, albeit quite general, of this behavior. The highly nonlinear behavior of the dynamics was discussed more generally by Csahók *et al.* (1999) and Pierre-Louis (2005).

1. Scaling arguments: Why a weakly nonlinear equation is not permissible

We now show explicitly how the highly nonlinear behavior arises in meander dynamics. We first define the appropriate small parameter for the expansion. Without desorption, the critical flux for instability F_c turns out to be zero: for small flux F, there is always a band of unstable modes [see Eq. (3.32)]

$$k < k_c = \sqrt{\Omega F \ell/(2D_S\Gamma)} \tag{3.38}$$

in a long-wavelength region of step modulation. Here we have neglected the Fk^4 term since F must be small enough, close enough to the critical point. We thus take a small parameter ϵ proportional to the flux F,

$$\epsilon \equiv (k_c\ell)^2 \ll 1. \tag{3.39}$$

The unstable modes we are interested in have long wavelengths $(k\ell)^2 \leq (k_c\ell)^2 \ll 1$.

The most unstable mode [corresponding to the maximum of $i\omega$ in Eq. (3.32)] has a wave number $k_m = k_c/\sqrt{2}$, and its wavelength λ_m reads

$$\lambda_m = 4\pi(D_S\Gamma/\Omega F\ell)^{1/2}. \tag{3.40}$$

As in the previous section we introduce the slow variables X and T [Eqs. (3.22) and (3.23)]. Omitting the factors which do not depend on ϵ, subtracting the contribution $\Omega F\ell$ in Eq. (3.36) (this means considering the motion in the moving frame), Eq. (3.36) can be rewritten as

$$\epsilon^2\zeta_T = -a\epsilon\partial_{XX}\zeta - b\epsilon^2\partial_{XXXX}\zeta - \sqrt{\epsilon}\partial_X J_n, \tag{3.41}$$

where we have used the linear part of the current (3.37) and J_n refers to the nonlinear part of the current, to be determined. Note that a is proportional to ϵ. Because of translational invariance, the current only depends on derivatives of ζ such as $\partial_x\zeta$, $\partial_{xx}\zeta$,… (but not on ζ itself; the origin of ζ is arbitrary). This current is composed of two contributions: (i) the equilibrium part and (ii) the nonequilibrium part.

a. The equilibrium contribution

The equilibrium contribution is easily determined as a derivative of a chemical potential. To leading nonlinear order, the equilibrium current takes the form $J_n^{\rm eq} \sim \partial_x\mu$. Since we are only seeking the nonlinear contribution, μ must at least be a quadratic function of ζ. A possible candidate is $(\partial_x\zeta)^2$. We have to remember, however, that μ must be written as a functional derivative of an energy (due to the thermodynamic nature of the equilibrium contribution). As seen, there is no functional whose derivative yields $(\partial_x\zeta)^2$. It is easier to focus first on the energy. The smallest power in the energy that produces a quadratic potential is 3, and thus the first attempt is $(\partial_x\zeta)^3$. This is not allowed by the parity symmetry (energy should be invariant under the transformation $x \to -x$). The next choice is $(\partial_x\zeta)^4$. Its functional derivative is $\sim\partial_x(\partial_x\zeta)^3$ (approximately the chemical potential) making the current $J_n^{\rm eq} \sim \partial_{xx}[(\partial_x\zeta)^3] \sim \epsilon^{5/2}\partial_{XX}[(\partial_X\zeta)^3]$ (recall that $X = x\sqrt{\epsilon}$).

b. The nonequilibrium contribution

The nonequilibrium part $J_n^{\rm neq}$ vanishes at $F=0$. It is natural to expect $J_n^{\rm neq} = F\bar{J}_n^{\rm neq} \sim \epsilon\bar{J}_n^{\rm neq} \sim \epsilon^{5/2}(\partial_X\zeta)^3$ [where the leading nonlinearity compatible with symmetry—the current is an odd function of the slope—is $(\partial_x\zeta)^3$; note that $\bar{J}_n^{\rm neq}$ may itself depend on F; what matters is that it vanishes with F]. Plugging the nonlinear contribution of the current into Eq. (3.41) (omitting factors which do not involve ϵ), we obtain

$$\epsilon^2\partial_T\zeta = -\epsilon^2\partial_{XX}\zeta - \epsilon^2\partial_{XXXX}\zeta - \epsilon^3\partial_X[(\partial_X\zeta)^3] - \epsilon^3\partial_{XXX}[(\partial_X\zeta)^3]. \tag{3.42}$$

The leading nonlinear term ($\sim\epsilon^3$) can balance the linear terms only if $\zeta \sim 1/\sqrt{\epsilon}$. This is the major difference compared with the case where allowance is made for desorption. This means that the standard ϵ truncation, encountered when dealing with nonlinear equations, breaks down.

The main reason for this "singular scaling" of ζ with respect to ϵ is that departure from equilibrium coincides with the occurrence of instability. This appeared above in the fact that F scaled as ϵ. This strongly contrasts with the case where a finite critical flux exists. In such cases, the nonequilibrium part does not have to vanish at $F=0$ but at $F=F_{\rm eq}$. Since $F-F_{\rm eq}$ is finite at the instability point $F=F_c$ (i.e., it is not in general of order $\epsilon^{1/2}$), the nonequilibrium contribution in the evolution equation would have scaled as $\epsilon^2\partial_{XX}[(\partial_X\zeta)^2]$ (instead of $\sim\epsilon^3$). Balancing the linear terms against this one yields $\zeta \sim 1$, which leads us to the conserved KS limit

$$\partial_T\zeta = -\partial_{XX}[\zeta + \partial_{XX}\zeta + (\partial_X\zeta)^2]. \tag{3.43}$$

This equation was derived in the context of bunching in the absence of desorption (Gillet *et al.*, 2001). It should be noted that without a conservation condition, we obtained $\zeta \sim \sqrt{\epsilon}$ and the KS equation as in the previous section.

2. Derivation of the highly nonlinear equation

A systematic analysis of the BCF equation revealed an astonishing fact (Pierre-Louis *et al.*, 1998; Gillet *et al.*, 2000): even in the presence of a small parameter ϵ the evolution equation is highly nonlinear and its precise form could not be inferred from the simple scaling argument. This regime is nonstandard in nonlinear systems. We saw above that the amplitude of ζ scales as $\epsilon^{-1/2}$. Note that the fact that the amplitude scales as $\epsilon^{-1/2}$ may

seem pathological. In reality, translational invariance means that only the derivative of ζ matters. By defining the variable $Z=\epsilon^{1/2}\zeta$ of order 1, $\partial_x\zeta=\partial_X Z$ is also of order 1. Because the natural quantity describing the step is the slope $\partial_x\zeta$, the nonlinear evolution equation can be expected to be highly nonlinear since the usual truncation in powers of $\partial_x\zeta$ is not legitimate here. Starting from the full BCF model it is possible to derive the evolution equation in a consistent manner. In terms of the physical variable ζ and the physical quantities x and t this equation takes the form (Gillet *et al.*, 2000)

$$\partial_t\zeta=-\partial_x\left[\sigma_0\frac{\partial_x\zeta}{1+(\partial_x\zeta)^2}-\frac{M_0\partial_x\kappa}{1+(\partial_x\zeta)^2}\right], \tag{3.44}$$

where κ is the step curvature [Eq. (2.59)], and we have defined

$$\sigma_0=\Omega F\ell^2/2, \quad M_0=D_S\ell\Gamma. \tag{3.45}$$

This equation is highly nonlinear as suspected from the above scaling argument. It must be noted that though ϵ appeared in the scaling of ζ, the final equation contains no ϵ and thus no "divergence" is expected when ϵ is small. After the nonregular expansion that led to Eq. (3.44), ϵ scaled out, so that its solution would lead to behavior not necessarily diverging with ϵ. Note that an expansion of Eq. (3.44) in powers of ζ to leading order yields the terms of Eq. (3.42) derived from phenomenology and symmetry.

We introduce the slope $m\equiv\partial_x\zeta$. Differentiating Eq. (3.44) with respect to x yields

$$\partial_t m=-\partial_{xx}\left[\frac{\sigma_0 m}{1+m^2}+\frac{M_0}{1+m^2}\partial_x\left(\frac{\partial_x m}{(1+m^2)^{3/2}}\right)\right], \tag{3.46}$$

where we have explicitly used the expression of the curvature $\kappa=-(\partial_x m)/(1+m^2)^{3/2}$. Equation (3.46) is somewhat similar to that used in the context of growth on a high symmetry surface [see Politi *et al.* (2000) for a review] and proposed as a phenomenological model inferred from numerical simulations. The first term inside the brackets, $m/(1+m^2)$, is indeed identical to that introduced by others in this context (however, growth on a singular surface from a beam is quite different from the present situation where atoms are deposited on terraces and the step advances in a step flow regime). The second part in our equation contains a distinct contribution from studies on high symmetry surfaces: the prefactor of the curvature term proportional to $1/(1+m^2)$. The presence of this term destroys the overall picture of coarsening found on high symmetry surfaces. Instead, dynamics in the step flow regime exhibit a frozen wavelength and an amplitude that grows indefinitely over time. We return to this point later.

The same equation [Eq. (3.44)] is derived in cases of meandering instability induced by electromigration drift (Sato *et al.*, 2002), by the coexistence of two phases close to the step (Kato *et al.*, 2003), or by surface reconstruction (Sato *et al.*, 2003).

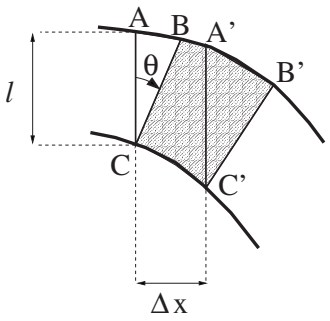

FIG. 19. Top view of an element of teracce area between two steps along $ABA'B'$ and CC' under step meandering.

3. Heuristic argument leading to the highly nonlinear equation

Following the same lines as in Sec. III.A, there is an edifying way to arrive at Eq. (3.44). In order to adapt the geometrical model of Sec. III.A to the present case of vicinal surfaces without desorption, we consider that the strip is now a terrace between two steps undergoing an in-phase meander.

Consider a curved part of the step as shown in Fig. 19. The number of atoms entering the step element CC' of arclength Δs is given by $V_n\Delta s/\Omega=V\Delta x/\Omega$, where V_n is the normal step velocity, V is the step velocity along the vertical z axis, and Δx is the length of CC' along the x axis. In the one-sided model, step motion results from incorporation of adatoms from the lower terrace. Mass conservation applied to the hatched region $CC'B'B$ between two steps determines the number of atoms entering the step element CC',

$$V\Delta x/\Omega=F\Delta S+J_\perp(x)-J_\perp(x+\Delta x), \tag{3.47}$$

where ΔS is the hatched area and $J_\perp(x)$ is the total flux across the BC segment in Fig. 19. ΔS is written as

$$\Delta S\approx\ell\Delta x-\mathcal{A}(x)+\mathcal{A}(x+\Delta x), \tag{3.48}$$

where $\mathcal{A}(x)$ is the area of the triangle ABC in Fig. 19 and is a function of $\partial_x\zeta$:

$$\mathcal{A}(x)=\frac{\ell^2}{2}\cos\theta\sin\theta=-\frac{\ell^2}{2}\frac{\partial_x\zeta}{1+(\partial_x\zeta)^2}, \tag{3.49}$$

where θ is the angle between the z axis and the normal to the step. In the long-wavelength limit, the local geometry of the terrace is described by $\ell_\perp=\ell\cos\theta$—the length of the BC segment in Fig. 19, κ—the step curvature, and their derivatives with respect to the arclength s along the steps. Since the flux $J_\perp$ arises only because of the change in the local terrace width, we have to leading order

$$J_\perp\sim\partial_s\ell_\perp\sim\partial_x(\partial_x\zeta)^2\ll\mathcal{A}\sim\partial_x\zeta, \tag{3.50}$$

which shows that the terms stemming from $J_\perp$ can be neglected at leading order in Eq. (3.47). Combining Eqs. (3.47)–(3.49) and letting Δx go to zero, we find

$$V = \Omega F \ell - \partial_x \left(\frac{\Omega F \ell^2}{2} \frac{\partial_x \zeta}{1 + (\partial_x \zeta)^2} \right). \tag{3.51}$$

Once the mean step velocity $\bar{V} = \Omega F \ell$ is subtracted, we recover the first (nonequilibrium) term of Eq. (3.44).

The second term is the classical equilibrium contribution. As described in Sec. II.B.2.b, diffusion along the terrace for long wavelengths can be seen as effective edge diffusion along the step. Using the same formal expression as Eq. (2.69), we have

$$\partial_t \zeta^{\mathrm{ED}} = \partial_x (M \partial_s \mu), \tag{3.52}$$

where step mobility (2.86) becomes

$$M = D_S \ell_\perp / k_B T \tag{3.53}$$

in the present notation and $\mu = \Omega \tilde{\gamma} \kappa$ is the chemical potential. Thus $J_{\mathrm{eq}} = -M \partial_s \mu$ is the mass current along the step, with the effective diffusion constant $D_S \ell_\perp / a$ (a refers to atomic length). After substituting $\ell_\perp = \ell / \sqrt{(\partial_x \zeta)^2 + 1} \simeq \ell$ and $\partial_s \simeq \partial_x$, the Mullins equation $\partial_t \zeta \sim \partial_{xx} \mu$, is recovered. In the present problem, full nonlinear dependence of mobility M on step slope $\partial_x \zeta$ must be maintained, therefore the evolution equation is not precisely of the Mullins type. We see that the presence of $\ell_\perp$ in the mobility is far from being innocuous since it completely destroys the nature of the dynamics. From Eqs. (3.52) and (3.53) we can finally write

$$\partial_t \zeta^{\mathrm{ED}} = \partial_x \left[\frac{D_S \ell \partial_x (\Gamma \kappa)}{1 + (\partial_x \zeta)^2} \right] = \partial_x \left[\frac{M_0 \partial_x \kappa}{1 + (\partial_x \zeta)^2} \right], \tag{3.54}$$

which is precisely the second term in Eq. (3.44). Adding the destabilizing contribution (3.51) and the stabilizing contribution (3.54), we obtain the full highly nonlinear evolution equation (3.44).

Note that if allowance is made for line diffusion along the step, the full equation remains the same except now the mobility acquires an additional term and reads

$$M = (D_S \ell_\perp + D_L a) / k_B T. \tag{3.55}$$

Interpretation is simple: besides the diffusion that occurs in a strip of width $\ell_\perp$ (terrace diffusion), a line diffusion occurs on a strip of atomic width of a.

4. Nonlinear meandering dynamics

a. Frozen wavelength

Besides the surprising effect for the scaling of ζ with ϵ which led to Eq. (3.44), step evolution in this model exhibits a perpetual increase in meander amplitude, while wavelength is frozen at the early stages of dynamics. Snapshots of the meander are shown in Fig. 20. After transients have decayed, the pattern wavelength is close to that of the linearly fastest growing mode λ_m defined in Eq. (3.40).

In the general case with finite attachment-detachment kinetics on both sides of the step with the kinetic coefficients $\nu_\pm$, the dispersion relation in the long-wavelength limit takes the form (Gillet *et al.*, 2000)

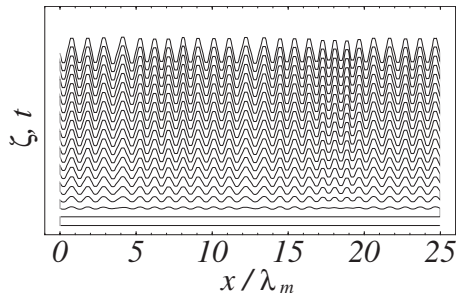

FIG. 20. Time evolution of step meandering as found from the solution of highly nonlinear equation (3.44), showing that the wavelength is fixed at early stages.

$$i\omega = -\frac{1}{2} \Omega F \ell^2 k^2 \frac{d_+ - d_-}{\ell + d_- + d_+} - \Gamma (D_S \ell + D_L a) k^4, \tag{3.56}$$

with the kinetics attachment lengths $d_\pm = D / \nu_\pm$ defined in Sec. II.B.4. Within the one-sided limit and with instantaneous kinetics from the lower side (a limit which was considered previously), this gives $d_+ \to 0$ and $d_- \to \infty$. If, in addition, we assume no line diffusion, the wavelength of the most unstable mode is λ_m, defined in Eq. (3.40). This result is appropriate provided that (i) line diffusion is neglected, (ii) the one-sided limit (only atoms from the lower terrace attach to the step) is legitimate, (iii) the attachment kinetics is fast for atoms from the lower terrace, and (iv) crystalline anisotropy is ignored. This scaling may be significantly altered if these assumptions are relaxed. For example, if line diffusion is allowed, Eq. (3.56) gives

$$\lambda_m = 4\pi \sqrt{\Gamma (D_S \ell + D_L a) / \Omega F \ell^2}. \tag{3.57}$$

If line diffusion is more efficient than terrace diffusion, then

$$\lambda_m = 4\pi \ell^{-1} \sqrt{\Gamma D_L a / \Omega F}. \tag{3.58}$$

The difference between pure terrace diffusion [Eq. (3.40)] and line diffusion [Eq. (3.58)] lies in the ℓ dependence; it is $\ell^{-1/2}$ in the first case and ℓ^{-1} in the second one. This difference is not beyond the reach of experiments. Finally we consider another situation where kinetic attachment at the step is not instantaneous but keep the condition that most atoms attach to the step when they come from the lower terrace ($d_- \gg d_+$). We also assume that ℓ is large in comparison to d_-. If line diffusion is negligible then

$$\lambda_m = 4\pi \sqrt{\Gamma D_S / \Omega F d_-}. \tag{3.59}$$

That is to say, the meander wavelength is independent of the interstep distance. Conversely, if line diffusion dominates over terrace diffusion, we have

$$\lambda_m = 4\pi \sqrt{\Gamma D_L a / \Omega F d_- \ell}. \tag{3.60}$$

This gives the same dependence with respect to ℓ and F as in the one-sided model [Eq. (3.40)]. However, Eq. (3.40) is obtained with pure terrace diffusion, while Eq.

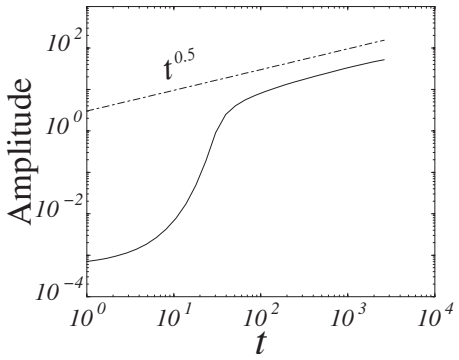

FIG. 21. Evolution of the meander roughness with time, corresponding to Fig. 20.

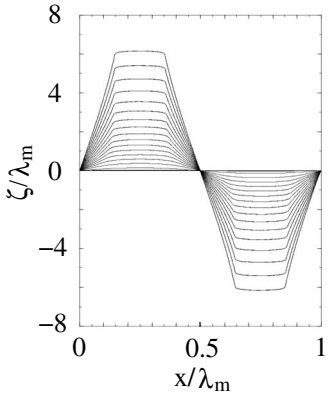

FIG. 22. A typical time evolution of the meander of a single wave in Fig. 20. The step develops plateaus.

(3.60) is based on the assumption that line diffusion prevails. Thus, it would be *a priori* difficult to discriminate experimentally between the two situations only from the ℓ dependence of λ_m. Other information would be needed, such as an analysis of the fluctuation correlation, as we saw in the section devoted to equilibrium.

b. Amplitude and shape

We summarize the results originating from the nonlinear evolution equation (3.44). Numerically, the amplitude is found to grow indefinitely as $\sim\sqrt{t}$ (Fig. 21). This behavior can be understood from a simple analytical argument.

Because wavelength is frozen, it is appealing to seek a solution to Eq. (3.44) in the steep slope region by

$$\zeta_s(x,t) = A(t)g(x). \tag{3.61}$$

For a large t, A is large and the first term in Eq. (3.44) dominates

$$A\partial_t A = \sigma_0 \partial_{xx} g/[g(\partial_x g)^2] = C, \tag{3.62}$$

where C is a constant. After integration, the result is

$$A = (2Ct)^{1/2}, \tag{3.63}$$

which agrees with the numerical solution of Eq. (3.44). Integration with respect to x provides us with the profile

$$g = (2\sigma_0/C)^{1/2}\,\mathrm{erf}^{-1}(4x/\lambda_s), \tag{3.64}$$

where λ_s is the width of a slope region. This function produces a cuspy structure at maximum amplitude instead of the plateau found numerically (Fig. 22). A plateau is induced by the second stabilizing term in Eq. (3.44). In order to deal with the plateau region of width $\lambda_0/2$ and meander amplitude of the order of $a_0 t^{1/2}$, the following *Ansatz* replaces Eq. (3.61) in the plateau region:

$$\zeta_p(x,t) = B_\pm(t) + h(x), \tag{3.65}$$

with $B_\pm(t) = \pm a_0 t^{1/2}$, where the plus and minus signs refer to the maxima and minima regions, respectively. After substitution in the evolution equation [Eq. (3.44)], the three parameters λ_0, a_0, and λ_s can be determined. This *Ansatz* is in good agreement with the simulation of the full evolution equation [for more details, see Gillet *et al.* (2000)].

We now make some general remarks. Because we are considering an in-phase mode (i.e., the steps move in synchronization), the evolution equation (3.44) takes the form of a conservation law, $\partial_t \zeta + \partial_x J = 0$. If the steps do not move in phase, this form ceases to be valid (Pierre-Louis, 1997) unless interlayer transport is forbidden. If allowance is made for an arbitrary phase shift between successive steps, then dynamics may prove to be much more complex. Currently some preliminary results have been published, showing complex dynamics involving topological defect generation and annihilation (Danker, 2007); see Sec. III.C.8.

5. The effect of elastic interaction on the meander: Modified nonstandard nonlinear equation

Since the meander amplitude increases with time indefinitely and the steps become closer and closer, it is natural to ask whether or not the elastic repulsion between steps may limit this behavior. The steps are known (provided that the two terraces adjacent to the step are identical) to be a location of force doublets (Marchenko, 1981). Two steps interact repulsively via the deformation of the underlying substrate with a law $1/\ell^2$, as described by Eq. (2.11). In order to include the elastic interaction, the equilibrium concentration (2.60) has to be modified by including both line tension and the elastic contribution in the chemical potential μ, defined by Eq. (2.61). The interstep interaction between modulated steps was first addressed by Houchmandzadeh and Misbah (1995) and introduced in the study of meandering by Paulin *et al.* (2001). We can infer the elastic contribution from the following reasoning. For curved steps (supposed to be synchronous for simplicity) and in the long-wavelength limit in which we are interested, we expect the elastic interaction law to remain the same provided that the interstep separation ℓ is substituted by the true distance $\ell_\perp = \ell/[1+(\partial_x \zeta)^2]^{1/2}$. Since this distance changes from one point to another along the step, the elastic free energy must be written as an integral over an energy density:

$$\mathcal{F}_{\rm elas} = \int_{-\infty}^{+\infty} ds \frac{\mathcal{A}}{\ell_\perp^2} = \frac{\mathcal{A}}{\ell^2} \int_{-\infty}^{+\infty} dx [1 + (\partial_x \zeta)^2]^{3/2}. \quad (3.66)$$

After a functional differentiation of $\mathcal{F}_{\rm elas}$ together with the contribution from line tension, Eq. (2.61), gives the chemical potential

$$\mu = \Omega\{\tilde{\gamma}\kappa + 3\mathcal{A}(\kappa/\ell_\perp^2)[1 + 2(\partial_x \zeta)^2]\}. \quad (3.67)$$

As shown by Paulin *et al.* (2001), this expression is identical to that obtained by Bonzel and Mullins (1996) starting from the usual macroscopic phenomenological free energy, expressed in terms of the step density $|\nabla h|$:

$$\mathcal{F}_{\rm surf} = \int dS(\gamma_0 + \gamma_1 |\nabla h| + \gamma_3 |\nabla h|^3), \quad (3.68)$$

where h is the surface height, dS is a surface element, and γ_0, γ_1, and γ_3 are constants. The above free energy was also derived in the section devoted to equilibrium [see Eq. (2.30), with $\rho = \nabla h/a$]. The new nonlinear equation for meander profile ζ can be obtained simply by substituting the equilibrium part [given in terms of μ in Eq. (3.52)] by the present μ [Eq. (3.67) into Eq. (3.44)]. More precisely, the meander evolution equation takes the form

$$V_n = \partial_s \left[-\frac{\Omega F l^2}{2} \frac{\partial_x \zeta}{1 + (\partial_x \zeta)^2} + \mathcal{M} \partial_s \mu \right], \quad (3.69)$$

where effective mobility is $\mathcal{M} = M/\sqrt{1+\zeta_x^2}$ and M is given (when both terrace and line diffusion are included) by Eq. (3.55) and μ by Eq. (3.67). The full equation can be rewritten in terms of the slope m as in the elasticity-free case [Eq. (3.46)]:

$$\partial_t m = -\partial_{xx} \left\{ \frac{m}{1+m^2} + \frac{1}{1+C_2} \left(\frac{1}{1+m^2} + \frac{C_2}{(1+m^2)^{1/2}} \right) \times \partial_x \left[\left(\frac{1 + C_1(1+m^2)(1+2m^2)}{1+C_1} \right) \kappa \right] \right\}, \quad (3.70)$$

where in order to show a minimal number of independent parameters we introduced rescaled variables. $C_1 = 3\mathcal{A}/\tilde{\gamma}\ell^2$ represents the elastic strength and $C_2 = D_L a/D_S \ell$ represents the contribution from line diffusion, while space (x and ζ) and time (t) were rescaled by $a_x = [2(D_S \ell + D_L a)\Gamma/\Omega F \ell^2]^{1/2}$ and $a_t = 2a_x^2/\Omega F \ell^2$, respectively. It is easy to see that Eq. (3.70) reduces to Eq. (3.46) if $C_1 = 0$ and $C_2 = 0$.

While both Eqs. (3.46) (without elasticity, $C_1 = 0$) and (3.70) (with elasticity, $C_1 \neq 0$) have strong similarities in their overall structures, they lead to two completely different dynamics. As seen in Sec. III.C.4, in the absence of elasticity there is a perpetual increase in meander amplitude, while wavelength is frozen at a value close to that corresponding to the fastest growing mode. Inclusion of elasticity leads to dynamics which are drastically different; coarsening occurs, that is to say, wavelength increases with time, as shown in Fig. 23(b). Amplitude also grows. Step roughness always increases with the same exponent $w \sim t^{1/2}$, exactly as in the elasticity-free case. However, the wavelength scaling exponent α (or coarsening exponent), defined by $\lambda \sim t^\alpha$, critically depends on the phenomena entering into play. More precisely, in the pure terrace diffusion regime ($C_2 = 0$), $\alpha = 0.17 \pm 0.02$ is found, whereas if allowance is made for line diffusion ($C_2 \neq 0$) $\alpha = 0.25 \pm 0.01$. These results are obtained from the full numerical solution of Eq. (3.70). A heuristic argument (see the next section), as well as a study based on phase diffusion, allows the capture of these exponents analytically (Politi and Misbah, 2006).

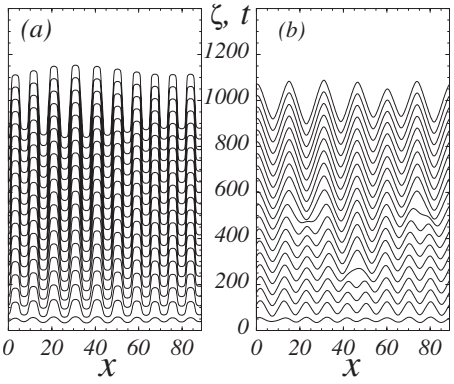

FIG. 23. Elastic effects on coarsening. (a) Without elasticity, $C_1 = 0$ and $C_2 \to \infty$ in Eq. (3.70), the wavelength is frozen. (b) With elasticity, $C_1 = 0.2$, endless coarsening is observed.

6. A heuristic argument for determining the exponents

There is a simple way to derive the above exponents analytically. The idea is based on the existence of a self-affine behavior for the meander $\zeta(x,t)$. The starting point is the use of the following scaling *Ansatz*:

$$\zeta = t^\beta f(x/t^\alpha). \quad (3.71)$$

We first note that $\alpha < 0$ is unphysical since it would characterize an endless decrease of lateral length scales, in contradiction with linear stability according to which there is a short length cutoff (stemming from line stiffness). In addition, we must exclude the case where $\alpha > \beta$ since this would be related to a step smoothening at long time (the slope would go to zero), which contradicts the presence of linear instability. Hence, we must have

$$\beta \geq \alpha \geq 0. \quad (3.72)$$

Indeed, the typical slope $\langle (\partial_x \zeta)^2 \rangle^{1/2} \sim t^{\beta - \alpha}$ increases with time in all simulations. For large slopes $m = \partial_x \zeta$, Eq. (3.70) behaves as

$$\partial_t m \sim -\partial_{xx}(1/m + m^\delta \partial_{xx} m), \quad (3.73)$$

where δ is an exponent whose value depends on the physical mechanisms involved in the smoothening of the step. With Eq. (3.70) we can check that in the presence of elastic interaction ($C_1 \neq 0$), we have $\delta = 0$ for a nonvanishing line diffusion ($C_2 \neq 0$) and $\delta = -1$ for $C_2 = 0$. Now, inserting the scaling form (3.71) into Eq. (3.73) and balancing the term on the left-hand side (lhs) of Eq. (3.73) with the first term on the right-hand side (rhs) yield the

following value for the roughness exponent:

$$\beta = \tfrac{1}{2}. \tag{3.74}$$

Balancing with the second term on the rhs of the same equation leads to

$$\alpha/\beta = (2+\delta)/(4+\delta). \tag{3.75}$$

This amounts to $\alpha=1/4$ when allowance is made for line diffusion and $\alpha=1/6$ otherwise. These results are in good agreement with the direct numerical integration of Eq. (3.70). Moreover, this analysis, which allowed extraction of the dynamics exponents, might be of interest for the problem of mound formation (Politi *et al.*, 2000).

In the absence of elastic repulsion between steps ($C_1=0$), similar analysis leads to an unphysical result, $\alpha=-1/2$. A more detailed analysis indicates the absence of coarsening (i.e., $\alpha=0$), and $\beta=1/2$ (Gillet *et al.*, 2000).

Generalizing the above analysis to an arbitrary power-law elastic repulsion $\sim 1/\ell^n$ with $n \geq 1$, the modified version of Eq. (3.70) gives $\delta=n-3$ for pure terrace diffusion and $\delta=n-2$ in the presence of line diffusion. Equations (3.74) and (3.75) fix the value of the coarsening exponent α, but the inequality $\beta > \alpha$ still holds: no power-law repulsion $\sim 1/\ell^n$ can prevent the shrinking of terrace widths, although this tendency slows down as n increases. The typical slope $m=\partial_x \zeta \sim t^{\beta-\alpha}$ increases according to a power law in all cases. This means that the local interstep distance $\ell_\perp \sim \ell/|m|$ tends toward zero. Elasticity does not prevent step crowding forced by the unstable meander. The distance between steps decreases until it reaches a few lattice spacings, below which the simple algebraic law of elastic interaction may be altered, and other effects such as entropic exclusion, should be properly taken into account. This question is not yet resolved and it constitutes an important task for future research.

7. The effect of anisotropy on the meander: Modified nonstandard nonlinear equation

This section will deal with the effect of anisotropy on the meander. We first ignore elastic interactions. Anisotropy is the rule rather than the exception in realistic crystals. We see that anisotropy leads to interesting new phenomena, such as *interrupted coarsening* or *tilted cellular structure* of the meander (i.e., periodic array of protuberances that are inclined with respect to the growth direction). Since the methodology of the evolution equation derivation has been previously discussed, here we focus on the results themselves. Detailed discussions of the effect of anisotropy on the meander can be found in Danker *et al.* (2003, 2004) and Danker (2007).

There are several sources of anisotropy: line diffusion, terrace diffusion, line stiffness, etc. First we consider anisotropy of the step properties only (line stiffness and line diffusion), while terrace diffusion will be introduced later.

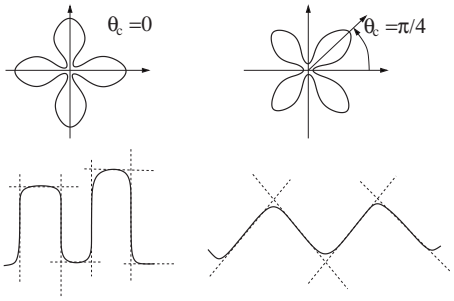

FIG. 24. Fourfold step anisotropy of A_Γ or A_L. Top left: A typical polar plot of an anisotropic function where $\theta=0$ is a maximum. In θ_c, the index c stands for Γ or L. Bottom left: A typical picture of the step profile (where the scenario of endless growth of the amplitude and frozen wavelength still holds). Top right: The function is maximum at an angle $\theta \neq 0$. Under some conditions the step may temporarily be pinned along the maximum anisotropy direction, as shown by the dotted lines at bottom right. (This case may lead to interrupted coarsening.)

a. Anisotropic step properties

Due to anisotropic line tension and line diffusion, the boundary conditions to be modified are (i) the equilibrium concentration at the step (3.13) expressing the effect of line tension Γ, where Γ is now treated as an anisotropic quantity; and (ii) the mass conservation condition at the step (3.14), which takes the form

$$V_n = \Omega D \hat{\mathbf{n}} \cdot \boldsymbol{\nabla} c|_+ + a\partial_s [D_L \partial_s (\Gamma \kappa)]. \tag{3.76}$$

We set $\Gamma(\theta)=\Gamma_0 A_\Gamma(\theta)$ and $D_L(\theta)=D_{L0}A_L(\theta)$. For definiteness, we adopt (see Fig. 24) a fourfold symmetry (any other symmetry can be dealt with along the same lines):

$$A_{\Gamma,L}(\theta) = 1 + \epsilon_{\Gamma,L} \cos[4(\theta - \theta_{\Gamma,L})]. \tag{3.77}$$

Here $\theta=\arctan(\partial_x \zeta)$ is the angle of the local normal to step with respect to the z axis, $\epsilon_{\Gamma,L} \in [0,1]$ measures the strength of the anisotropy, and $\theta_{\Gamma,L}$ denotes the angle along which Γ or D_L reaches its largest value.

The linear stability analysis (Danker *et al.*, 2003) provides us with the fact that the most unstable mode is the in-phase mode and that the corresponding modulation wavelength is given by

$$\lambda_m = 4\pi \{\Gamma(\bar{\theta})[D_S \ell + D_L(\bar{\theta})a]/\Omega F l^2\}^{1/2}, \tag{3.78}$$

where $\bar{\theta}$ is the average orientation of the step. Thus the wavelength has exactly the same form as in the isotropic case [Eq. (3.57)], where the anisotropic functions Γ and D_L are evaluated at $\theta=0$. As discussed in Sec. III.C.1 the instability occurs however small the incoming flux is. Extraction of the nonlinear equation follows exactly the same strategy as in Sec. III.C.1. We only provide the result for the meander evolution (Danker *et al.*, 2003)

$$\partial_t m = -\partial_{xx}\{\sigma_0 m/[1+(m)^2] - \tilde{M}_0(\theta)\partial_x [A_\Gamma(\theta)\kappa]\}, \tag{3.79}$$

where

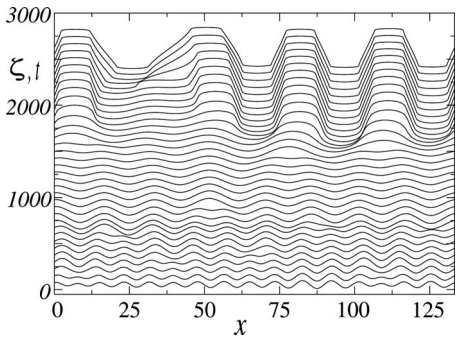

FIG. 25. A snapshot of a typical pattern when allowance is made for anisotropy [Eq. (3.79)]. Interrupted coarsening may take place. Here we show the case where steps are stabilized by anisotropic line diffusion and isotropic line tension. We have chosen $A_\Gamma(\theta)=1$ and $A_L(\theta)=1+0.92\cos[4(\theta-\pi/4)]$.

$$\tilde{M}_0(\theta)=\tilde{M}_0=[D_S\ell_\perp+D_L(\theta)a]\Gamma_0/(1+m^2)^{1/2}. \quad (3.80)$$

This gives the same equation as in the isotropic case [Eq. (3.44)]. The difference lies in the dependence of D_L and Γ on θ.

As seen in Sec. III.C.4, in the isotropic model the wavelength is frozen at the early stage of dynamics while the amplitude grows as $\sqrt{t}$. Due to anisotropy, the system may first undergo coarsening up to a certain wavelength beyond which the wavelength is frozen, while the amplitude continues to increase over time as $\sqrt{t}$. We refer to this situation as interrupted coarsening. Figure 25 shows the evolution of the meander as a function of time. The final wavelength may significantly exceed the value λ_m corresponding to the fastest growing mode. Criteria for coarsening will be discussed later.

The interrupted coarsening scenario occurs for the type of anisotropy considered here only if $\theta_{\Gamma,L}>\theta^0_{\Gamma,L}$, where $\theta^0_{\Gamma,L}$ is a critical angle (maximum anisotropy occurs at $\pm\pi/4$ with respect to the z axis), and if the strength of crystalline anisotropy measured by ϵ_Γ exceeds a certain value. The main physical reason for this behavior is a balance between diffusion, which tends to increase amplitude indefinitely (as shown for the isotropic case) leading to increasingly larger slopes, and anisotropy, which tends to pin the structure along $\pm\theta^0_{\Gamma,L}$ (Fig. 24). Anisotropy triggers these solutions to a certain cellular width λ beyond which the gain in diffusion overcomes the loss in crystalline pinning. Finally, we note that there is no qualitative difference in the role of stiffness and line diffusion anisotropies, denoted as A_Γ and A_L, respectively. That is to say, both give rise to interrupted coarsening.

b. Symmetry and drift of solutions

The cells of the meander (i.e., periodic array of protuberances) are tilted with respect to growth direction because of anisotropy. Since the step advances, we may expect the cellular structure to drift sideways. The numerical solution of Eq. (3.79), however, reveals no drift. This is *a priori* rather surprising. Close inspection of Eq. (3.79) reveals that the evolution equation in terms of $m=\partial_x\zeta$ enjoys $(x)\to(-x)$ symmetry. The equation in terms of ζ enjoys the combined symmetry group $(x,\zeta)\to(-x,-\zeta)$. The apparent dilemma is thus resolved.[10]

Drift occurs, however, when higher-order nonlinear contributions in the evolution equation are considered. Indeed, these contributions destroy the above-mentioned symmetry group. For details see Danker *et al.* (2003, 2004) and Danker (2007).

Finally, it should be noted that loss of parity symmetry may lead to drift only if the evolution equation is nonvariational or nonpotential; i.e., it cannot be written as $\partial_t\zeta=\partial_x[M\partial_x(\delta\mathcal{F}/\delta\zeta)]$, where $\mathcal{F}$ is a functional. The physical reason is obvious and interested readers can find simple formal proof in Danker *et al.* (2003).

c. Terrace diffusion anisotropy

Another important source of anisotropy lies in the diffusion of adatoms on the terraces. The mass current on the terrace reads

$$\mathbf{J}=-\underline{\underline{D}}\,\nabla c. \quad (3.81)$$

Due to anisotropy mass diffusion is represented by a tensor

$$\underline{\underline{D}}=\begin{pmatrix}D_{11} & D_{12}\\ D_{12} & D_{22}\end{pmatrix}. \quad (3.82)$$

Studies (Danker *et al.*, 2003; Danker, 2007) have shown that this problem can be mapped onto that of the previous section. Thus, mapping by coordinate transformation

$$\bar{x}=x-\frac{D_{12}}{D_{22}}z,\quad \bar{z}=\frac{D_0}{D_{22}}z,\quad \bar{\ell}=\ell\frac{D_0}{D_{22}}, \quad (3.83)$$

with $D_0=\sqrt{D_{11}D_{22}-D_{12}^2}$ allows transmission of the terrace anisotropy into effective step parameters which depend on orientation.

Thanks to the mapping equation (3.83) there is of course no need to rederive the nonlinear evolution equation. We only need to refer to Sec. III.C.7.a [more precisely Eq. (3.79)]. This does not mean, however, that the dynamics will be the same. Indeed the precise dependence of the effective step parameters on anisotropy originating from terrace diffusion is quite different in nature from that treated previously. This leads to new features summarized as follows. (i) Unlike the case where either step stiffness or step edge diffusion are anisotropic, terrace diffusion anisotropy may lead to tilted meandering ripples because of x and z coordinate mixing in the transformation (3.83). (ii) If the fast diffusion axis is perpendicular to the steps, the instability is weaker (i.e., longer time scales and longer wavelengths are obtained) and does not exhibit coarsening. (iii) If the fast diffusion direction is along the steps, the instability

[10]In principle, spontaneous parity symmetry breaking may occur (Misbah and Valance, 1994), but this scenario has not been observed so far for step meandering.

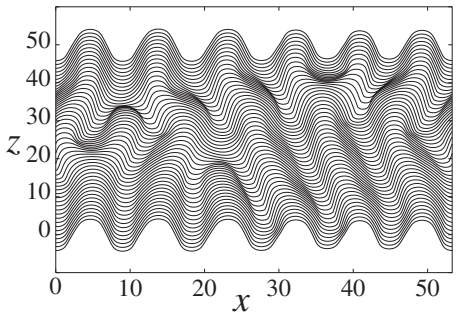

FIG. 26. Snapshot of a train of unstable steps. Solution of the coupled highly nonlinear evolution equations (Gillet, 2000; Danker, 2005, 2007).

is stronger, and interrupted coarsening is found. (iv) When anisotropy is very strong, the instability is weaker for most orientations except if the fast diffusion axis is almost perfectly aligned with the steps. For more details see Danker *et al.* (2003) and Danker (2005).

8. Two-dimensional meandering dynamics

Hitherto, the steps were supposed to move in phase (in a synchronized fashion). When this assumption is relaxed, several interesting features are revealed. Each step has its own dynamics and is coupled to its neighbors by a diffusion field and elasticity. Although the linear stability analysis shows that the in-phase mode prevails, the subsequent nonlinear evolution leads generically to defects (Fig. 26). The defects correspond to a phase shift jump between successive steps. These are topological defects. The dynamics of these coupled nonlinear equations has been investigated partially (Danker, 2007). The qualitative novelty is the occurrence of slow coarsening (most likely logarithmic) of the meander wavelength due to the drift and annihilation of topological defects of opposite signs. Furthermore, if the in-phase motion assumption leads to a frozen wavelength (if elastic interactions are disregarded), the allowance for arbitrary phase shifts (thus allowing for the generation of topological defects) seems to trigger coarsening. This problem constitutes an interesting area for future investigations.

D. Nonequilibrium line diffusion: Kink ES effect

In several systems, such as Cu surfaces (Giesen-Seibert *et al.*, 1995), the experimental study of equilibrium fluctuations proved that diffusion of mobile atoms along steps plays a major role. Here, we discuss the effect of line diffusion on the surface morphology during growth.

The nonequilibrium dynamics of the steps may be described by a model for kink motion along the steps. The main idea is the following: During growth, the step ES effect—asymmetry in attachment kinetics at the steps—was shown to lead to stabilization (as opposed to step bunching) of vicinal surfaces by Schwoebel (1969) (see Sec. IV.A.1). Moreover, it was also shown to lead to the destabilization of nominal surfaces (i.e., by creating islands) by Villain (1991). It is therefore expected that the kink ES effect—asymmetry of attachment of mobile step atoms to kinks—also leads to the stabilization of vicinal steps and to the destabilization of nominal steps during growth. From the analogy with the case of surfaces, a vicinal step is a step which has a slight misorientation with respect to a high symmetry orientation, and a nominal step is a step lying along a high symmetry orientation. Here we discuss some ideas which have been put forward regarding the ES effect at the kinks (i.e., along the steps and not along the vicinal surfaces). It has been suggested that this may lead to step instability in the form of meandering. In order to be able to translate known results on step dynamics to the case of kink dynamics, there is a prerequisite: the distance between kinks should be large enough, i.e., much larger than atomic distance so that the kinks are well-separated entities. This is not the case at high temperatures (due to thermodynamic roughening) or during fast growth (due to kinetic roughening) or for some step orientations where the kinks may be very close to each other.

During growth, the main processes are as follows. Atoms from an atomic beam or a vapor land on the terraces and become adatoms. These adatoms diffuse and may reach the steps. If the kink density is low enough, they attach to the steps somewhere between kinks and become mobile step atoms. Mobile step atoms may either detach and go back to the terrace or diffuse along the step and attach to a neighboring kink. Kink motion therefore results from the incorporation of mobile step atoms. Hence, kink dynamics are very similar to step dynamics expect that kinks have no lateral length. Aleiner and Suris (1992) were the first to notice that kink dynamics during growth have an effect on step stability. As expected, they showed that vicinal steps are stabilized during growth in the presence of a normal kink ES effect (i.e., attachment is more difficult for a mobile step atom moving around the kink). It was then pointed out by Murty and Cooper (1999) and Pierre-Louis *et al.* (1999) that the kink ES effect also leads to destabilization of nominal steps. We now mention the main components of the models. In the presence of a mass flux J_L along the step, mass conservation at the step takes a generalized form of Eq. (2.66):

$$(1/\Omega + c_- - c_+)V_n = \mathbf{n}\cdot\mathbf{J}_+ - \mathbf{n}\cdot\mathbf{J}_- - \partial_s J_L, \tag{3.84}$$

where $\mathbf{J}_\pm$ are fluxes from both terraces, as defined in Eq. (2.57). Flux along the step J_L consists of two contributions. First is an equilibrium one driven by the chemical potential gradient [Eq. (2.68)]. The second contribution is stabilizing from the stochastic nucleation process (Politi and Villain, 1996). It was found that (Politi and Villain, 1996; Pierre-Louis *et al.*, 1999)

$$J_L^{k\ \mathrm{ES}} = \frac{F_s}{2}\frac{(1-|m|)L_s}{[1+L_s(|m|+1/L_c)]}\frac{m}{(|m|+1/L_c)}, \tag{3.85}$$

where $m=\partial_x\zeta$ and $|m|<1$. F_s is the accretion flux of adatoms onto steps, L_c is a cutoff length related to 1D nucleation by aggregation of mobile atoms on the steps,

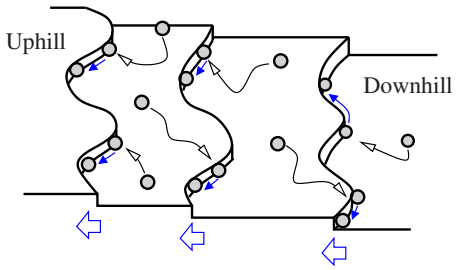

FIG. 27. (Color online) During growth on a vicinal surface, atoms from a molecular beam land on terraces and become adatoms. Adatoms diffuse on the terrace up to a step and become mobile step atoms. Mobile step atoms diffuse along steps. If line diffusion is stabilizing, mobile step atoms diffuse toward the concave parts of the steps (as shown with arrows), thereby creating an uphill mass flux.

and L_s is the Schwoebel length (a typical excursion length before overcoming an ES barrier). Incorporating the flux (3.85) in the mass conservation condition (3.84) reproduces the expected stability or instability of the steps with respect to meandering. A detailed study (Rusanen *et al.*, 2002) based on kinetic Monte Carlo simulations revealed that the shape of the meander is consistent with the nonlinear theory developed for mound formation by Politi *et al.* (2000).

By continuously changing the step orientation from nominal to vicinal, the morphological stability of the step may be changed. This transition was studied by Pierre-Louis *et al.* (1999), where it was shown that fluctuations play an important role. The literature also points out that the stability of vicinal surfaces with respect to mound formations is always metastable (Politi and Krug, 2000; Kallunki and Krug, 2004; Vilone *et al.*, 2005). Kallunki and Krug (2004) reported that at a small enough ES effect the vicinal surface is stable. This does not seem to agree with other results. Metastability means that a surface may be stable with respect to small fluctuations, but after some finite time a large fluctuation may occur, initiating instability. These studies were not explicitly extended to the case of vicinal steps, and this question remains open.

A more surprising effect is the possibility of inducing mound formation or step bunching from the kink ES effect. For simplicity, we assume that no step ES effect is present. It is then shown in Fig. 27, that line diffusion may lead to a mass flux along vicinal surfaces (Murty and Cooper, 1999; Pierre-Louis *et al.*, 1999). Since line diffusion is stabilizing against the meander, the flux is uphill, as seen in Fig. 27. If it is destabilizing, the flux is downhill. This effect is not specifically related to the kink ES effect. Indeed, any line diffusion mechanism, stabilizing or destabilizing, may lead to an average mass flux along vicinal surfaces. As shown in Sec. V, this flux may then induce various instabilities.

A calculation of the flux induced by a kink ES effect obtained using kinetic Monte Carlo (KMC) simulations is given by Murty and Cooper (1999). It was shown that these mass fluxes can lead to mound formation (Murty and Cooper, 1999; Pierre-Louis *et al.*, 1999). They can also lead to step bunching (Politi *et al.*, 2000) or to step meandering (Nita and Pimpinelli, 2005).

E. Simulations of the meander instability

Three main questions have been addressed by means of KMC simulations. (1) Can the behavior expected from the analytical study in the nonlinear dynamics be reproduced (Bena *et al.*, 1993)? Specifically, can the spatiotemporal chaos related to the KS dynamics in the presence of desorption and the power-law increase of amplitude $t^{1/2}$ in the absence of desorption be observed (Pierre-Louis *et al.*, 1998)? (2) How do the different mechanisms for instability (ES effect vs kink ES effect), as well as the stabilizing processes (terrace or edge diffusion), compete or combine during the dynamics? (3) When and how may mounds be formed on a surface which undergoes a meandering instability?

1. Dynamics of the amplitude

Shortly after the derivation of the KS equation for a single step (Bena *et al.*, 1993), chaotic dynamics of the KS instability were rapidly confirmed by KMC simulations (Saito and Uwaha, 1994) using a terrace-step-kink model, where overhangs are forbidden. Recently the full solution of the step model with the help of a phase-field model also confirmed chaotic dynamics (Pierre-Louis, 2003a). Using a terrace-step-kink model once again, but without desorption, the expected $t^{1/2}$ scaling law of the meandering (without interactions) was found by Pierre-Louis *et al.* (1998). Subsequent simulations did not show this result and no general scaling law applies (Kallunki *et al.*, 2002). These results point to the fact that it is difficult to reach the asymptotic $t^{1/2}$ scaling law; since the amplitude of the meander becomes large while the wavelength is fixed, the distance between steps reaches the atomic scale. Within this limit a BCF-type model should be revised to evoke microscopic dynamics and interactions that should prevent steps from coming too close together. This issue should be clarified further in the future.

2. Competition between the different mechanisms

The exponent β for the growth of the meanders in the case of kink ES instability has been found to depend on the model. For example, Pierre-Louis *et al.* (1999) found that $\beta \approx 0.3$ for the weak kink ES effect led to rounded shapes with cusps and $\beta \approx 0.6$ for the strong kink ES effect gave zigzag shapes. On the other hand, a more systematic study by Rusanen *et al.* (2001, 2002) in the regime of strong kink ES effect showed that $\beta \approx 1/3$, with a shape transition from zigzag in the early stages to rounded with cusps in the late stages. Moreover, the shape of the meander and the meandering wavelength from KMC simulations were shown to be in agreement with the continuum theory previously presented (Rusanen *et al.*, 2002). It was further found (Kallunki *et al.*, 2002) that the amplitude of the meander in KMC simu-

lations seems to saturate (i.e., $\beta=0$) for the kink ES effect instability while it increases linearly (i.e., $\beta=1$) for the step ES effect instability. The difference in the asymptotic behavior in different simulations may be caused by large meandering amplitudes, leading to large surface slopes where the meaning of step and terrace structures may be lost. Complete understanding of the dynamics in these high slope regions (which were shown to control asymptotic behavior; see Sec. III.C.4.b), is still lacking.

Finally, although asymptotic dynamics are not well understood, the meandering wavelength from the KMC simulations was shown to be in good agreement with continuum models for both kink ES effect and step ES effect (Kallunki *et al.*, 2002; Rusanen *et al.*, 2002).

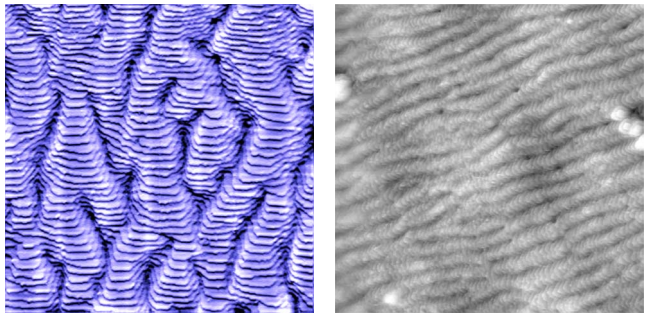

FIG. 28. (Color online) Step meandering during MBE growth on (a) Cu(1,1,17) and (b) Cu(0,2,24). From Maroutian *et al.*, 2001.

3. Nucleation and mound formation in the presence of meandering instability

Up to now we have considered growth on vicinal surfaces in the absence of nucleation on terraces. The assumption which lies behind this regime is the fact that steps are not too far apart so that adatoms, which land and diffuse on terraces, will most probably find a step and attach to it before meeting another atom. It is natural to ask whether or not—even when it is rare—nucleation may ultimately lead to the formation of mounds, and if so, how would this couple to the meandering instability. The study of mound formation within a one-dimensional model for the growth of vicinal surfaces has been addressed (Rost *et al.*, 1996; Vilone *et al.*, 2005). The main conclusion is that step flow is metastable (Vilone *et al.*, 2005) with respect to the formation of mounds. Indeed, there is a critical size of the mound above which its growth is fast enough to prevent being erased by steps coming from uphill in the vicinal. So, if statistical fluctuations lead to the formation of a mound, whose size surpasses the critical size, the mound will grow indefinitely. Further studies have shown that mounds may form in the presence of meandering instability (Rost *et al.*, 1996; Kallunki *et al.*, 2002; Rusanen *et al.*, 2002). Nevertheless, the precise coupling between the two instabilities, such as the existence of a preferred location for nucleation events on a vicinal surface exhibiting meanders, needs further clarification. Another mechanism leading to the breakdown of the vicinal character of surfaces may be triggered by the meandering itself. Indeed, KMC simulations (Kallunki and Krug, 2004) have shown that the meander leads to the formation of two-dimensional voids behind the step. These voids then grow in depth as other steps pass through, leading ultimately to pits, as discussed by Pierre-Louis and Misbah (1998a).

F. Experiments

Several methods, such as x-ray diffraction, have been used to probe surfaces in and out of equilibrium (Vlieg *et al.*, 1988; Robinson and Tweet, 1992; van der Vegt *et al.*, 1992; Conrad, 1996). Unlike fluctuations at equilibrium (Sec. II) and bunching (Sec. IV), quantitative experimental data on meandering are rather sparse. This issue merits greater attention in the future since x-ray diffraction itself lends naturally to ensemble average and thus to a more adequate comparison with the theoretical description.

We focus here on a few experimental studies of step meandering performed on metals or semiconductors during growth. The most systematic work concerns the study of growth on vicinal surfaces of Cu(100); see Fig. 28. The instability was first identified by means of helium-atom beam scattering (Schwenger *et al.*, 1997), but the most systematic analysis was performed from direct imaging with STM (Maroutian *et al.*, 2001).

The main results can be summarized as follows. (i) Scaling of the wavelength with temperature and incoming flux seems to disagree with the prediction of the Bales-Zangwill instability [such as the typical wavelengths (3.57)–(3.60)], and to be in qualitative agreement with the instability due to an ES effect at the kink. The experimental results of Maroutian *et al.* (2001) indicated that the observed wavelength scales as $\sim F^{-0.21}$. The step Schwoebel effect leads to a wavelength $\sim F^{-0.5}$ for all cases discussed in Sec. III.C.4.a. In the case of an instability induced by a kink Erhlich-Scwoebel effect (Pierre-Louis *et al.*, 1999), the initial wavelength can be derived from an analogy with mound formation models in 1+1 dimensions. A strong or weak kink Scwhoebel effect would thus lead to a wavelength $\sim F^{-1/4}$ (Krug, 1997) or $\sim F^{-3/8}$ (Politi and Villain, 1996), respectively. However, a more careful analysis and identification of the relevant stabilizing mechanism are still needed before a conclusive answer can be given. Indeed, it is still unclear if the stabilization is due to the cost of the meander in step free energy or rather to the 1D nucleation process that occurs along steps. (ii) So far, no measurable change of wavelength as a function of time has been observed on this system. This may suggest that coarsening is absent and the system should select a length scale.[11] If the mini-

[11]As discussed in Sec. III.C.8, however, the presence of topological defects may affect coarsening and render it extremely slow.

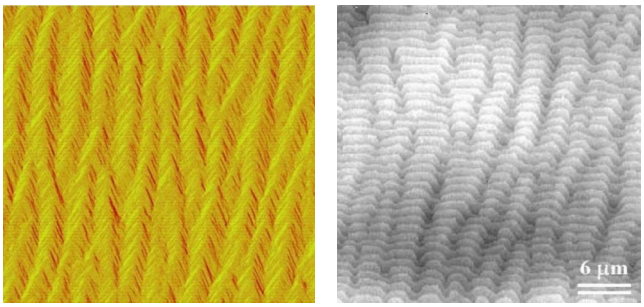

(a) (b)

FIG. 29. (Color online) STM images of step meander on Si(111). (a) From Omi and Ogino, 2000. (b) From Hibino *et al.*, 2003.

mal model of BCF is adopted and instability is taken to be due to the ES barrier at the step, then on the basis of Sec. III.C.5 we may speculate that elastic interactions between steps may affect dynamics. This is based on the study according to which elastic interactions trigger coarsening (see Sec. III.C.5). However, due to the fact that the instability wavelength does not follow the expected scaling with the flux [as obtained by Bales and Zangwill; Eq. (3.40)], we refrain from taking this conclusion as granted. It is clear that further analyses will be needed before drawing conclusive answers. (iii) The amplitude of the wave modulation grows as a power law but seems to be closer to $t^{1/3}$ than to $t^{1/2}$. As mentioned, this is still a formidable task for both theory and simulations. A kinetic Monte Carlo simulation which could account accurately for high slopes [including facets other than (100)] would be very useful. (iv) Mounds appear in the late stages of the instability, as expected from Sec. III.E.3.

Other experiments were carried out on Si(111) surfaces [see Fig. 29(b)]. For temperatures lying in the vicinity of the transition $(1\times1)\leftrightarrow(7\times7)$, meandering is observed (Hibino *et al.*, 2003). The instability is interpreted as being due to an effective step Ehrlich-Schwoebel effect induced by the partial (7×7) reconstruction of the terrace on the upper side of the steps, which locally modifies the diffusion constant (Hibino *et al.*, 2003). This induces asymmetry in the step attachment. Other observations of meandering in the form of a zigzag pattern on Si(111) surfaces were reported by Omi and Ogino (2000), as shown in Fig. 29(a).

IV. STEP BUNCHING

In this section we consider another type of instability of nonequilibrium surfaces: step bunching. We consider a situation where a surface with a step train is exposed to an external flux F but adsorbed atoms may desorb with a desorption time τ. Many different mechanisms are known to produce step bunching. We consider specific ones in detail: bunching induced by the Ehrlich-Schwoebel effect during sublimation, by electromigration, and by elasticity in heteroepitaxy.

It must be emphasized that there are many other physical ingredients that may lead to step bunching but will not be discussed here. We believe, however, that their nonlinear description should enter one of the classes presented in this section. To cite just a few examples, step bunching also occurs (i) by surface contamination (van den Eerden and Müller-Krumbhaar, 1986; Kandel and Weeks, 1992), (ii) due to nonquasistatic effect (Keller *et al.*, 1993; Ranguelov and Stoyanov, 2008), (iii) in the presence of several species at the surface (Wheeler *et al.*, 1992; Vladimirova *et al.*, 2001), (iv) as a result of the coupling between composition and elasticity (Duport *et al.*, 1995; Tersoff, 1996), and (v) due to oscillations of macroscopic fields (Derényi *et al.*, 1998; Pierre-Louis and Haftel, 2001).

A. The Schwoebel instability

1. The instability mechanism

Here we recall the Ehrlich-Schwoebel (ES) effect discussed in Sec. II.B.2.b. This corresponds to an asymmetric attachment at the step. This asymmetry was discovered experimentally by Ehrlich and Hudda (1957) and analyzed theoretically by Schwoebel (1969). Under nonequilibrium conditions, this asymmetry induces a net mass flux, which may be either uphill or downhill. This depends on whether the surface is under growth or sublimation. A step-bunching instability under sublimation was discovered by Schwoebel (1969).

For simplicity, we often consider the extreme case where there is no interlayer mass transport. This is the "one-sided model," where adatoms only attach or detach from the lower terrace. During sublimation a step emits atoms onto the terrace in front. The number of emitted atoms increases with the terrace size. This means that the wider the terrace, the faster the step recession. This explains the step-bunching instability.

Consider a train of steps during sublimation, where the terrace width is ℓ for all terraces, except one which is narrower [Fig. 30(a)]. Atoms detached from the step desorb into the atmosphere after a lifetime τ. If the terrace in front of the step is narrow [the second step from the left in Fig. 30(a)], a detached adatom may reattach to the original step and be reincorporated. Therefore, its retraction speed is slower than that of the others. Since the step at the front end of the narrow terrace (the third step from the left) recedes faster, two steps approach each other: bunching instability follows. How the instability evolves in the nonlinear regime is a question which will be addressed later.

Had we considered growth instead of sublimation, we would have seen the reverse situation. Indeed, the narrower terrace [that now moves to the right in Fig. 30(b)] will get fewer landing atoms attaching to the step delimiting the wide terrace on the left side. That step would then move more slowly than the others, causing the narrow terrace to expand. The vicinal surface is *stable*. In short, a vicinal surface is unstable regarding step bunching under sublimation and is stable under growth. This scenario is valid as long as a direct ES effect (mass ex-

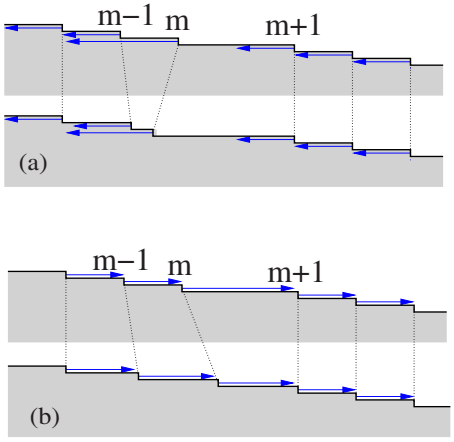

FIG. 30. (Color online) Consequences of the ES effect on the stability of a train of steps. The arrows represent the step velocities, which are proportional to the downhill terrace width. The dotted line indicates the motion of the steps. For both (a) and (b), we have plotted the steps and their velocities for an initial configuration where one terrace is larger than the others. Below, the steps are shown at a later time, having subtracted step motion of the unperturbed surface for the sake of clarity. (a) During sublimation, the wider terrace becomes increasingly wider resulting in step-bunching instability. (b) During growth the opposite is obtained (see text) and the surface is stabilized.

change between a step and its adjacent lower terrace is predominant) is assumed. If the opposite is adopted (an inverted ES effect), the result will be just the reverse: stability under sublimation and instability under growth.

2. One-dimensional step model

We consider a simple 1D one-sided model under sublimation. Adatoms diffuse and may desorb after a characteristic time τ. We first disregard deposition ($F=0$). The diffusion equation (2.73) becomes

$$D\partial_{zz}c - c/\tau = 0. \tag{4.1}$$

We assume fast step kinetics ($\nu_+ \to \infty$) together with an infinite ES barrier ($\nu_- = 0$). It follows from Eqs. (2.57) and (2.74) that

$$\partial_z c_- = 0, \quad c_+ = c_{\rm eq}^m, \tag{4.2}$$

where + and − refer to the lower and the upper sides of the step, respectively. The first equation expresses a zero flux across a descending step (one-sided attachment), while the second equation corresponds to equilibrium on the ascending side (rough steps). The local equilibrium concentration $c_{\rm eq}^m$ at the mth step contains a contribution from the elastic step-step interaction, $\mathcal{F}_{\rm elas} \sim \mathcal{A}/\ell_m^2 + \mathcal{A}/\ell_{m-1}^2$ (nearest-neighbor approximation). Here $\mathcal{A}$ is the strength and $\ell_m = z_{m+1} - z_m$ and z_m are the terrace width and position of the mth step, respectively. The chemical potential μ_m is obtained by taking the functional derivative of $\mathcal{F}_{\rm elas}$ with respect to z_m instead of ζ in Eq. (2.61), and using Eq. (2.60) the following is obtained:

$$c_{\rm eq}^m = c_{\rm eq}^0[1 + A(1/\ell_m^3 - 1/\ell_{m-1}^3)], \tag{4.3}$$

where we have defined the elastic volume as $A = \Omega\mathcal{A}/k_BT$.

Assuming $\Omega c \ll 1$, mass conservation at the steps reads

$$V_m \equiv \partial_t z_m = \Omega D \partial_z c_+|_m. \tag{4.4}$$

The model presented above can be solved explicitly and the step velocity can be expressed as a function of the position of the neighboring steps,

$$V_m = -(\Omega c_{\rm eq}^m x_s/\tau)\tanh(\ell_m/x_s), \tag{4.5}$$

where $x_s = (D\tau)^{1/2}$ is the desorption length [Eq. (2.87)]. Note that the elastic effect is hidden in $c_{\rm eq}^m$.

3. Linear stability analysis

In order to perform the linear stability analysis we define the deviation ζ_m from the regular step flow motion with average velocity $\bar{V}$:

$$z_m = m\ell + \bar{V}t + \zeta_m. \tag{4.6}$$

This expression is substituted into Eq. (4.5) and expanded for small ζ. At leading order (i.e., for $\zeta = 0$), we obtain the step velocity of a uniform train:

$$\bar{V} = -(\Omega c_{\rm eq}^0 x_s/\tau)\tanh(\ell/x_s). \tag{4.7}$$

Then the well-known BCF result (Burton *et al.*, 1951) is found.

To first order in ζ, we find

$$\dot{\zeta}_m = a_{ne}(\zeta_m - \zeta_{m+1}) - a_{\rm eq}(2\zeta_m - \zeta_{m+1} - \zeta_{m-1}), \tag{4.8}$$

where we have set $a_{ne} = -\partial\bar{V}/\partial\ell = (\Omega c_{\rm eq}^0/\tau)\cosh^{-2}(\ell/x_s) > 0$ and $a_{\rm eq} = 3(\Omega c_{\rm eq}^0/\tau)\tanh(\ell/x_s)Ax_s/\ell^4 > 0$. The first term on the right-hand side of Eq. (4.8) represents the nonequilibrium contribution due to diffusion, while the second term corresponds to the part representing the elastic stabilizing effect. Note also that the first term contains only a contribution from steps m and $m+1$. This is a consequence of the one-sided model: the dynamics of step m depend only on the diffusion field in front. Unlike the nonequilibrium part, the equilibrium contribution involves step $m-1$ since it originates from the elastic interaction. We also see that the first term is destabilizing whereas the second is stabilizing (because the elastic interaction is repulsive).

As in the sections devoted to equilibrium fluctuations, we define the Fourier transform and its inverse as

$$\zeta_{\omega\phi} = \int dt \sum_m e^{-i\omega t - im\phi} \zeta_m(t),$$
$$\zeta_m(t) = \int \frac{d\omega}{2\pi} \int \frac{d\phi}{2\pi} e^{i\omega t + im\phi} \zeta_{\omega\phi}, \tag{4.9}$$

where $\zeta_m(t)$ is decomposed into Fourier modes $\zeta_{\omega\phi}$. In a linear regime, Fourier modes are decoupled, so it is sufficient to consider a single mode $\zeta_m(t)=\zeta_{\omega\phi}\exp[i\omega t + i\phi m]$. The variable ϕ corresponds to a phase shift between steps and $\phi=2\pi/N$ represents a perturbation with a spatial periodicity N. Hence, $\phi=\pi$ corresponds to the formation of step pairs ($N=2$). This is a short-wavelength mode. $\phi=0$ corresponds to a global translation of the train. Modes with $\phi\to 0$ correspond to long-wavelength ($\lambda=2\pi\ell/\phi \gg 1$) perturbations along the $\hat{z}$ direction.

By defining $i\omega=\mathrm{Re}[i\omega]+i\,\mathrm{Im}[i\omega]$, we can write

$$e^{i\omega t + im\phi} = e^{\mathrm{Re}[i\omega]t} e^{im'\phi}, \tag{4.10}$$

where $m'=m-V_{\mathrm{phase}}t$ with $V_{\mathrm{phase}}=-\mathrm{Im}[i\omega]/\phi$. A positive $\mathrm{Re}[i\omega]$ indicates instability. $\mathrm{Im}[i\omega]$ accounts for the propagation of the perturbation at velocity V_{phase}.

Taking the Fourier transform of Eq. (4.8), we obtain

$$i\omega = [a_{ne} - 2a_{\mathrm{eq}}][1-\cos\phi] - ia_{ne}\sin\phi. \tag{4.11}$$

Since there is instability if $\mathrm{Re}[i\omega]>0$, it occurs if $a_{ne}>2a_{\mathrm{eq}}$. Using the expressions of a_{ne} and a_{eq} given above, this condition reads

$$r \equiv \ell^3/3A(x_s/\ell)\sinh(2\ell/x_s) > 1. \tag{4.12}$$

When $r<1$, the train of steps is stable. The most unstable mode (maximum growth rate $\mathrm{Re}[i\omega]$) is the pairing mode $\phi=\pi$.

Actually, a distinction must be made between two scenarios:

(i) The weak desorption limit where $x_s \gg \ell$ and $r \approx \ell^3/6A$. From a dimensional analysis (Houchmandzadeh and Misbah, 1995) it is to be expected that $A \sim Ea^3/k_BT$, where E is the Young modulus of the solid and a is an atomic length. Using typical values ($E\sim 10^{10}$ Pa and $a\sim$ Å), we obtain $A \sim 1$ Å$^3 \ll \ell^3$. Therefore, the instability condition $r>1$ is safely satisfied: the train of steps is unstable for sufficiently weak desorption rates.

(ii) For high desorption rates $x_s \ll \ell$, we have $r<1$ and the uniform train is stabilized [the denominator in Eq. (4.12) dominates]. Atoms detaching from a step will most probably desorb to the atmosphere before reaching another step, and the desorption acts as a short circuit preventing steps from "attraction" via the diffusion field, qualitatively described in Sec. IV.A.1. Steps then only interact via (repulsive) elastic distortion, which stabilizes the train.

It must be remembered that for silicon experiments are performed in the limit $x_s \gg \ell$ [case (i)], therefore the condition $r<1$ is unlikely. Note that the one-sided model (strong ES effect) assumption is still controversial. The experimental study of step bunching in the presence of electromigration has proven to be clearer and has given rise to an interesting interaction between experiments, theory, and simulations. Note that, as discussed in Sec. V, the Schwoebel instability can also be understood within a macroscopic picture.

4. Interlayer exchange

At high enough temperatures where sublimation takes place and steps recede, the ES barrier is usually not strong enough to prevent interlayer mass transport. It is thus essential to set a finite barrier so that interlayer exchange becomes permissible. With a finite ν_- but infinitely fast incorporation $\nu_+=\infty$, Eqs. (2.57) and (2.74) yield the following boundary conditions:

$$c_+ = c_{\mathrm{eq}}, \tag{4.13}$$

$$D\partial_z c_- = \nu_-(c_- - c_{\mathrm{eq}}). \tag{4.14}$$

As seen, these relations introduce a kinetic attachment length $d_-=D/\nu_-$ that an adatom has to travel on average before it descends a step. Mass conservation at a step now reads

$$V_m/\Omega = D\partial_z c_+|_m - D\partial_z c_-|_m. \tag{4.15}$$

As in the previous section, the model can be solved explicitly. We defer presentation of the explicit solution in favor of some qualitative discussion. Quantitatively allowing for interlayer mass transport changes the dynamics close to the instability threshold. Indeed, surface diffusion across the steps becomes an efficient channel to stabilize the vicinal surface at short scales. To demonstrate this, consider two simple linear models where step evolution is dictated locally by a chemical potential difference μ_m. In the first model (referred to as model A, according to the traditional nomenclature), no interlayer transport is allowed. The terraces exchange mass only with a three-dimensional phase (a reservoir). Therefore, the rate of detachment of adatoms from the mth step is $\mu_m G_{\mathrm{A}}^m$, where G_{A}^m is a given function of the neighboring terrace widths. Consider the other extreme limit, model B, where only interlayer mass transport is allowed. The mass flux from the mth to the $(m+1)$th step is given in this case by $(\mu_{m+1}-\mu_m)G_{\mathrm{B}}^m$. For the two models we have

$$\text{model A:}\quad V_m = -\mu_m G_{\mathrm{A}}^m,$$
$$\text{model B:}\quad V_m = (\mu_{m+1}-\mu_m)G_{\mathrm{B}}^m - (\mu_m - \mu_{m-1})G_{\mathrm{B}}^{m-1}. \tag{4.16}$$

Due to translational invariance, a shift of all steps by the same distance does not change the chemical potential. From this, and by taking into account nearest-neighbor interaction, the chemical potential assumes the following form in the linear regime:

$$\mu_m \approx -(\ell_m - \ell_{m-1})H = -(\zeta_{m+1} - 2\zeta_m + \zeta_{m-1})H, \tag{4.17}$$

where H is a function of the average terrace width ℓ. It follows that the step velocity is given by

$$\text{model A:} \quad V_m = HG_A\Delta_2\zeta_m, \tag{4.18}$$

$$\text{model B:} \quad V_m = -HG_B\Delta_4\zeta_m, \tag{4.19}$$

where G_A and G_B correspond to G_A^m and G_B^m evaluated at a value ℓ. We have defined $\Delta_2\zeta_m = \zeta_{m+1} - 2\zeta_m + \zeta_{m-1}$ and $\Delta_4\zeta_m = \Delta_2(\Delta_2\zeta_m)$. Models A and B depict two basic relaxation processes for one-dimensional vicinal surfaces. If the variations of ζ are smooth on the scale of ℓ, the finite difference operators Δ_2 and Δ_4 can be approximated by partial derivatives ∂_{yy} and ∂_{yyyy}, respectively (see Fig. 9 for the coordinate axes). The usual diffusion (or Edwards-Wilkinson) and (linearized) Cahn-Hilliard (or Mullins) equations result. From Eqs. (4.18) and (4.19), the dispersion relations are obtained:

$$\text{model A:} \quad \mathrm{Re}[i\omega] = -2[1 - \cos(\phi)]H(\ell)G_A(\ell), \tag{4.20}$$

$$\text{model B:} \quad \mathrm{Re}[i\omega] = -4[1 - \cos(\phi)]^2H(\ell)G_B(\ell), \tag{4.21}$$

and $\mathrm{Im}[i\omega]=0$. At long wavelength $\phi \to 0$, $\mathrm{Re}[i\omega] \sim -\phi^2$ is found in model A and $\mathrm{Re}[i\omega] \sim -\phi^4$ in model B. Therefore, for long enough wavelengths [i.e., $\phi^2 \ll G_A(\ell)/G_B(\ell)$], the nonconserved contribution (model A) always dominates. Nevertheless, we must remember that at short wavelengths [i.e., $\phi \sim O(1)$] the balance between the two contributions depends on the precise microscopic components of the model.

Now, consider the specific case of the step flow model (steps recede due to a net surface desorption) with interlayer exchange as introduced at the beginning of the present section. The step velocity of a uniform train is modified from Eq. (4.7) to

$$\bar{V} = -\frac{\Omega c_{eq}\mathcal{L}}{\tau}\frac{d_- + 2\mathcal{L}}{d_- + \mathcal{L}} \tag{4.22}$$

with the cutoff length

$$\mathcal{L} = x_s \tanh(\ell/x_s) \approx \min(\ell, x_s), \tag{4.23}$$

which has the same form as that introduced in Eq. (3.10). The dispersion relation reads [following from the analog of Eq. (4.5) after including the ES effect]

$$\mathrm{Re}[i\omega] = 2\left(\frac{\Omega c_{eq}^0 d_-}{2\tau}\partial_\ell B - \bar{V}\frac{A}{\ell^4}\right)(1 - \cos\phi) - 4\Omega c_{eq}^0 DB\frac{A}{\ell^4\mathcal{L}}(1 - \cos\phi)^2,$$

$$\mathrm{Im}[i\omega] = i\sin\phi\,\partial_\ell\bar{V}, \tag{4.24}$$

where

$$B = 1/(1 + d_-/\mathcal{L}). \tag{4.25}$$

The coefficient B which multiplies the diffusion constant D in Eq. (4.24) accounts for the kinetic slowing down of adatoms diffusing across the steps: the steps introduce an extra barrier to surface diffusion.

The dispersion relation (4.24) has the generic form

$$\mathrm{Re}[i\omega] = a_2[1 - \cos(\phi)] - a_4[1 - \cos(\phi)]^2, \tag{4.26}$$

with $a_4 > 0$. This dispersion relation is a combination of models A and B introduced above. This form arises whenever the step velocity is a function of the nearest- and next-nearest-neighboring step positions and when the basic state (i.e., the uniform vicinal surface) possesses translational invariance.

From the behavior of $\mathrm{Re}[i\omega]$ as plotted in Fig. 31, the results of the linear stability can be summarized in the following three categories:

(i) If $a_2 < 0$, the train of steps is stable (the lowest curve in Fig. 31). Stabilization is most efficient for the pairing mode $\phi = \pi$. The typical time for stabilization of the pairing mode is $t_s = -2\pi/\mathrm{Re}[i\omega]|_{\phi=\pi}$. It is expressed as

$$t_s = \pi/(2a_4 - a_2). \tag{4.27}$$

The mode $\phi = 0$ is always marginally stable since $\mathrm{Re}[i\omega] = 0$. This is traced back to the translational invariance of the uniform train and corresponds to a global shift of the train.

(ii) If $0 < a_2 < 2a_4$, there is a range $0 < \phi < \phi_c$ of unstable modes (i.e., $\mathrm{Re}[i\omega] > 0$), as shown by the middle curve in Fig. 31. ϕ_c and the most unstable mode ϕ_m are calculated by

$$\phi_c = \arccos(1 - a_2/a_4), \quad \phi_m = \arccos(1 - a_2/2a_4). \tag{4.28}$$

The typical time for the appearance of the instability is $t_m = 2\pi/\mathrm{Re}[i\omega]|_{\phi=\phi_m}$. We find

$$t_m = 2\pi 4a_4/a_2^2. \tag{4.29}$$

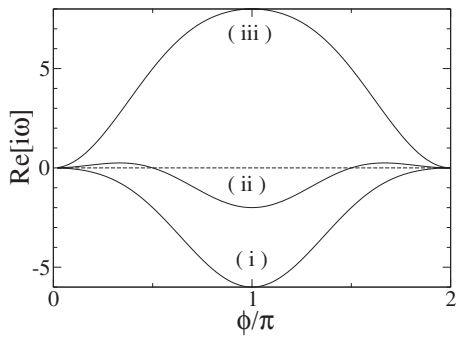

FIG. 31. The dispersion relation (4.26) for the three different cases: (i) $a_2 < 0$, (ii) $0 < a_2 < 2a_4$, and (iii) $a_2 > 2a_4$.

(iii) When $a_2 > 2a_4$, all modes are unstable, as shown by the top curve in Fig. 31. The most unstable mode is $\phi = \pi$, with

$$t_m = \pi/(a_2 - 2a_4). \tag{4.30}$$

The linear analysis provides us with information on the initial stability or instability against small perturbations and on typical time and length scales that are likely to grow first. Because $a_4 > 0$, a fact which is related to the stabilizing effect of the elastic interactions with A, the instability occurs at long wavelengths (small ϕ) in the vicinity of the instability threshold (where a_2 is small). This result introduces a small parameter $\sim\phi$ that renders a systematic nonlinear expansion possible. Next we analyze the nonlinear evolution.

5. The Benney equation: A compromise between solitons and spatiotemporal chaos

Following the same lines as in Sec. III, we perform a systematic nonlinear expansion which allows derivation of simplified nonlinear equations from the initial full BCF model. This task will also allow us to put dynamics into a more general context.

The first step consists of identifying the spatial and temporal scales in the vicinity of the instability threshold. Since the distance to the instability threshold vanishes when $a_2 = 0$, we define a small parameter

$$\epsilon = a_2/a_4 \tag{4.31}$$

around the threshold, with $a_2 > 0$. Then, from Eq. (4.28), the relevant mode for the bunching dynamics has a phase shift of $\phi \sim \phi_m \sim \phi_c \sim \epsilon^{1/2}$ with a characteristic time scale given by Eq. (4.29). Hence, the spatiotemporal scales at which the instability develops follow the scaling

$$t \sim 1/\mathrm{Re}[i\omega] \sim \epsilon^{-2}, \tag{4.32}$$

$$m \sim 1/\phi \sim \epsilon^{-1/2}. \tag{4.33}$$

Therefore, we expand the model equation with a finite ES barrier using Eqs. (4.32) and (4.33) together with the *Ansatz*

$$\zeta \sim \epsilon^{\vartheta}. \tag{4.34}$$

We then take the same general scaling arguments developed for meandering and look for the largest value ϑ_c of ϑ for which nonlinearities enter into play. We find $\vartheta_c = 1$ (i.e., $\zeta \sim \epsilon$) and the evolution equation reads at leading order in ϵ,

$$\partial_t \zeta_m = (\partial_\ell \bar{V})\Delta_1 \zeta_m - a_2 \Delta_2 \zeta_m - a_4 \Delta_4 \zeta_m + \tfrac{1}{4}(\partial_{\ell\ell}\bar{V}) \times [(\Delta_1 \zeta_{m+1})^2 + (\Delta_1 \zeta_{m-1})^2], \tag{4.35}$$

where $\bar{V}$ is given in Eq. (4.22) and $\Delta_1 \zeta_m = (\zeta_{m+1} - \zeta_{m-1})/2$. This equation may be called the discrete-advected Kuramoto-Sivashinsky (DAKS) equation.

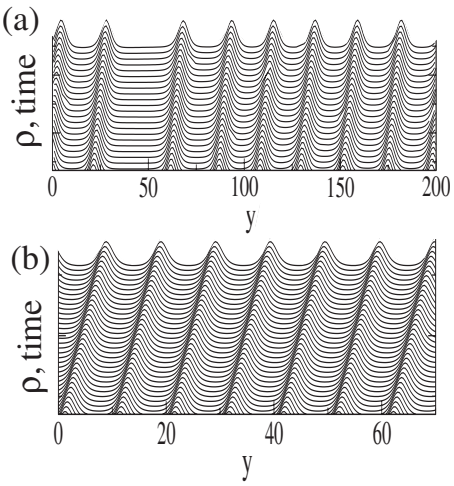

FIG. 32. Benney dynamics: (a) Dynamics of the step density $\rho = 1/\partial_y z$ [$z(y)$ is the surface profile] from the Benney equation (4.38) with $b = 24.6$. (b) Evolution of the step density ρ from the full solution of the step model for 200 steps [Eqs. (4.13) and (4.14)]. Parameters are chosen such that $D = 1$ and $\ell = 1$. We took $\tau = 0.28$, $A = 0.01$, $c_{\mathrm{eq}}^0 = 10$, and $\nu_- = 1$. These parameters lead to $b = 24.6$ from Eq. (4.40).

Since dynamics occurs at large scales, it is natural to take the continuum limit of the DAKS equation. To do so, define the "vertical" coordinate y, as indicated in Fig. 9(a), so that the mth step has a height $y = ma$, where a is the step height. The finite difference derivatives in Eq. (4.35) are then expanded to

$$\Delta_1 \zeta_m = a\partial_y \zeta(y) + (a^3/3!)\partial_{yyy}\zeta(y) + O(a^5) \tag{4.36}$$

and similarly for Δ_2 and Δ_4. Substituting these into Eq. (4.35) and absorbing $a(\partial_l \bar{V})\partial_y \zeta$ into a Galilean transformation, $y' = y - a(\partial_\ell \bar{V})t$, we obtain

$$\partial_t \zeta = -a_2 a^2 \partial_{y'y'}\zeta + (a^3/6)(\partial_\ell \bar{V})\partial_{y'y'y'}\zeta - a^4 a_4 \partial_{y'y'y'y'}\zeta + (a^2/2)(\partial_{\ell\ell}\bar{V})(\partial_{y'}\zeta)^2. \tag{4.37}$$

After dropping the primes and rescaling time, space, and amplitude, we find

$$\partial_T Z = -\partial_{YY} Z + b\partial_{YYY} Z - \partial_{YYYY} Z + (\partial_Y Z)^2, \tag{4.38}$$

where

$$T = \frac{a_2^2}{a_4} t, \quad Y = \left(\frac{a_2}{a^2 a_4}\right)^{1/2} y, \quad Z = \frac{(\partial_{\ell\ell}\bar{V})}{2a_2}\zeta, \tag{4.39}$$

and

$$b = (\partial_\ell \bar{V})/6(a_2 a_4)^{1/2} \sim \epsilon^{-1/2}. \tag{4.40}$$

Equation (4.38) is known as the Benney equation (Benney, 1966). The Benney equation is a combination of the Kuramoto-Sivashinsky (KS) equation [Eq. (3.26), encountered in the study of meandering] and the Korteweg–de Vries (KdV) equation [Eq. (2.108), with $\delta\rho \to Z$, introduced in the study of kinematic waves]. The KS equation shows spatiotemporal chaos, while the KdV equation exhibits solitons. The Benney equation is

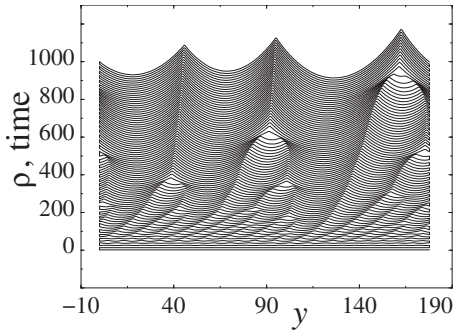

FIG. 33. Surface profile showing coarsening in a conserved system when dynamics is described by Eq. (4.41).

thus known to produce a transition from chaos to order upon increasing b. Its numerical solution is shown in Fig. 32(a). Since $b \sim \epsilon^{-1/2}$, we took a large value of b as $b = 24.6 \gg 1$ and ordered bunches appear as expected. We do not exclude the fact that the physical prefactor entering b might make b of order 1, in which case spatiotemporal chaos would prevail. This depends on physical systems, parameter ranges, etc.

It is interesting to note that a comparison between the solution of the Benney equation and the full solution (without any expansion and without taking the continuum limit) reveals good agreement as shown in Fig. 32. The Benney equation was derived in the context of bunching caused by electromigration (Sato and Uwaha, 1995; Misbah and Pierre-Louis, 1996), a topic discussed in Sec. IV.C. It was also derived in the context of step meandering under electromigration with a current oriented in a titled direction with respect to the step normal (Sato *et al.*, 1998).

B. Large diffusion length: Conserved dynamics—The conserved Benney equation

In most experimental situations, and especially on Si(111), desorption of adatoms is a rare event on the scales of interest. Therefore we do not expect the Benney equation in this case. Indeed, as in Sec. III.C, the quadratic nonlinearity $(\partial_y \zeta)^2$ should vanish since it is not a divergence of a flux. This is a consequence of mass conservation. This limit has been tackled by Gillet *et al.* (2001). It has been shown that in the limit of a large desorption length, if ES effect is weak, the surface profile obeys the following equation:

$$\partial_t \zeta = -\partial_{yy}[\zeta + b\partial_y \zeta + \partial_{yy}\zeta - (\partial_y \zeta)^2]. \tag{4.41}$$

This equation exhibits drastically different dynamics from that of the Benney equation. A typical profile is shown in Fig. 33. The profile undergoes a coarsening process. It was found numerically (Gillet *et al.*, 2001) that the wavelength increases as $t^{1/2}$ and the amplitude increases as t. The same equation appeared slightly earlier in the context of sand ripple formation (Csahók *et al.*, 2000). A heuristic analytical argument was given by Csahók *et al.* (2000) to show the $t^{1/2}$ coarsening behavior. A more recent study of this equation can be found in Frisch and Verga (2006). We note that the above equation does not always hold and it may happen that the equation is highly nonlinear (nonstandard regime), as encountered in the study of meandering in Sec. III.C (see Sec. IV.C.3.c for the analog situation regarding step bunching).

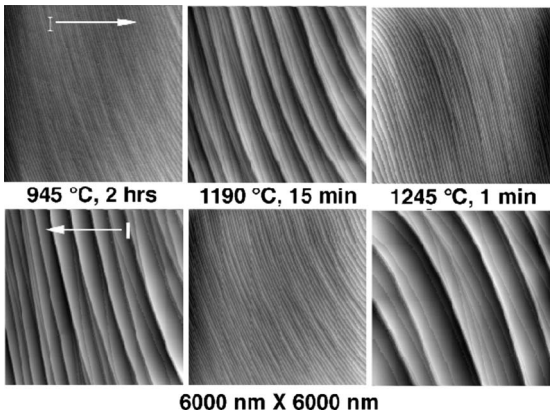

FIG. 34. STM observation of the Si(111) vicinal surface as a function of the direction of heating current (arrow) and the temperature range. In the upper panel the current is ascending ($I<0$) and thus the vicinal surface is stable in regimes I and III (left and right panels), while it is unstable in the middle range (regime II). Reversal of the direction of the electric current (lower panel) inverts the situation. From Yang *et al.*, 1996.

C. Migration

1. Observations on Si(111)

In 1989, Latyshev *et al.* (1989) investigated vicinal surfaces of Si(111) heated by the Joule effect due to a direct electric current. The current is perpendicular to the average step orientation. Depending on temperature and the sign of the electric current, bunches of steps may form (Fig. 34): the regular surface becomes unstable against step bunching. When the current is reverted, the vicinal surface is restored (it becomes stable). The current direction (up step or down step) for which bunching is observed depends on temperature. Métois and Stoyanov (1999) performed new experiments using a technique allowing the adaptation of supersaturation so that both growth and sublimation could be studied. A summary of the stability in the plane of parameters (supersaturation σ and the current I) is shown in Fig. 35.

Above the transition temperature T_R for $(7\times7)\rightarrow(1\times1)$ reconstruction ($T_R \approx 830\,^\circ$C), four different regimes are known. The diagram in Fig. 35(a) represents the results in the range $T_R < T < T_1$ (regime I) and $T_2 < T < T_3$ (regime III). In ranges I and III, the vicinal surface behaves qualitatively in the same manner. Figure 35(b) contains the results in the second temperature regime $T_1 < T < T_2$ (regime II), which differs from regimes I and III. Finally, at very high temperature $T > T_3$, bunching is observed during sublimation for an uphill current ($I<0$) and no instability is found for a downhill current. The only work which reports on this regime is

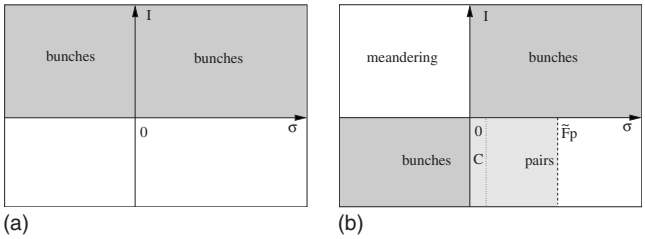

FIG. 35. Surface morphology of Si(111) under electromigration. $I>0$ for downhill current and σ is the supersaturation. $\sigma>0$ corresponds to growth and $\sigma<0$ corresponds to sublimation. (a) Temperature ranges I (low temperatures) and III (high temperatures). Bunching instability occurs irrespective of the supersaturation sign (no difference between sublimation and growth). (b) Intermediate temperatures, range II. The bunching instability critically depends on the sign of the supersaturation. There are also additional instabilities. The "pairs" region corresponds to the case where step pairs form, while in the "C" region small bunches are observed whose width does not increase with time. $\tilde{F}_p$ denotes a critical supersaturation below which step pairs form.

that of Latyshev *et al.* (1989). Note that the values of the transition temperatures mentioned above vary from one experiment to another due to the difficulty of measuring temperatures accurately at the surface $T_1=1000-1100\,^\circ$C, $T_2=1180-1250\,^\circ$C, and $T_3=1300\,^\circ$C. The transition temperatures also exhibit a weak dependence on the interstep distance (Degawa *et al.*, 2001).

The discovery of meandering (Degawa *et al.*, 1999) instability and pairing (Pierre-Louis and Métois, 2004) instability (shown in Fig. 36) further increases the complexity of the stability diagram. Furthermore, small bunches whose size did not increase (unlike all the other bunches which underwent coarsening) with time were also found during growth in range II (Pierre-Louis and Métois, 2004); region C in Fig. 35(b).

Note that in the late stages of the bunching instability antibands appear, i.e., there is an alternation between the usual bunches and bunches forming in the opposite direction (see Fig. 37). In range II, step meandering is also found to take place in the antibands. After a long time, bunches may become so large that they are visible in an optical microscope (Degawa *et al.*, 1999).

Under an ac heating electric current bunching was predicted to occur below a certain frequency (Houchmandzadeh *et al.*, 1994). This prediction was confirmed experimentally (Métois and Audiffren, 1997) and the result was used in order to estimate the effective charge of the drifting atoms along the vicinal surface (see the next section for a discussion on the effective charge).

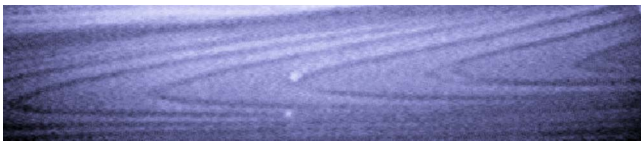

FIG. 36. (Color online) REM image of pairs of steps on Si(111) under dc current. From Pierre-Louis and Métois, 2004.

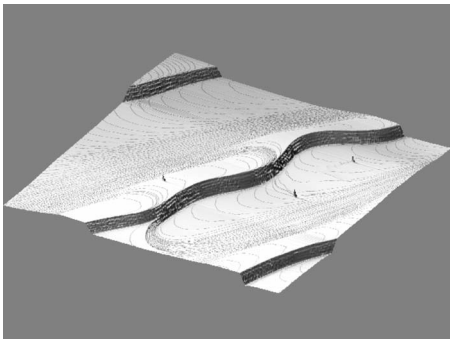

FIG. 37. Late-time morphology of bunches (the quite visibile macrsotep) with antibunches (less visible in between the macrosteps). Courtesy of E. D. Williams

Since surface stability depends on current direction, there is no doubt about the relevance of the heating current in the mechanism by which the instability takes place. Stoyanov (1990) suggested that electromigration, i.e., the drift of adatoms on the surfaces, is responsible for this instability.

Latyshev *et al.* (1989) observed that the size of the bunches increases with time (i.e., bunches undergo coarsening). Systematic analysis of the experimental evolution of bunches over time reveals that the size of the bunch behaves according to $t^{1/2}$ (Yang *et al.*, 1996). While bunches succumb to coarsening, step meandering occurring under a heating current seems to keep a constant wavelength (Degawa *et al.*, 1999).

Other experimental studies have focused on the slope and shape of the bunches. More precisely, the smallest terrace width $\ell_{\min}$ within a bunch is found to scale with the bunch size N (the number of steps within the bunch) as a power law: $\ell_{\min}\sim N^{-\alpha}$ (Fujita *et al.*, 1999). The exponent α varies slightly from one regime to another: $\alpha=0.68\pm0.03$ in regime II and $\alpha=0.60\pm0.04$ in regime III (both experiments were performed during sublimation).

Overall, it seems that surface evolution under a heating current is rich and complex, and this has given rise to a number of theoretical studies that we present in some detail hereafter.

2. The notion of electromigration

When a crystal is subjected to an electric current, defects and impurities may drift. The drift may be due to the fact that either atoms carry a real charge and/or to the transfer of momentum from the charge carriers in the metal or semiconductor to the mobile atoms. This phenomenon is called electromigration. Electromigration is an important problem since it is one of the major causes of collapse of many electronic circuits (Blech, 1976): migration of impurities, vacancies, etc., may accumulate at various junctions, weakening the device, which may then easily rupture at those sites. Although electromigration has been widely studied in crystal bulk, surface electromigration is still poorly understood.

We consider a mobile atom diffusing on a high symmetry surface. Two origins of the drift may be identified.

The first is a direct force $f_d = z_d eE$ on a charge carrier with an effective valence z_d under the electric field E and e is the absolute value of the electron charge. The second origin arises from the scattering of charge carriers on an atom (even neutral), resulting in a partial momentum transfer. The resulting force is known as wind force and will be denoted f_w. The wind force is easily calculated using a ballistic model (Fiks, 1959). Let n denote the electron (or hole) density at the surface, v their average velocity, λ their mean free path, and σ_a the cross subsection of the atom. The number of collisions per unit time is $\sigma_a n v_e$. We now assume that during each collision the electron transfers all its momentum $eE\tau$ to an atom, where $\tau = \lambda / v_e$ is the relaxation time of the electron. Then, we have $f_w = -(\sigma_a n v_e) eE\tau = -(\sigma_a n \lambda) eE$. An effective wind force valence z_w can be defined using $f_w = z_w eE$. We find for the effective valence,

$$z_w = -\sigma_a n \lambda. \tag{4.42}$$

In a metal, typically $n \sim 10^{-2}$ Å^3, $\lambda \sim 10^2$ Å, and $\sigma_a \sim 1$ Å^2. This leads to $z_w \sim -1$. From a more sophisticated model, Rous *et al.* (1994) calculated $z_w \sim -21$ on a Cu(111) surface. Thus, wind force seems to dominate over direct force. Further investigations of electromigration in the bulk (Bosvieux and Friedel, 1962; Turban *et al.*, 1976; Lodder, 1989) showed that there is a screening of the direct charge from the conduction electrons, meaning that direct force should vanish totally. Nevertheless, we cannot simply extend this result to the surface. A quantitative analysis of step fluctuations on Ag surfaces allowed one to extract the value of the migration force (Williams *et al.*, 2007). Surprisingly, a very strong migration force is found for atoms along steps, with $z_w \sim -10^2$.

On semiconductors, using bulk values for Si at 1150 °C (Kandel and Kaxiras, 1996) $n \sim 10^{-5}$ Å^3, $\lambda \sim 3$ Å, and $\sigma_a \sim 1$ Å^2, we find $z_w \sim -10^{-4}$. The smallness of the effective wind charge raises the question of the relevance of a direct force once again. Some attempts have been made to obtain a quantitative value for the effective charge (Kandel and Kaxiras, 1996), but the question, remains open for the surface of semiconductors. Indeed, Kandel and Kaxiras (1996) proposed that charge will change with temperature. This disagrees with experimental observations of the shape changes of a rectangular groove (Degawa *et al.*, 2000; Yagi *et al.*, 2001). Indeed, experiments showed that the direction of migration does not change with temperature. The electromigration force can also be derived indirectly from the observation of its consequences on step dynamics. Several works showed that the effective charge is positive and $z_w \sim 10^{-2}$–10^{-1} on Si(111) surfaces. These results may, for example, be obtained from the critical frequency for an oscillatory electric current to produce step bunching (Métois and Audiffren, 1997) or from the shape of steps that run between two bunches (Thürmer *et al.*, 1999).

From the Einstein relation, mobile adatoms on terraces drift at an average velocity[12] given by

$$v_e = Df/k_B T, \tag{4.43}$$

where $f = zeE$ is the total force. The linear relation (4.43) is accurate for small forces, and its form does not depend on the microscopic details of the migration process. The total mass flux on terraces (i.e., far from steps) which accounts simultaneously for diffusion and migration then reads

$$\mathbf{J} = -D\nabla c + c\mathbf{v}_e = D(-\nabla c + c/\xi \mathbf{e}_m), \tag{4.44}$$

where $\xi = k_B T/f$ is a length scale characterizing migration and $\mathbf{e}_m$ is a unit vector pointing in the direction of the migration force. Other effects may come into play on Si surfaces, such as microvacancy diffusion and migration, as studied by Misbah *et al.* (1995). We shall not consider this effect here, although it may have important consequences on the stability of the surface.

3. Opaque steps and highly nonlinear continuum equations and facets

Because the various scenarios of the Si(111) instability cannot be described by a single model in all temperature ranges, several authors were led to introducing new ingredients related to the fact that steps may be opaque (the usual picture, meaning that atoms are absorbed at a step site) or transparent (atoms may not be absorbed at a step but wander around several steps before absorbtion). It seems that adopting the opaque picture in ranges I and III and the transparency assumption in range II allows the various scenarios to be described. It should be stated that the link between transparency or opacity and the atomistic description is not obvious and it is quite astonishing *a priori* that by further increasing the temperature (range III) the steps become opaque.

a. Mechanism of the instability

As Eq. (4.11) reveals, the basic ingredient for the occurrence of instability is the presence of an asymmetric dependence of step motion on the width of the neighboring terraces. Therefore, electromigration may be viewed as a bias which induces an effective ES effect. This effective ES barrier may lead to an instability which is similar to that mentioned in Sec. IV.A.1. The effective value of the ES effect due to electromigration can be calculated quantitatively, as shown by Houchmandzadeh *et al.* (1994).

To be more precise we use a heuristic argument. Consider a 1D conserved model under electromigration with neither adsorption nor desorption. The steps are considered to be straight and perpendicular to the z axis. The migration force is taken to be along the z axis: $\mathbf{e}_m = \hat{\mathbf{z}}$. The motion of the steps results from mass exchange between steps themselves via terrace diffusion and drift due to electromigration. On each side of the step, at-

[12] We have assumed that the surface is isotropic for simplicity.

tachment is proportional to the local concentration, while detachment occurs at a fixed rate. Assuming symmetric kinetics [which is probably valid for Si(111) surfaces at a high enough temperature, as mentioned in Sec. IV.C.1], at the steps we have

$$\mathbf{J}_+ \cdot \mathbf{n} = -D\partial_z c_+ + Dc_+/\xi = -\bar{\nu}(c_+ - c_{\rm eq}),$$
$$\mathbf{J}_- \cdot \mathbf{n} = -D\partial_z c_- + Dc_-/\xi = \bar{\nu}(c_- - c_{\rm eq}), \tag{4.45}$$

where $\bar{\nu}$ is a kinetic coefficient, $\mathbf{J}_\pm$ are the mass fluxes (4.44) on both sides of the step, and $\mathbf{n}=\hat{\mathbf{z}}$ is the normal to the steps. Mass conservation at the steps reads

$$V = -\Omega(\mathbf{J}_+ - \mathbf{J}_-)\cdot\mathbf{n} = \Omega\bar{\nu}[(c_+ - c_{\rm eq}) + (c_- - c_{\rm eq})]$$
$$= 2\Omega\bar{\nu}(\bar{c} - c_{\rm eq}), \tag{4.46}$$

where

$$\bar{c} = (c_+ + c_-)/2 \tag{4.47}$$

is the average step concentration.

In the quasistatic approximation, concentration on the terraces is assumed (on step motion time scales) to reach a steady state. Therefore, $\nabla\cdot\mathbf{J}=0$, where the mass flux $\mathbf{J}$ is given by Eq. (4.44). Within our 1D description, this can be written as

$$D\partial_{zz}c - (D/\xi)\partial_z c = 0. \tag{4.48}$$

Consider the case where attachment-detachment kinetics at steps are slow. Adatoms have ample time to diffuse on the terrace before being incorporated into the steps. Thus, a steady state is reached on terraces where the mass flux is small: $\mathbf{J}\approx 0$. Using Eq. (4.44), this reads $\partial_z c - c/\xi \approx 0$. We also consider a very small migration force, so that concentration is only slightly perturbed: $c \approx c_{\rm eq}$. Hence, $\partial_z c \approx c_{\rm eq}/\xi$. For clarity, we also disregard the stabilizing effect of elastic interactions and set $c_{\rm eq} \approx c_{\rm eq}^0$ accordingly. We thus find that the concentration gradient on the terraces is constant and does not depend on the terrace width:

$$\partial_z c \approx c_{\rm eq}^0/\xi. \tag{4.49}$$

The concentration on a terrace then varies linearly with z:

$$c \approx c_{\rm eq}^0(1 + z/\xi). \tag{4.50}$$

Moreover, since adsorption and desorption are neglected on the terraces, the average concentration must be $c_{\rm eq}^0$. Therefore we should place the origin $z=0$ in the middle of the terrace, so that $\ell^{-1}\int dz c = c_{\rm eq}^0$ on a terrace of width ℓ. The average concentration (4.47) at a step then reads

$$\bar{c} \approx c_{\rm eq}^0[1 + (\ell_- - \ell_+)/4\xi]. \tag{4.51}$$

Finally, using Eq. (4.46) for the speed of the mth step we have

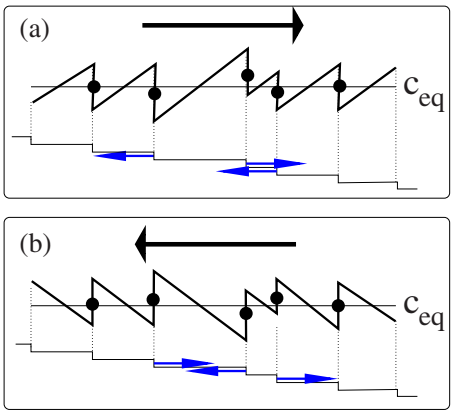

FIG. 38. (Color online) Instability of a vicinal surface under migration. The sawtoothlike profile (4.50) of the concentration is plotted. Black dots indicate the average concentration $\bar{c}$ at the steps. If $\bar{c} > c_{\rm eq}$ ($\xi>0$), the step moves forward, and if $\bar{c} < c_{\rm eq}$ ($\xi<0$), it moves backward. The surface is (a) destabilized for downhill migration and (b) stablilized for uphill migration. The large arrow shows the migration direction and the small ones indicate step motion.

$$V_m \approx (\Omega c_{\rm eq}^0\bar{\nu}/2\xi)(\ell_- - \ell_+)$$
$$= -(\Omega c_{\rm eq}^0\bar{\nu}/2\xi)(\zeta_{m+1} + \zeta_{m-1} - 2\zeta_m). \tag{4.52}$$

Schematics of the instability in terms of microscopic step motion are shown in Fig. 38. $V_m = \partial_t\zeta_m$ and the finite difference becomes $\sim\partial_{zz}\zeta$ in the continuum limit so that the above equation becomes a diffusion equation with the diffusion constant $\sim -\Omega c_{\rm eq}\bar{\nu}/2\xi$. This is negative if $\xi>0$ (descending direction) and positive if $\xi<0$. This means that there is instability if $\xi>0$ and stability if $\xi<0$. Note that we could also perform a stability analysis on the discrete version, as in Sec. IV.A.3. The fastest mode is the $\phi=\pi$ mode.

b. Nonlinear nonconserved dynamics: The Benney equation

The electromigration process is often accompanied by a strong Joule heating process induced by the electric current. As reported in Sec. IV.C.1, the substrate temperature sometimes exceeds 1000 °C. At such temperatures, desorption of atoms from the surface to the atmosphere (or vacuum) is not negligible. At high temperatures, where desorption is large enough, it is also likely that the ES effect is weak, so that the instability discussed in Sec. IV.A induced by the ES effect is irrelevant. Hence instability is basically expected to be driven by electromigration only. The linear stability of the model equations was first studied by Stoyanov (1990). The nonlinear dynamics are studied by means of a multiscale analysis, following the same lines as in Sec. IV.A. We obtain the same DAKS equation (4.35) of step evolution in a discrete step picture. Under growth or sublimation where the steps are moving at a finite average velocity, the evolution equation acquires a term proportional to $\Delta_1\zeta_m$ and nonlinear terms $\sim(\Delta_1\zeta_{m\pm1})^2$. As exemplified in Eq. (4.52), electromigration leads to the term $\sim\Delta_2\zeta_m$, which governs the instability of the mor-

phology. Step repulsion always gives a stabilizing contribution represented here by the term $\sim\Delta_4\zeta_m$. In a continuum limit, the form of the final equation is identical to the Benney equation (4.38) (Sato and Uwaha, 1995; Misbah and Pierre-Louis, 1996). The length scales and time scales on which Benney dynamics are relevant depend on the parameter values. We shall not, however, dwell on this question.

Note that by "nonconserved" we do not only mean "sublimation" but also that the diffusion length x_s is small (or of the same order) compared to length scales of interest. The opposite situation enters the class of conserved dynamics since sublimation appears just as an additive global term in the evolution equation (Gillet *et al.*, 2001), like a negative flux F in MBE.

c. Nonlinear conserved dynamics: A highly nonlinear continuum equation and facets

If no allowance is made for desorption, and in the quasistatic limit (as adopted throughout this review), mass conservation imposes

$$V_m = -J_m + J_{m-1}, \tag{4.53}$$

where J_{m-1} and J_m are the mass fluxes at the mth step from the left and right terraces, respectively. This conservation constraint drastically changes the nonlinear dynamics of the surface. We saw in Sec. IV.B that in the limit of fast kinetics and under growth, the evolution equation is given by the conserved Benney equation which leads to coarsening. In the general situation, analysis may require special treatment. For example, we may find a somewhat similar situation to that encountered in the study of step meandering in the zero desorption limit, described in Sec. III.C. Indeed, it may happen that (Chang *et al.*, 2006) the dynamics are highly nonlinear (nonstandard regime) and $\zeta\sim\epsilon^{-1/2}$, making a weakly nonlinear analysis illegitimate. Since we have electromigration in mind, we stick to this situation and discuss the appropriate evolution equation. The evolution equation obtained from the multiscale analysis is (Chang *et al.*, 2006)

$$\partial_t\zeta = -a\partial_y\left[\frac{\Omega D c_{\rm eq}^0}{1+d\rho}\left(\frac{1}{\xi} - A\rho a^2\partial_{yy}\rho^3\right)\right], \tag{4.54}$$

where $\rho=1/(\ell+a\partial_y\zeta)$ is the local step density, A is the elastic interaction parameter, and $d=2D/\nu$. It can be checked that if d is small enough and if there is weak desorption (or growth), then the front profile equation reduces to Eq. (4.41), derived by Csahók *et al.* (1999) and Gillet *et al.* (2001), otherwise the highly nonlinear equation (4.54) results. This is the nonstandard regime. More details are given by Misbah *et al.* (2008).

The above equation quite naturally follows from an elementary consideration. From Eq. (4.53) in a continuum limit, we must have $\partial_t\zeta=-a\partial_y J$, where the mass flux J contains one contribution from electromigration and one from elasticity. The electromigration current (see also Sec. IV.C.3) is from Eq. (4.45) given as $\sim Dc_{\rm eq}^{(0)}/\xi$. The contribution due to elasticity appears in the equilibrium concentration as Eq. (4.3). In the continuum limit where $l_m=1/\rho$, the elastic contribution in $c_{\rm eq}$ is proportional to $A(\ell_m^{-3}-\ell_{m-1}^{-3})\to Aa\partial_y\rho^3$. The stabilizing flux on a terrace is therefore proportional to $(D/\ell_m)(c_{\rm eq}^{m+1}-c_{\rm eq}^m)\to D\rho a^2 c_{\rm eq}^0 A\partial_{yy}\rho^3$. Finally, we must remember (see also Sec. IV.C.3) that the bare diffusion constant D must be replaced by $DB=D/(1+d\rho)$ stating that diffusion is reduced by the presence of steps due to noninstantaneous kinetics at the steps. The evolution equation (4.54) follows naturally.

The set of periodic steady-state solutions of Eq. (4.54) can be analyzed (Chang *et al.*, 2006). Because of the special form of Eq. (4.54), the explicit value of the flux for any periodic steady state can be calculated from a simple integration over one period. In a steady state the flux in the partial derivative by y on the rhs of Eq. (4.54) is constant and equal to $\bar{J}$. Integrating $\bar{J}(1/\rho+d)$ along y on a distance Na (or equivalently along z on a width Λ by incorporating $dy/dz=\rho a$) gives

$$\frac{\bar{J}}{\Omega D c_{\rm eq}^0}(\Lambda+Nd) = \frac{\Lambda}{\xi} - Aa(\partial_y\rho_+^3 - \partial_y\rho_-^3), \tag{4.55}$$

where $\partial_y\rho_\pm^3$ are the values of $\partial_y\rho^3$ at the boundaries of the integration domain. If integration is performed over one period or $\Lambda=\lambda$, we have $\partial_y\rho_+^3=\partial_y\rho_-^3$ and $N/\Lambda=\bar{\rho}$ is the average slope. Finally, the flux of a steady state is obtained by

$$\bar{J} = \frac{\Omega D c_{\rm eq}^0}{1+d\bar{\rho}}\frac{1}{\xi}, \tag{4.56}$$

which generalizes the law derived by Liu *et al.* (1998) from a phenomenological argument within the limit of a large d. An important result can be drawn from Eq. (4.56): the flux $\bar{J}$ only depends on the average slope $\bar{\rho}$ and not on the precise surface profile. Therefore, $\bar{J}$ is the same for all periodic steady states of a given surface. Under this constant flux $\bar{J}$, various properties of the periodic steady states of Eq. (4.54) are determined by Chang *et al.* (2006), whose main results will be summarized shortly. The wavelength λ as a function of the size of the largest terrace L_0 (proportional to the inverse of the smallest slope in the period) is given in Fig. 39(a). The wavelength of the continuum steady-state solutions is always smaller than the critical wavelength λ_c [defined by $\mathrm{Re}(i\omega)=0$] since for $\lambda>\lambda_c$ the basic trivial solution is linearly unstable. On the basis of the results reported by Politi and Misbah (2004)—which are presented in Sec. V.C.2—one is tempted to say that a frozen wavelength of the bunches should be observed instead of coarsening.

The real behavior of the branch of steady-state solutions turns out to be more subtle. Inspection of the density profile computed from Eq. (4.54) reveals the existence of cusps, as shown in Fig. 39(b). A cusp position corresponds to a height y of very small step density or large isolated terraces. This hints that the surface splits into bunches separated by wide terraces instead of having a gradual density profile. This result is confirmed by

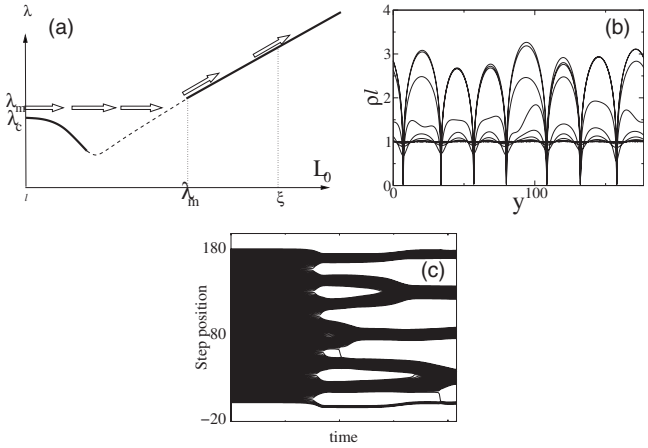

FIG. 39. A step bunching scenario for conserved systems. (a) Wavelength λ of the periodic steady-state solutions as a function of the largest terrace width L_0. The solid line represents the steady state obtained by solving the continuum and semicontinuum models, as explained in Sec. IV.C.3, Eq. (4.53). The arrows show that, in principle, for $\lambda > \lambda_m$ the system will choose the ascending branch; the arrows also show the path followed by the system upon coarsening. The solid decreasing part of the curve is not essential since the system does not explore it; it is an unstable branch. (b) Time evolution of the local step density ρ obtained by the numerical integration of the nonlinear equation (4.54). (c) Full evolution of step positions in conserved dynamics.

the full solution of the step model as shown in Fig. 39(c). Since wide terraces form in the course of time, the continuum description of the surface profile should break down. This singular behavior may be analyzed by means of a semicontinuum approach. We consider wide isolated terraces coupled with a bunch in which step density is treated in the continuum limit. The boundary conditions at the edge of the bunches are extracted from the full step model (Chang *et al.*, 2006). From this model, which explicitly takes into account dense regions (treated in the continuum limit) and wide terraces (treated in a discrete manner), the wavelength of the periodic steady states is calculated and shown in Fig. 39(a). As a function of the width of the largest terrace L_0, the periodicity λ of the steady states exhibits a minimum. We expect endless coarsening (as discussed in Sec. V.C.2).

Figure 39(a) shows three different regimes. The first regime corresponds to the situation where $\lambda_m \ll L_0 \ll \xi$, in which

$$\lambda_m = 2\pi[6A\xi\bar{\rho}^3 a^2(\bar{\rho} + 1/d)]^{1/2} \tag{4.57}$$

is the wavelength of the linearly most unstable mode (Chang *et al.*, 2006). It is also found that the width of the largest terrace L_0 is greater than that of the bunch W as $L_0 \gg W$. Hence, $N = \bar{\rho}(W + L_0) \approx \bar{\rho} L_0$. Moreover, $\bar{J}$ still obeys the generalized Liu-Weeks relation (4.56). A systematic analysis of this regime (Chang *et al.*, 2006) yields the following scaling:

$$W \sim N^{1/3} \lambda_m^{2/3} \bar{\rho}^{-1/3}, \tag{4.58}$$

$$L_{\min} \sim N^{-2/3} \lambda_m^{2/3} \bar{\rho}^{-1/3}, \tag{4.59}$$

$$L_1 \sim N^{-1/3} \lambda_m^{2/3} \bar{\rho}^{-1/3}, \tag{4.60}$$

where W is the bunch width, $L_{\min}$ is the width of the smallest terrace in the bunch, and L_1 is the width of the terrace at the border of the bunch. Interestingly, the bunches are abrupt, which means that there is no tangential matching (no zero slope at the facet) between the bunch and the terrace. In the limit of very large bunches $L_0 > \xi$, which we refer to as the second regime, and if $N \gg \xi^{3/2} A^{-1/2}$ (Chang *et al.*, 2006),

$$\bar{J} \sim N^{-1/2}, \tag{4.61}$$

$$W \sim \xi^{5/6} A^{1/18} N^{1/2}, \tag{4.62}$$

$$L_{\min} \sim (A\xi)^{1/4} N^{-1/2}. \tag{4.63}$$

This means that Eq. (4.56) is no longer valid. Indeed, it appears that this equation relies on the assumption that all terrace widths are smaller than ξ. Using orders of magnitude that are adapted to the case of Si(111), we find that $N \gg \xi^{3/2} A^{-1/2}$ implies $N \gg 10^{12}$, which is unreasonably large. Therefore, this regime, though interesting from a conceptual point of view, is not relevant to Si(111) experiments. We cannot exclude this regime *a priori* for other systems, such as metals. Finally, it is worth noting that there is an additional intermediate regime where $L_{\min} \sim N^{-1/3}$ [see Chang *et al.* (2006)].

The first regime [Eqs. (4.58) and (4.59)] was studied by Liu *et al.* (1998), Stoyanov and Tonchev (1998), and Sato and Uwaha (1999). It should be mentioned that they did not use the boundary condition at bunch edge by analyzing the matching between bunch and terrace (as discussed in this section). Careful analysis, however, reveals that the scaling (4.58) and (4.59) is not altered and only the numerical prefactor is different (Chang *et al.*, 2006).

Stoyanov and Tonchev (1998) and Sato and Uwaha (1999) studied the limit of fast attachment kinetics $d\bar{\rho} \ll 1$. The important point is that the maximum slope $L_{\min}$ (as seen above) does not depend on $\bar{\rho}$ in this limit, unlike Eqs. (4.58) and (4.59) (however, scaling with the other parameters remains the same). The opposite limit of slow attachment kinetics has been studied by Liu *et al.* (1998). They found that the maximum slope $L_{\min}$ depends on $\bar{\rho}$ and is therefore a function of the position of the neighboring bunches. In both cases of fast and slow attachment kinetics regimes, $L_{\min} \sim N^{-2/3}$ as in Eq. (4.59). Quantitative comparisons of bunch thermal relaxation with experiments on Si(111) (Liu *et al.*, 1998) seem to indicate that attachment kinetics are slow. Moreover, the scaling of the smallest terrace size $L_{\min}$ was confirmed experimentally by Fujita *et al.* (1999). The scaling of the width of the first terrace L_1, given by Eq. (4.60), has not yet been measured experimentally, as far as we know.

Finally, we discuss the time dependence of bunch size. While a full analysis can be made from the step dynamics equations (Sato and Uwaha, 1999), here we have cho-

sen to present a heuristic argument that does not need the model equation to be specified. This argument was presented by Liu *et al.* (1998). The crux of their analysis is the assumption that dynamics depend on a unique length scale, which we consider to be the typical number of steps in the bunch $N \sim t^{\beta}$. We then expect both mass flux $\bar{J}$ and surface profile z to be described by the self-affine *Ansätze*,

$$J(y,t) = t^{\alpha_J} \mathcal{J}(y/t^{\beta}), \tag{4.64}$$

$$z(y,t) = t^{\alpha_\zeta} \mathcal{Z}(y/t^{\beta}). \tag{4.65}$$

These scaling forms are constrained by two relations. First, from Eq. (4.56), $J=\bar{J}$ is constant (as discussed above, this is valid in the experimentally relevant regime, where $L_0 \ll \xi$). Using Eq. (4.64), the relation $J=\bar{J}$ suggests $\alpha_J=0$. As a second constraint, the average slope $\bar{\rho}$ is fixed. This latter property may be written as $\langle \partial_y z \rangle = 1/\bar{\rho}$, where $\langle\ \rangle$ denotes a spatial average along y. Substitution into Eq. (4.65) now suggests $\alpha_\zeta = \beta$. Using these *Ansätze* in mass conservation, written as

$$\partial_t z(y,t) = -\partial_y J(y,t), \tag{4.66}$$

we find $\beta = 1/2$. This result is in agreement with experiments (Yang *et al.*, 1996).

d. Hierarchical bunching

It was first noticed by Sato and Uwaha (1998) that step bunching might occur via a scenario where steps initially form pairs and then pairs may form quadruplets, which in turn coalesce to produce increasingly larger bunches [see Fig. 39(c)]. The analysis of Sato and Uwaha (1998) was made under global equilibrium conditions (neither growth nor sublimation, but only electromigration inducing mass transport from one step to the other). This inverted-tree-like scenario is found to occur when elastic interactions are sufficiently weak. In the regime of weak elasticity, it is known that the linearly most unstable mode is the step pairing mode (in this regime all modes are unstable); see Sec. IV.A.4. In principle, we should expect step pairing to occur first. The parameters used by Sato and Uwaha (1998) create the regime where all modes are unstable, and the initially fastest growing mode is the pairing mode.

In this scenario, the bunches maintain their identity: bunches are distinctly separated from each other. Therefore, the resulting dynamics may be analyzed with the help of the semicontinuum description of Sec. IV.C.3.c. Their regime corresponds to that described by the scaling equations (4.58) and (4.59).

D. Differential diffusion and step transparency

The existence of regime II observed in the Si(111) experiment as described in Sec. IV.C cannot be explained using the previous model. An *a priori* quite natural assumption is that the effective charge changes sign in regime II (Kandel and Kaxiras, 1996). This assumption is ruled out by the experiment of Degawa *et al.* (2000). Another alternative is the activity of advacancies (Misbah *et al.*, 1995) that naturally explains the change of regime. At present it is not easy to experimentally test this idea. Another idea which has been put forward is that the step may be viewed as "transparent" in regime II (Stoyanov and Tonchev, 1998): in this image they suggest that adatoms visit many terraces before attaching to the crystal phase or leaving the surface by sublimation. Perfect transparency would mean that concentration is continuous at the steps, $c_+ = c_-$. Actually, another process which could force $c_+ = c_-$ is that atoms attach instantaneously to the step regardless of the side from which they arrive (upper or lower terrace). This limit means $\nu_+ = \nu_- = \infty$ (fast attachment from both sides of a step). Referring to Eqs. (4.45), this implies $c_+ = c_{\rm eq}$ and $c_- = c_{\rm eq}$, and hence $c_+ = c_-$. This idea explains the occurrence of step bunching in regime II during sublimation and growth (Pierre-Louis, 2003a). This theory does not, however, explain the simultaneous occurrence of both bunching and meandering, as seen experimentally [see Fig. 35(b)]. For that purpose, it has been argued (Zhao *et al.*, 2004) that there should still be finite kinetics attachment at the step [ν_+ and ν_- are finite; symmetric attachment is assumed $\nu_+ = \nu_- = \nu$ (Zhao *et al.*, 2004)] in regime II, but that adatom diffusion in the step zone becomes faster than that in the terrace (diffusion is enhanced in the vicinity of the step). This may be called the *differential diffusion* model. As shown by Zhao *et al.* (2004) this results in *negative* kinetic coefficient ν. This idea has accounted for the occurrence of meandering in regime II. Nevertheless, the formation of pairs, as seen experimentally in regime II [see Fig. 35(b)], could not be captured by this model.[13] Based on the same physical ingredient of differential diffusion, Pierre-Louis and Métois (2004) proposed that steps would be partially transparent and have a negative transparency kinetic coefficient. Such a model accounts for the observed formation of stable pairs in regime II. In addition, it was found recently (Pierre-Louis, 2006) that a variation of the migration force in the vicinity of the steps would have similar consequences as the differential diffusion hypothesis.

Partial transparency has been considered (Sato *et al.*, 2000; Pierre-Louis, 2003b). The modification brought by transparency is that boundary conditions (4.45) transform to

$$\begin{aligned} \mathbf{n}\cdot\mathbf{J}_+ &= -\nu_+(c_+ - c_{\rm eq}) - \nu_0(c_+ - c_-), \\ \mathbf{n}\cdot\mathbf{J}_- &= \nu_-(c_- - c_{\rm eq}) - \nu_0(c_+ - c_-), \end{aligned} \tag{4.67}$$

where ν_0 is a transparency coefficient. $\nu_0 = 0$ means opaque steps, while $\nu_0 \to \infty$ imposes $c_+ = c_-$, meaning perfectly transparent or permeable steps. In the latter case, a combination of the above two equations and the use of

[13] Note that the pairing evoked by Zhao *et al.* (2004) simply means that the mode corresponding to a phase shift $\phi = \pi$ is the most unstable one, but the nonlinear dynamics does not select step pairing, contrary to the explanation provided.

the mass conservation law (4.46) lead to [see Eq. (2.60)]

$$c_+ = c_- = c_{\rm eq}^* = c_{\rm eq}^0(1 + \mu/k_BT + \beta V), \tag{4.68}$$

where μ accounts for other contributions (e.g., elasticity) to the concentration, and

$$\beta = 1/c_{\rm eq}^0 D\Omega(d_+^{-1} + d_-^{-1}) \tag{4.69}$$

is the kinetic coefficient. A generalization of these boundary conditions has been given by Pierre-Louis (2003a, 2006). Relation (4.68) allows for another interpretation of the transparency. When $\beta=0$, meaning that step attachment-detachment kinetics are fast on both sides, then concentration at the step (on both sides) is at local equilibrium. Conversely, when the kinetic coefficient β is large, the above boundary condition means that the concentration at the step may vary due to nonequilibrium conditions, but it is kept permanently at the same values on both sides of the steps.

1. The instability mechanism

In a perfectly transparent case, concentration is continuous across the steps (i.e., $c_+=c_-$) and the instability mechanism depicted in Sec. IV.C.3.a (Fig. 38) cannot be invoked. Indeed, in the absence of growth and sublimation, the surface is linearly stable since atom fluxes equilibrate due to transparency. The situation is quite different, however, under growth or sublimation. The number of atoms per time unit landing on a terrace depends on the terrace size (the larger the terrace, the larger the amount of mass). Figure 40 summarizes this situation. Here we have an instability only for downhill migration during growth and only for uphill migration during sublimation. This is consistent with observations in regime II (Sec. IV.C).

An interesting consequence of transparency with a finite kinetic coefficient β is the occurrence of the instability at a well-defined (and maybe long) wavelength even in the absence of step-step repulsion (Liu *et al.*, 1998). We ignore elasticity for the moment. With transparency, it is found that instead of the dispersion relation shown in Fig. 31, the dispersion relation takes the form given in Fig. 41. In the opaque regime $\nu_0=0$, all modes are unstable, and the maximum growth rate is at $\phi=\pi$ as shown by the black curve in Fig. 41. With finite transparency coefficient ν_0, all modes are unstable but the maximum growth rate occurs at a small ϕ. This results from the fact that the destabilizing effect related to step transparency is weaker for short wavelengths (like $\phi=\pi$) since atoms can equilibrate more easily from one terrace to another. Since the most unstable modes are those with long wavelengths (and not the pairing mode), we do not expect a hierarchical bunching scenario as for opaque steps.

Transparency has another consequence on the scaling laws. Remember that in the opaque regime (Sec. IV.C.3), the minimal terrace width within the bunch, for example, has a scaling property $L_{\rm min}\sim N^{-2/3}$. Stoyanov and Tonchev (1998) analyzed the scaling laws of bunches in this regime and proposed $L_{\rm min}\sim N^{-1/2}$ for close-to-equilibrium sublimation and $L_{\rm min}\sim N^{-3/5}$ for far-from-equilibrium sublimation. The latter result is in agreement with the experimental measurement of the bunch shape (Fujita *et al.*, 1999).

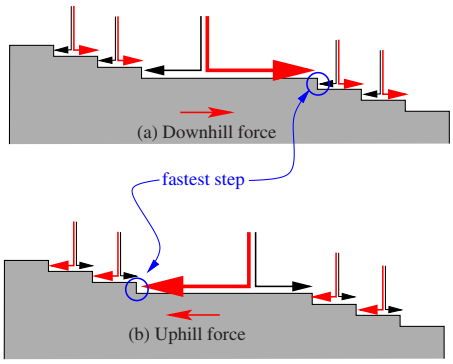

FIG. 40. (Color online) Schematic of the instability for fast step kinetics (either instantaneous step kinetics or strong step transparency) during growth and in the presence of migration. Atoms are deposited on terraces where they diffuse and attach to steps. The arrows indicate the mass flow of freshly landed atoms (i.e., atoms which have not yet reached a step). Their thickness is proportional to the amplitude of the mass flow. (a) A downhill migration force produces a downhill attachment bias on each terrace. We have assumed that one terrace is wider than its neighbors (for example, due to statistical fluctuations). The fastest step is indicated, showing that the large terrace widens for a downhill force, thereby leading to amplification of the surface perturbation, which gives rise to the instability. (b) An uphill migration force produces an uphill attachment bias. Following the same reasoning, the large terrace retracts for an uphill flux and the surface is stable. The situation is reversed during sublimation.

2. Pairs

If we consider a stable regime, for example, sublimation and downhill migration, the growth rate of a small perturbation is simply the opposite of that correspond-

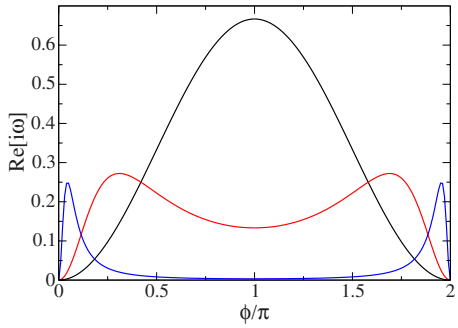

FIG. 41. (Color online) Dispersion relation for transparent steps under growth and downhill migration (or sublimation and uphill migration). In order to focus on the consequences of migration, the elastic interactions have been neglected (i.e., $A=0$). As transparency increases, the peak splits into two. For sublimation the corresponding curves are obtained by up-down symmetry ($\mathrm{Re}[i\omega]\rightarrow-\mathrm{Re}[i\omega]$). From Pierre-Louis, 2003b.

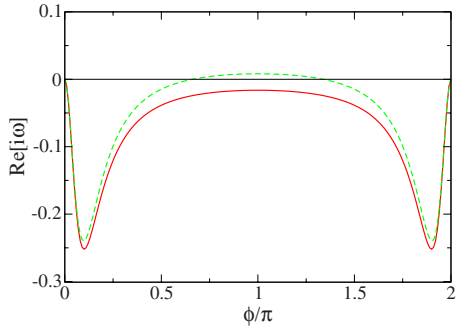

FIG. 42. (Color online) Dispersion relation for sublimation and downhill migration (Sec. IV.D.2). The solid curve is obtained from the curve in Fig. 41 from an up-down symmetry (Re[$i\omega$]→−Re[$i\omega$]). The dashed curve is obtained by slightly reducing transparency; opacity favors $\phi=\pi$ as we know from Sec. IV.C.3.a.

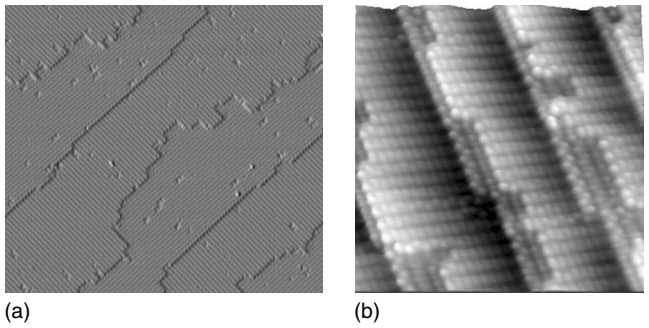

FIG. 43. STM images of Si(100). (a) Single-step biperiodic vicinal surface. Two successive steps fluctuate with significantly different amplitudes. The strongly fluctuating one is called S_B, while the other is referred to as S_A. (b) Double steps. Courtesy of M. Lagally.

ing to the unstable regime, as shown in Fig. 42, obtained from the curve in Fig. 41 by up-down symmetry. Reducing transparency, the mode $\phi=\pi$ is promoted (as we know opacity favors this mode; see curve in Fig. 42). The modes around $\phi=\pi$ are unstable, while the modes away from $\phi=\pi$ are stable. Provided that the unstable band is small enough around $\phi=\pi$, pairing instability should occur and no coarsening process is expected (since the only unstable mode is $\phi=\pi$, while its higher harmonics are stable). Note that once the steps within pairs are close enough to each other, the interstep distance within the pairs saturates due to elastic repulsion (or entropic). The nonlinear pairing steady state can be calculated (Pierre-Louis and Métois, 2004) and the transition to pairing may be found to be subcritical (this is the analog of a first-order transition).

Recent experiments on Si(111) have confirmed the existence of step pairing (Pierre-Louis and Métois, 2004) which requires, according to theory, that $d_0=\nu_0/D$ is negative or that the migration force varies in the step region (Pierre-Louis, 2006). The former assumption is consistent with the assumption of Zhao *et al.* (2004). Why should a kinetic coefficient become negative in regime II, while remaining positive in regimes I and III, and how could one develop a simple and unified picture taking into account this feature, and account for bunching, meandering, and pairing, is still a largely open problem.

E. The Si(100) surface

1. Equilibrium

The Si(100) surface looks very different from the Si(111) surface described in Sec. IV.C.1 at the microscopic level due to the (2×1) dimer-row reconstruction. The orientation of the dimer rows is alternated from one terrace to the other, and the resulting vicinal surface is sometimes called a biperiodic grating. Accordingly, there are two types of single steps, S_A and S_B [see Fig. 43(a)], which run parallel and perpendicular to the dimer rows on the adjacent upper terrace, respectively.

At equilibrium, these surfaces experience a step-doubling transition if the step density is sufficiently high (Alerhand *et al.*, 1990). On the one hand, the free energy of double steps E_d proved to be smaller than E_L, the energy of separate single steps. On the other hand, separation of the double steps into single steps leads to relaxation of the elastic energy of the (2×1) reconstruction. This relaxation is known to lead to the spontaneous formation of strips of stress domains on nominal surfaces (Alerhand *et al.*, 1988). The total difference of energy per unit area between double-step and single-step vicinal surfaces is

$$E_d - E_L = -(1/\ell)[\delta/2 - \lambda \ln(\ell/\pi a)], \tag{4.70}$$

where $\delta>0$ is the difference in step free energy between S_A plus S_B steps and one double step. The second term results from the elastic energy. The logarithmic dependence can be traced back to the fact that the (2×1) reconstruction leads to anisotropic surface stress. This results in net force density at a step which separates the two domains. Since elasticity is essentially a Laplacian field (such as electromagnetism), the interaction energy between two forces applied at a distance r is proportional to $1/r$. We then have to integrate along both steps and consider the energy per unit length. This leads to an interaction energy per unit length $\sim\ln(\ell)$ between two steps separated by a distance ℓ. Finally, since the step density per unit area is $\sim1/\ell$, we obtain the second contribution in Eq. (4.70). The surface undergoes a step-doubling transition when E_d-E_L becomes negative, i.e., when $\ell<\ell_c$, with

$$\ell_c = \pi a \exp[\delta/2\lambda]. \tag{4.71}$$

This result is in quantitative agreement with experiments at 500 °C, giving a transition at a miscut angle of $\theta_c=2°$ [terrace width given by $\ell_c=a\tan(\theta_c)$]. Nevertheless, the details of this transition seem to be more complex, as shown by Pehlke and Tersoff (1991a, 1991b), for example.

2. Growth

During growth, fast pairing and subsequent bunching of the pairs have been observed in experiments. This appears in an intermediate regime, where the temperature is neither too low (so that no nucleation is observed on terraces) nor too high (so that thermodynamic smoothening is not too efficient). Interestingly, a novel coarsening scenario is proposed (Myslivecek *et al.*, 2002), called the "ripple-zipper" mechanism.

Experimental measurement of the decay of mounds (Tanaka *et al.*, 1997) seems to support the idea of transparent steps. The dynamics of biperiodic grating has been studied (Frisch and Verga, 2005, 2006).[14] Here we assume that Eq. (4.68) applies for the two types of steps, with different kinetic coefficients, β_A and β_B [see Eq. (4.69)]. Due to the fact that there are fewer kinks in S_A steps than in S_B steps [see Fig. 43(a)], it is tempting to set $\beta_A \gg \beta_B$, which means that attachment is much easier on S_B steps. For simplicity, we take $\beta_B=0$. The diffusion equation on each terrace reads

$$0 = D_\perp \partial_{zz} c + F \quad \text{on A terraces}, \tag{4.72}$$

$$0 = D_\parallel \partial_{zz} c + F \quad \text{on B terraces}, \tag{4.73}$$

where $D_\parallel$ and $D_\perp$ are the diffusion constants along and perpendicular to the dimer rows. In a simple model, we consider the interaction of neighboring steps only. Since we have seen that this interaction is logarithmic, the chemical potential μ, which is proportional to the derivative of the energy with respect to ℓ, scales as ℓ^{-1}. Then, in the same way as for the boundary condition (4.68), we write the boundary conditions for concentrations c^A and c^B at steps S_A and S_B, respectively. They include the elastic interaction,

$$c^A = c^A_{eq} = c^0_{eq}\left[1 + A\left(\frac{1}{\ell_B} - \frac{1}{\ell_A}\right) + \beta_A V\right], \tag{4.74}$$

$$c^B = c^B_{eq} = c^0_{eq}\left[1 + A\left(\frac{1}{\ell_A} - \frac{1}{\ell_B}\right)\right], \tag{4.75}$$

where ℓ_A and ℓ_B are the widths of the A terraces with dimer rows parallel to the steps and the B terraces with dimer rows perpendicular to the steps, respectively. Finally, mass conservation at the step reads

$$V_m/\Omega = D_+ \partial_z c_+|_m - D_- \partial_z c_-|_m, \tag{4.76}$$

where $D_\pm$ and $c_\pm$ are the diffusion constants and the concentrations on both sides of the steps, respectively. Without desorption, steady-state growth is obtained when all steps move at the same velocity $V=\Omega F \ell$ with $\ell=(\ell_A+\ell_B)/2$. The steady-state condition implies that

$$c^A_{eq} = c^B_{eq}, \tag{4.77}$$

which results into

$$1/(\alpha-1) + 1/\alpha = \beta_A V \ell / A, \tag{4.78}$$

where $\alpha=\ell_A/(\ell_A+\ell_B)$. Since the lhs of Eq. (4.78) is a monotonously decreasing function of α, there is a unique solution. In the limit of fast growth or weak interactions, steps in the pairs are very close to each other and

$$\alpha = \ell_A/(\ell_A+\ell_B) \approx A/\beta_A V \ell. \tag{4.79}$$

It is obvious that the A terraces shrink because the B steps, where attachment is easy, move faster than the A steps. Due to elastic repulsion, the B steps slow down when they get too close to A steps. Care must be taken, however, as the coupling of this pairing with (equilibrium) step doubling may render the picture more complex. This constitutes an interesting task for future investigations.

The step with fast kinetics ($\beta_B=0$) catches up with the slow kinetics step, thus forming a pair. The pair may then be viewed as a single effective step, with an effective negative Schwoebel barrier (since atoms would attach more easily at the back of the pair; the step where kinetics are fast lies at the rear). It must be remembered that the picture may be more complex because the distance between the steps in a pair is not fixed. Recent analysis of a similar model with nontransparent steps (Frisch and Verga, 2005) was found to lead to pairs. They found two pairing steady states for small fluxes, and no pairing steady state for large fluxes. This is different from the transparent case where there is always a solution. They then proved the occurrence of bunching from a stability analysis of the train of pairs and from the numerical solution of the full step model.

More complex patterns, such as zigzags, have been observed during the growth of Si(100) vicinal surfaces (Schelling *et al.*, 1999). From the complexity of its structure, the Si(100) surface produces a large number of morphologies during growth. A complete and quantitative description remains a challenge.

3. Electromigration

In the presence of an electric current, one of the two terraces dominates, while the other one shrinks thus leading to step pairs. This was observed experimentally by Ichikawa and Doi (1992) and analyzed theoretically by Stoyanov (1990).

The bunching of these pairs of steps was observed by Litvin *et al.* (1991) and Latyshev *et al.* (1998) for both directions of the electric current (for small miscuts). They observed that the number of steps in the bunches increases as $\sim t^{1/2}$ and the average width W of the bunches follows $W \sim N^{-1/2}$ [similar to the situation with Si(111) in the intermediate temperature range under sufficiently weak nonequilibrium conditions (Stoyanov and Tonchev, 1998; Fujita *et al.*, 1999)]. Further theoretical investigations can be found by Sato *et al.* (2005) and Zhao *et al.* (2005).

For large miscuts (i.e., small terrace widths), step bunching is seen only for step-up current. These results

[14] These studies were performed without the transparency assumption, leading to qualitatively similar results.

are difficult to analyze due to the interference of this effect with the spontaneous (equilibrium) pairing transition induced by elastic interactions on these surfaces, as mentioned above. Experiments with arbitrary current orientations have also been reported (Nielsen *et al.*, 2001) and analyzed by Zhao *et al.* (2005).

F. Elastic relaxation in heteroepitaxy

In heteroepitaxial growth, material of the adsorbed epitaxial layer is different from the substrate material. Since in general there is a lattice misfit, the elastic stress accumulates in epilayers and induces various surface instabilities.

1. The instability mechanism and linear analysis

Two mechanisms of step bunching related to the elastic relaxation of the crystal during heteroepitaxy have been reported. The first mechanism (Tersoff *et al.*, 1995) is the transcription of the Asaro-Tiller-Grinfeld (ATG) instability (Asaro and Tiller, 1972; Grinfeld, 1986) to vicinal surfaces. The ATG instability results from the fact that the elastic energy of a solid under biaxial stress can be lowered by undulation of the surface. This undulation is not due to the buckling of the solid but results from mass transport from valleys to summits.

In the case of vicinal surfaces, the kinetics of mass transport and elastic relaxation are governed by crystal steps. During heteroepitaxy, a density of force monopoles is present at the steps. These forces are necessary in order to achieve mechanical equilibrium (discontinuity of the height across a step means that the stresses on both sides of a step are unequal; the step is then a location of a force monopole). Unlike Si(001) (see Sec. IV.E), successive steps here have forces pointing in the same direction, changing repulsion (Marchenko, 1981) into attraction. As for Si(001), the interaction is logarithmic with ℓ. Since our aim is to analyze step bunching, we first consider the case where steps are straight. In this case, the chemical potential at the steps, obtained from the derivative of the energy, is $\sim 1/\ell$. We then have (Tersoff *et al.*, 1995)

$$\mu_m = \sum_{n\neq m} \left[-\frac{\alpha_1}{(z_n - z_m)} + \frac{\alpha_2}{(z_n - z_m)^3} \right], \tag{4.80}$$

where α_i's are constants. α_1 is positive (Tersoff *et al.*, 1995) due to the above-mentioned attraction. This atttraction obviously leads to instability. In Eq. (4.80), there is no term $\sim 1/(z_n - z_m)^2$. This can be explained with simple symmetry arguments. Indeed, expanding the force distribution around the steps gives a force density at leading order and a density of dipoles to subdominant order. Interaction between the forces leads to the term proportional to α_1 in Eq. (4.80) and interaction between the dipoles leads to the term proportional to α_2 (in homoepitaxy, there are no net forces at the steps and $\alpha_1 = 0$). However, the interaction between the forces and the dipoles—which would scale as $1/(z_n - z_m)^2$—vanishes. Consider two steps denoted 1 and 2. The interaction energy between dipoles at step 1 with the forces at step 2 is opposite to that between the forces at step 1 with the dipoles at step 2. The two contributions counterbalance each other.

Consider conserved dynamics, with instantaneous attachment kinetics at the steps under an incoming flux F. This gives

$$\partial_t z_m = \frac{\Omega F}{2}(z_{m+1} - z_{m-1}) + B\Delta\left[\frac{\Delta\mu_{m+1}}{\Delta z_{m+1}}\right], \tag{4.81}$$

where $\Delta f_m = f_m - f_{m-1}$ is the finite difference operator.

Following Tersoff *et al.* (1995), a stability analysis of these equations can be performed. Note that the incoming flux F only enters in the imaginary part of the growth rate of small perturbations. Therefore, it only leads to propagative effects and is irrelevant to the analysis of stability in the linear regime. The instability is driven by elasticity. If the destabilizing force is small, the instability appears at long wavelength and the linear dispersion relation is expanded to

$$\mathrm{Re}[i\omega] \sim \tilde{\alpha}_1 |\phi|^3 - \tilde{\alpha}_2 \phi^4, \tag{4.82}$$

where $\tilde{\alpha}_i$ are positive constants proportional to α_i. This dispersion relation is different from that reported previously. The odd destabilizing term $|\phi|^3$ results from α_1. The absolute value expresses the fact that elasticity is of long range.[15] In real space, the Fourier transform of $|\phi|$ leads to an integral representation (the Hilbert transform) pointing thus to nonlocality. The term proportional to ϕ^4 is the traditional term leading to surface relaxation (the Mullins term).

There is a second mechanism, treated by Duport, Nozières, and Villain (1995) (DNV). As mentioned, a step is a location of a force density. These forces interact with the force dipoles located around each adatom. The interaction potential between an adatom and a straight step at a distance r is $U \sim 1/r$ (since the interaction energy of a force and a dipole is $\sim 1/r^2$ and that of a line of forces and a dipole is $\sim 1/r$). The presence of the external potential U created by the step leads to an additional (drift) term in the quasistatic diffusion equation

$$D\partial_z\left[\partial_z c + \frac{c}{k_B T}\partial_z U\right] + F = 0, \tag{4.83}$$

$$U(z) = -\sum_{m=-\infty}^{\infty} \frac{\alpha_0}{z - z_m}. \tag{4.84}$$

We are dealing with a situation with an adsorption flux F but no desorption. The gradients of the interaction potential $\partial_z U$ lead to a drift of the adatoms perpendicular to the steps.

The DNV effect is similar to an effective Schwoebel barrier in the sense that it makes the concentration

[15] Actually, ϕ^3 is a product of $|\phi|$ (resulting from elasticity) and ϕ^2 due to the conservation constraint.

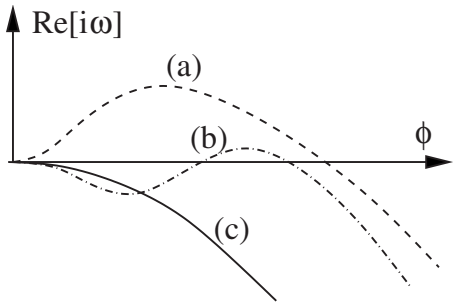

FIG. 44. Dispersion relation (4.85) for bunching at long wavelength $\phi \ll 1$ during heteroepitaxial growth. (a) $A_0=\tilde{\alpha}_0+\tilde{\mathcal{S}}$ positive: instability at long wavelength. (b) A_0=negative and small: instability at finite wavelength. (c) A_0=negative and large: the surface is stable.

asymmetric. Unlike the ATG instability, the main contribution of this effect is local and to linear order it may be viewed as a renormalization of the Schwoebel effect. From Sec. IV.A, the additional term which comes into play in the long-wavelength dispersion relation may be inferred so that Eq. (4.82) now reads

$$\mathrm{Re}[i\omega] \sim F(\tilde{\alpha}_0+\tilde{\mathcal{S}})\phi^2+\tilde{\alpha}_1\epsilon|\phi|^3-\tilde{\alpha}_2\phi^4, \tag{4.85}$$

where $\tilde{\mathcal{S}}$ is a term proportional to the Ehrlich-Schwoebel effect, and $\tilde{\alpha}_0$ is proportional to α_0. If the sum of the DNV and the Schwoebel effects, $A_0=\tilde{\alpha}_0+\tilde{\mathcal{S}}$, is positive (i.e., uphill diffusion bias), there is instability [Fig. 44(a)], which dominates the ATG instability at long wavelength (the growth rate of which is $\sim\phi^3$).

If FA_0 is negative and small, there is instability at finite wavelength, as shown in Fig. 44(b). If FA_0 is negative and sufficiently large, the surface is linearly stable [Fig. 44(c)].

2. Nonlinear dynamics: Highly nonlinear equation

Due to mass conservation, the resulting evolution equation for the surface height h takes the form

$$\partial_t h=\bar{F}-\partial_z J, \tag{4.86}$$

where $\bar{F}=\Omega aF$. The mass flux J takes the form (Xiang, 2002)

$$J=\frac{\bar{F}}{12}\partial_z\rho^{-2}+\bar{F}\frac{\mathcal{B}}{2}\left(d_-+\frac{\alpha_0}{k_BT}\ln(2\pi a|\rho|)\right)+\mathcal{B}\frac{\Omega D c_{\mathrm{eq}}}{k_BT}\partial_z\frac{\delta\mathcal{E}}{\delta h}. \tag{4.87}$$

The two first terms in Eq. (4.87) account for the breakdown of the up-down symmetry (Politi and Villain, 1996) induced by step motion and for the uphill mass flux forced by the ES effect. In light of this formulation, the DNV effect appears as a slope-dependent straightening of the ES effect. As in previous sections [see Eqs. (4.24) and (4.54)], the prefactor $\mathcal{B}$ accounts for diffusion slowing down due to the fact that atoms have to jump over the ES as well as diffusion barriers (with a kinetic attachment length d_- and $d_+=0$). It reads

$$\mathcal{B}=1/(1+d_-\rho). \tag{4.88}$$

The energy $\mathcal{E}$ accounts for elastic interactions between steps and takes the form

$$\mathcal{E}=\int dz\left(-a^2\pi\alpha_1\frac{\tilde{h}}{2}H(\rho)+\frac{a^3}{2}\alpha_1\rho\ln(\rho)+\frac{a^3\pi^2}{12}\alpha_2\rho^3\right) \tag{4.89}$$

with $\tilde{h}=h-z\bar{\rho}$, where $\bar{\rho}$ is the average step density. We have defined the Hilbert transform as

$$H(u)=\frac{1}{\pi}\int dy\frac{u(y)}{z-y}. \tag{4.90}$$

It can be checked that the second and third terms in the energy (4.89) account for the force monopole-monopole and dipole-dipole interactions, respectively. The first term expresses the effect of deviation from the uniform train and is related to a $|\phi|$ dependence in the linear dispersion relation. This type of term was also derived in the context of the ATG instability (Kassner and Misbah, 2002).

From the numerical solution of Eq. (4.81), it was found by Tersoff *et al.* (1995) that growth plays an important role in nonlinear dynamics. Indeed, in the absence of growth, coarsening is observed, with a scaling law for the bunch size $N\sim t^{1/4}$. If allowance is made for an incoming flux ($F>0$, growth), the bunch size exhibits saturation after some finite amount of coarsening. This is reminiscent of two effects mentioned earlier for local nonlinear dynamics. First, propagative terms (as in the Benney equation; see Sec. IV.A.5) seem to change the dynamics equation qualitatively. Here the propagative term is the first term on the rhs of Eq. (4.87). Second, the coarsening process seems to be similar to the interrupted coarsening observed on the meanders of anisotropic steps in Secs. III.C.7.a and III.C.7.c. It is then tempting to speculate that, as in the case of meandering, the interrupted coarsening might be related to the presence of a bounded branch [Fig. 46, (iii)] (the wavelength as a function of amplitude exhibits a maximum) of steady states. Clearly, further nonlinear analysis is needed for a full understanding of the late stages of this instability.

It is also natural to expect the ATG instability to appear via step meandering. The elastic relaxation related to meandering was analyzed by Houchmandzadeh and Misbah (1995). The competition between bunching and meandering instabilities in the limit of small perturbations was studied by Leonard and Tersoff (2003). It appears that, while both instabilities are usually present, the meandering instability always dominates when the distance between steps is sufficiently large.

V. MACROSCOPIC PHENOMENOLOGICAL DESCRIPTION AND COARSENING

In this section we present a phenomenological picture for the study of instabilities on a vicinal surface and analyze the limit of a singular high symmetry surface. We admit, on the basis of several explicitly studied examples, that the instability occurs at long wavelength. This limit is encountered, for example, for step meandering when the incoming flux is small enough. Typically this holds if the step relaxation frequency which is of the order of V/Γ is small in comparison to diffusion time over a terrace, given by D/ℓ^2 [see Eq. (3.32) where one finds that typical length scales $(k\ell)^2 \sim V\ell^2/D_S\Gamma$ and the hydrodynamic limit corresponds to $(k\ell)^2 \ll 1$]. Using typical values one finds that the condition is satisfied. For step bunching the hydrodynamic limit corresponds to the situation where the length scale is large in comparison with the interstep distance. This condition always holds at the scale of the bunch. If the instability is of short wavelength (an exception is step pairing), a long-wavelength limit makes sense if one concentrates on the close vicinity of the bifurcation point (see Sec. IV.D.2). We also present our current understanding regarding criteria for the occurrence or not of coarsening.

A. Nonconserved dynamics

At a macroscopic scale, we may attempt to present a general phenomenological continuum model. We first consider a one-dimensional model. To leading order we may write the normal velocity of the surface

$$v_n = A_0(\theta) + A_1(\theta)\kappa, \tag{5.1}$$

where κ is the curvature and θ is the angle between the normal and a reference axis. The presence of κ is a natural consequence of the intrinsic character of curvature [see also Csahók *et al.* (1999)]. Keeping the first term only, we obtain the Frank model (Frank, 1958; Pimpinelli and Villain, 1998), which was used to explain the (apparent) anisotropic growth shape of crystals in solutions. Due to the orientation dependence of A_0, an initially circular seed may assume either a smooth profile or facets. The precise form of A_0 determines which scenario prevails. Following the same picture, we may extend the analysis to a vicinal surface, with a local misorientation θ with respect to the high symmetry plane of the terraces. Ignoring the curvature term for the moment, the local step velocity is given by $V_{\text{step}} = v_n/\sin\theta = A_0(\theta)/\sin\theta$, where the surface orientation angle θ is related to local surface slope $\rho = |\partial_z y/a|$ as $\rho = |\tan\theta|/a$ (in the present section, we shall deal with step nucleation, so that the vicinal restriction breaks down, and the surface slope does not necessarily correspond to the step density anymore). Thus, V_{step} is simply a function of ρ. Such a ρ-dependent velocity is the starting point of the kinematic wave theory. The approach presented in Sec. II.C may then be applied.

Before proceeding further, we make a comment regarding singular surfaces. This analysis cannot, in principle, be easily extended to nonvicinal surfaces for two reasons: (i) A_0 is expected to be nonanalytic around facets (i.e., at $\theta=0$); (ii) for orientations close to a facet, when θ is small, 2D nucleation would take place, so that step density may be a complex function of the orientation.

As discussed in Sec. II.C (a section dedicated to kinematic waves) a description in terms of ρ only cannot account for morphological instability and higher-order derivatives are necessary. This is encoded in the the subdominant term $A_1\kappa$. It is simple to recognize that when $A_1(\theta) > 0$, a flat surface of orientation θ is linearly unstable and is stable otherwise.

In order to deal with the stability of a vicinal surface with respect to both bunching and meandering, a two-dimensional model is required. A generalization of Eq. (5.1) must include in the subdominant term the two principal curvatures. For simplicity, we assume that the steps have isotropic properties. Moreover, we consider a scalar space-independent driving force (such as a deposition flux, but no electromigration, for example). To parametrize the surface we use the step curvature κ_s (along the step direction) and the surface slope gradient $\partial_n\rho$ in the direction orthogonal to the step. The simplest leading order continuum model therefore reads

$$\partial_t h = A_0(\rho) + A_s(\rho)\kappa_s + A_n(\rho)\partial_n\rho. \tag{5.2}$$

We now use this model to study the linear stability of a vicinal surface. Consider an initial vicinal surface with an average step density $\bar{\rho} > 0$ along the z axis (i.e., along the vicinal direction). The actual surface height can be written $h = A_0(\bar{\rho})t - a\bar{\rho}z + \delta h$, where δh is the deviation from the homogeneous profile. Expansion of Eq. (5.2) to linear order in δh yields

$$a\partial_t \delta h = -\partial_\rho A_0(\bar{\rho})\partial_z \delta h - [A_s(\bar{\rho})/\bar{\rho}]\partial_{xx}\delta h + A_n(\bar{\rho})\partial_{zz}\delta h. \tag{5.3}$$

The first term on the right-hand side is purely imaginary in Fourier space; it expresses a propagative (or a drift) effect. The second term accounts for meandering modes; step meandering occurs if $A_s > 0$. The last term accounts for step-bunching modes; a step-bunching instability is indicated by $A_n < 0$.

Note that the above analysis cannot be applied to a nominal surface with $\bar{\rho} = 0$ since curvature κ_s and unit vector normal to a step $\mathbf{n}$ are meaningless in this case.

B. Conserved dynamics

Now consider dynamics with a conservation constraint, such as deposition with no desorption. This model was first discussed by Villain (1991) in the context of mound formation induced by the ES effect. In one dimension, we have

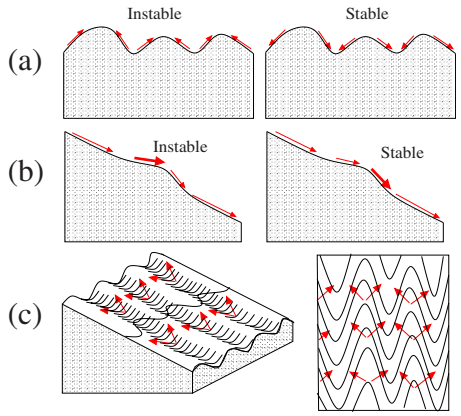

FIG. 45. (Color online) Surface mass fluxes may stabilize or destabilize the surface. There are three basic instabilities: (a) mound formation induced by an uphill mass flux, (b) step bunching induced by slope-dependent variations of the mass flux, and (c) step meandering induced by an uphill mass flux. We observe that mound formation and step bunching may be described within the frame of a 1D model, while step meandering requires a 2D description of the surface.

$$\partial_t h = \bar{v} - \partial_z J(\theta), \tag{5.4}$$

where $\bar{v}$ represents the average velocity, obeying (on average over the surface) $\langle \partial_t h \rangle = \bar{v}$. In a gradient expansion, the dominant contribution to J is a simple angle dependence $J = J(\theta)$. As shown in Figs. 45(a) and 45(b), instability occurs if $\partial_\theta J > 0$.

As in the nonconserved case, a two-dimensional generalization of this criterion is easily obtained:

$$\partial_t h = \bar{v} - \boldsymbol{\nabla} \cdot \mathbf{J}. \tag{5.5}$$

For an isotropic step model, with a scalar driving force, the mass flux is to leading order[16] along the normal to the steps and only depends on surface slope

$$\mathbf{J} = -\mathbf{n} J(\rho) \tag{5.6}$$

if $\mathbf{n}$ is the normal to the step. Consider a slight deviation δh. As before, the height is written $h = \bar{v}t - a\bar{\rho}z + \delta h$. A linear expansion of the model equation leads to

$$a\partial_t \delta h = -[J(\bar{\rho})/\bar{\rho}]\partial_{xx}\delta h - \partial_\rho J(\bar{\rho})\partial_{zz}\delta h. \tag{5.7}$$

As compared to the nonconserved case [Eq. (5.3)], no propagative term appears (to leading order only). This is related to the fact that kinematic waves, as presented in Sec. II.C, do not exist within this type of conserved equation (this fact was mentioned in Sec. II.C).

When $\bar{\rho} \neq 0$, we have a vicinal surface. Stability is then deduced from Eq. (5.7). Namely, if $\partial_\rho J(\bar{\rho}) > 0$ step bunching occurs and if $J(\bar{\rho}) > 0$ (i.e., uphill mass flux) meandering takes place [see Fig. 45(c)]. The limit $\bar{\rho} \to 0$ appears to be problematic. This difficulty may be circumvented by evoking a general physical argument. Indeed, symmetry leads us to expect that $J(0) = 0$ and that the flux should be continuous for $\rho = 0$. An expansion of the current around $\rho = 0$ should thus yield

$$J(\rho) \approx \rho \partial_\rho J(0). \tag{5.8}$$

The limit $\rho \to 0$ can then be taken directly from Eq. (5.7), leading to

$$a\partial_t \delta h = -\partial_\rho J(0)[\partial_{xx}\delta h + \partial_{zz}\delta h], \tag{5.9}$$

which expresses the fact that mound formation instability takes place when $\partial_\rho J(0) > 0$. From Eq. (5.8), the condition for mounding instability can also be written as $J(\rho) > 0$, i.e., an uphill flux. If we do not assume that $J(\rho \to 0) \to 0$ then the dynamics around a nominal surface ($\rho = 0$) would not be well defined. Nevertheless, mounds may be well defined if it is accepted that small slopes are forbidden by (more or less *ad hoc*) dynamics. This question was addressed in this context by Elkinani and Villain (1993) for the Zeno model, for which slopes smaller than the inverse of the nucleation length are forbidden. Later Politi and Villain (1996) put forward the idea that stochastic nucleation could solve this problem since the limit of $\rho \to 0$, J vanishes. Finally, studies of mound formation in the presence of a finite ES effect have shown that dynamics are in fact nonlocal at the top of mounds, leading to a nonanalytic shape with a truncated mound [curiously similar to the shape of the step meander studied by Gillet *et al.* (2000)]. In the limit of a strong ES effect, the width of the top terrace tends to zero and a singular peaked shape is obtained (Krug, 1997; Politi, 1997).

Similar problems are encountered when dealing with the decay of mounds as shown by Chame *et al.* (1996). In this case, although global stability can be expected, causing structure decay, the dynamics are still not well defined around facets at $\rho = 0$. The results of the conserved model are qualitatively shown in Fig. 45. There is now significant literature on the phenomenological modeling of flux J (Politi *et al.*, 2000). Additional higher-order terms in the flux, which may account for the up-down symmetry breaking of the surface and/or for short wavelength surface stabilization, have been introduced. Here we have attempted to show how a consistent picture could be produced for the derivation of nonlinear evolution equations when nucleation is absent. The incorporation of nucleation, which is an essential ingredient in the study of dynamics of nominal surfaces, is to date largely phenomenological.

C. Coarsening

1. Scaling and universality classes

We first recall the work of Paulin *et al.* (2001) on step meandering in the presence of elastic interactions, which was presented in Sec. III.C.5. In this work it was shown that when meandering leads to endless coarsening, a self-affine *Ansatz* can be used to find the coarsening exponents from a simple power-counting argument. This

[16] By this we mean to leading order in variation of the geometry of the surface; for example, if we include a curvature term as in the nonconserved case, we produce higher-order derivatives in the final equation in terms of δh.

method was also applied to step bunching (Pimpinelli *et al.*, 2002). The basic assumption is a self-affine *Ansatz*: $h(x,t)=t^{\alpha/z}H(x/t^{1/z})$. The exponents are extracted from a power-counting method by comparing the different terms in the nonlinear equation.

As pointed out by Krug *et al.* (2005) and Chang *et al.* (2006), the existence of more than one type of steady state for the highly nonlinear equation [such as Eq. (4.54)] casts doubt on the general validity of the criterion.

It should be stressed that this type of reasoning (power counting) has not been proven to work, for example, for weakly nonlinear equations. There are at least three terms in weakly nonlinear equations (destabilizing, stabilizing, and nonlinear) such as the Benney equation and Eq. (4.41). Therefore, it is not clear how the power-counting methods can be extended to these equations.

A more powerful tool for determining the coarsening exponent has been put forward (and proved for a large class of equations). It is based on analysis of the phase diffusion equation (Politi and Misbah, 2004, 2006). This will be discussed next.

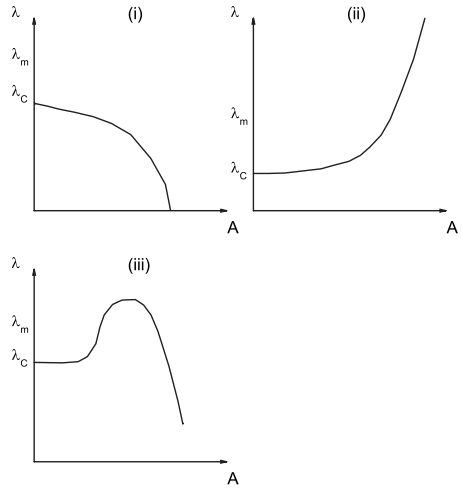

FIG. 46. Three scenarios for coarsening. (i) No steady state above the most unstable wavelength λ_m. No coarsening. (ii) Perpetual coarsening. (iii) Steady states up to a value of λ corresponding to maximum of the curve $\lambda(A)$. If λ_m is larger than that value, no coarsening occurs; if it is lower, interrupted coarsening takes place.

2. Coarsening versus noncoarsening of the pattern

So far we have seen that dynamics can broadly be classified into three main categories: (i) fixed wavelength, (ii) perpetual coarsening, and (iii) interrupted coarsening; this intermediate stage may occur, in which wavelength increases significantly beyond that of the fastest growing mode before freezing at a typical value. It is quite puzzling to see that some equations first appear to be quite similar (as encountered in Sec. III) but lead to drastically different scenarios (such as coarsening and wavelength selection). We want to understand if there are criteria that allow a distinction to be made between these types of dynamics. We attempt to classify the dynamics that is likely to take place without resorting to a systematic numerical integration of the evolution equations.

The interesting feature is that a connection can be made between the shape of the steady-state branch, expressed in terms of the amplitude A of the pattern as a function of periodic structure wavelength λ, and the occurrence or absence of coarsening. This connection is possible for a certain class of equations as presented by Politi and Misbah (2004, 2006).

Three different generic scenarios may occur: (i) $\lambda(A)$ is a decreasing function of A [Fig. 46, (i)], (ii) $\lambda(A)$ increases indefinitely [Fig. 46, (ii)], and (iii) $\lambda(A)$ increases then attains a maximum before decreasing [Fig. 46, (iii)]. In (i) it is found that there is no coarsening while the wavelength is frozen at a value close to that of the fastest growing mode. In (ii) there is coarsening. In (iii) there is coarsening until the wavelength reaches the maximum value where coarsening is interrupted. While there is no coarsening [case (i)] or when coarsening is interrupted [case (iii)], the amplitude increases indefinitely over time. We may refer to these solutions as "diverging solutions." Note that there are other variations. For example, in case (ii), $\lambda(A)$ may first decrease before increasing [see Fig. 39(a) and Politi and Misbah (2004)]. In this case, coarsening occurs. We may even have several minima. What matters is that $\lambda(A)$ increases at large λ.

Finally, a fourth important distinct generic scenario may occur: the steady-state branch increases up to a maximum value of amplitude A, then reaches a turning point before going back to lower values of A. Such a case indicates that no standard coarsening can be obtained and more complex behavior might occur; see Politi and Misbah (2004, 2006) for a detailed discussion.

In a recent work (Politi and Misbah, 2004, 2006) it has been argued that the absence or manifestation of coarsening may be linked to the so-called *phase diffusion constant*. This is not restricted to crystal growth or sublimation only but to classes of equations that may occur in different domains.

More precisely, suppose that there is a steady-state solution $h_0(x)$ with periodicity λ, $h_0(x+\lambda)=h_0(x)$. This steady state may become unstable with respect to wavelength modulation, i.e., a sudden local increase in wavelength may be enhanced due to intrinsic instability, which is referred to as *phase instability*. Thus, if the steady branch is always unstable (this is taken to mean for "all wavelengths") with respect to the phase, then we expect perpetual coarsening to occur. Conversely, if the branch is stable with respect to phase modulation, then we expect the wavelength to be fixed.

For a steady-state periodic solution, the phase of the pattern is $\phi=kx$, where $k=2\pi/\lambda$. If the wavelength λ is locally perturbed (due to an inherent fluctuation), then the phase ϕ becomes a function of space and time (either relaxing toward the initial local wavelength or deviating away from it; these two situations correspond to

stable and unstable patterns with respect to phase fluctuations). The (slow) phase $\psi(X,T)=\phi(x,t)/\epsilon$ (where ϵ is a small parameter measuring the strength of phase modulation and $X=x\sqrt{\epsilon}$ and $T=\epsilon t$ are the slow variables) can be shown (Politi and Misbah, 2004, 2006) to obey a diffusion equation

$$\partial\psi/\partial T = D\partial^2\psi/\partial X^2, \tag{5.10}$$

where D is the phase diffusion coefficient which is a function of the steady-state solution h_0, which itself is parametrized by the wave number. Consider the following evolution equation:

$$\partial_t h = \partial_x^2 h - F(h), \tag{5.11}$$

where F is a general function of h. This is referred to as the generalized Ginzburg-Landau equation in Politi and Misbah (2004). $h_0(x)$ is its steady-state solution with periodicity λ and amplitude A. It can be shown (Politi and Misbah, 2004, 2006) that D in Eq. (5.10) is given by

$$D = \partial_k\langle k(\partial_\phi h_0)^2\rangle/\langle(\partial_\phi h_0)^2\rangle \equiv D_1/D_2. \tag{5.12}$$

In the above, $\langle\cdots\rangle=(2\pi)^{-1}\int_0^{2\pi}\cdots d\phi$ is the inner product, the denominator D_2 is always positive, and the sign of D is fixed by the numerator $D_1=\partial_k\langle k(\partial_\phi h_0)^2\rangle$. Using mechanical analogy [since the steady version of Eq. (5.11), $\partial_t h=0$, is analogous to Newton's equation of a fictitious particle having a position $h_0(x)$ and x plays the role of time; thus $\partial_x^2 h$ is acceleration and F force] it has been shown (Politi and Misbah, 2004, 2006) that the sign of D_1 is the same as that of $-\partial_A\lambda$. Consequently, if $\lambda(A)$ is an increasing function of λ, as in scenario (ii) (Fig. 46), then $D<0$ and the pattern is always unstable with respect to wavelength modification and coarsening occurs.[17]

Politi and Misbah (2004, 2006) extended the argument based on phase diffusion constant analysis to other equations and seemed to work perfectly well according to the three scenarios presented above. We have seen throughout that these three scenarios and their dynamics are consistent with the general picture drawn above.

3. Coarsening exponents

It has been argued and shown by Politi and Misbah (2006) that the phase diffusion equation could be exploited to determine the coarsening exponent.

A negative D implies unstable behavior of the phase diffusion equation $\partial_t\psi=-|D|\partial_{xx}\psi$, which displays exponential growth. The idea by Politi and Misbah (2006) is based on the fact that if coarsening takes place, only time measurement t and pattern length scale λ are expected to survive as the essential scales over a long time and large spatial scales. Since coarsening is triggered by phase instability, represented by its diffusion coefficient D, there is only one way to link these quantities together, namely,

$$|D(\lambda)| \approx \lambda^2/t. \tag{5.13}$$

In general $D(\lambda)$ can always be determined, at least numerically, without resorting to any time-dependent calculation [it is determined only from knowledge of steady-state solutions as in Eq. (5.12)]. It turns out that for a large class of equations, $D(\lambda)$ can be extracted analytically in the asymptotic limit (large λ), and thus an analytical expression of the coarsening exponent can be derived (Politi and Misbah, 2006). For all known equations in the class of equations studied by Politi and Misbah (2006), the exact exponent was recovered. As discussed by Politi and Misbah (2006), an analytical derivation of a coarsening exponent is made for some classes of equations where the one-dimensional character of the equation is essential. While a link between the phase diffusion coefficient and the behavior of a steady-state branch is currently difficult to achieve beyond 1D, the phase diffusion equation can be derived at an arbitrary dimension. This suggests that $t\sim\lambda^2/D$ is worth testing in a higher dimension. If it works, since D only contains information on the periodic steady-state solutions, it is sufficient to obtain these solutions to determine the coarsening law. Numerical determination of these solutions is straightforward and thus the behavior of D as a function of λ can easily be extracted. Thus the coarsening law can be obtained without resorting to a time-dependent simulation. This presentation partially answers the challenging question: When and under which conditions does coarsening take place? It is hoped that this type of analysis will be extended to other nonlinear equations and to higher dimensions.

VI. CONCLUSION AND FUTURE DIRECTIONS

This review presents the major results known for vicinal surfaces regarding both bunching and meandering. Both standard and nonstandard nonlinear regimes are encountered. In conclusion, we discuss the major problems, constituting important tasks for future investigations.

The meandering study, together with bunching, have led to various nonlinear equations; some of them are known in other nonlinear systems, while others were yet unrevealed. The nonlinear equations are derived analytically from BCF equations. Their numerical solutions reveal four basic scenarios: (i) chaotic dynamics, (ii) fixed wavelength with increasing amplitude, (iii) perpetual coarsening, and (iv) interrupted coarsening. Integration of the BCF model [without approximation, which consists in reducing the BCF system into nonlinear partial differential equations (PDEs)] and lattice gas simulations capture the same essential features (Saito and Uwaha, 1994; Kallunki *et al.*, 2002; Danker, 2005). This points to the fact that the above scenarios are intrinsic properties of the basic BCF model. A deep math-

[17] In principle one could think that $D<0$ may also lead to a decrease of the wavelength (via cell splitting). However, this is not consistent with the fact that for $\lambda<\lambda_c$, the straight step is stable. Thus only an increase of λ should be expected, *a priori*.

ematical understanding on why, for example, two apparently similar PDEs exhibit entirely different dynamics is lacking; some preliminary work has been undertaken (Politi and Misbah, 2004, 2006). The task, which consists in developing general criteria on the properties of the PDEs and their far-reaching consequences, offers a major panel of research in applied mathematics in this field with increasing importance and embraces a wide spectrum of scientific communities, ranging from fundamental research to applications.

From the physical point of view many questions remain unsolved or continue to be a matter for debate. To explain meandering instability two mechanisms have been evoked: (i) the Ehrlich-Schwoebel effect at the step and (ii) the same effect at the kinks. It has not yet been determined whether one prevails over the other or if it depends mainly on the systems and the parameter values. More refined experiments, together with microscopic simulations, are necessary in order to shed further light on these questions.

Bunching occurs in many circumstances, but here the emphasis has been on bunching caused by electromigration since many experimental data are available in this case. The intermediate temperature range for experiments on Si(111) has proven rather mysterious at first sight. Several ideas have been put forward to resolve the dilemma raised by this regime: (i) change of effective charge with temperature (ruled out by experiments), (ii) step transparency to atoms (or fast kinetics attachment on both sides of the step), (iii) differential diffusion model (in that atoms diffuse faster closer to the step than elsewhere), (iv) partial transparency, (v) change of electromigration of atoms close to a step, and (vi) advacancy effect. While each model has its own merit, there is a need for a clear understanding of the physics of Si(111) surfaces at the microscopic level. In addition, why transparency or differential diffusion should occur just in the intermediate temperature range remains as a major challenge. Further experiments on other systems should help guide and promote a deeper understanding of nonequilibrium-driven interfaces.

It must be stressed that in many cases step bunching has been regarded within a one-dimensional picture. The extraction of nonlinear PDEs from the BCF equations including 2D dynamics is largely an unexplored area of research. Beyond step flow dynamics a systematic incorporation of nucleation on terraces in a continuum description of surface evolution is also lacking.

More recent different types of approaches for deriving continuum nonlinear equations have been published (Haselwandter and Vvedensky, 2008). These are based on the renormalization of stochastic lattice models leading to continuum surface equations. While this approach is appealing, scenarios like those leading to highly nonlinear equations, as those met here, are not captured. It will be an interesting task for future studies to conceive of approaches of this type in order to deal with more general scenarios.

Besides analytical tools which have proved successful in extracting nonlinear evolution equations from the basic growth model, it is essential to pursue analyses on phase-field modeling (Pierre-Louis, 2003a) and level set approaches (Ratsch *et al.*, 2002), together with kinetic Monte Carlo (KMC) simulations (Saito and Uwaha, 1994; Kallunki *et al.*, 2002; Rusanen *et al.*, 2002). These analyses should also be made in a concerted fashion with more atomistic (e.g., *ab initio*) calculations in order to determine energetic and kinetic parameters to be injected into more coarse-grained theories. This last step is essential if we want to use the knowledge accumulated in this field in a more quantitative application to specific systems. Several numerical studies have focused on the dynamics of nominal surfaces on the basis of KMC simulations, and some key ingredients are beginning to emerge. It is an important task for future investigations to determine whether or not dynamics may be captured by simple prototypical continuum evolution equations.

The field of this review is, on the one hand, a major area of research in fundamental science, providing a plethora of examples of nonequilibrium and nonlinear statistical physics. On the other hand, this field is at the frontier of technological applications. One important promising issue is the possibility (or ability) of taking advantage of the deterministic instabilities to monitor vicinal surfaces and use them as a template for nanostructure formation.

Periodic arrays of nanofeatures, such as nanoislands (or nanodots), are useful as a basis of a variety of nanodevices, including electronic, acoustic, photonic, and magnetic devices. These arrays are traditionally obtained by means of lithographic techniques. Nowadays there is an increasing interest toward the use of spontaneous self-organization of islands and wires. It may now also be envisaged to take advantage of the meandering instability offering a 2D ordered template (see, for example, Fig. 29). Deposition of new species on the template that have preferential nucleation sites either at the summits of the zigzag pattern or at the valleys may lead to an ordered array of quantum dots. This goal may be achieved thanks to a control of the following features of the instability: (i) the functional dependence of the wavelength with parameters (which will thus allow one to fix the size of the dots at will) and (ii) the control of long-range order of the instability (which ensures high ordered nanostructures). In many optical applications (e.g., light emitting devices), monodisperse quantum dots should allow coherent peaked emission spectra. The typical size requirement of quantum dot application in optics is the range 10–20 nm. The nonperiodic arrangement of such memory devices and logic devices may reduce the effectiveness and usefulness of the nanopatterned device array. For example, in the case of magnetic hard disk media, undesirable switching or read error of magnetically written bits may occur if periodicity is not sufficiently precise (tolerance in inhomogeneity should be much smaller than the size of the reading device).

Examples of nanostructure production have been demonstrated for the growth of wires and platelets along atomic steps (Gambardella *et al.*, 2000; Li *et al.*, 2000;

Himpsel *et al.*, 2001; Gai *et al.*, 2002). The width of these wires is usually several atomic spacings. Several attempts have focused on the organization of nanodots on step bunches (Ronda *et al.*, 2003; Goldfarb, 2007). But, long-range order has not been produced yet on these surfaces. Another possible direction is to use templates which simultaneously undergo bunching and meandering instabilities, leading to a 2D pattern, such as in Néel *et al.* (2003). But, to our knowledge, no 2D meandering-bunching pattern with long-range order has been obtained yet in experiments. This promising route toward directed self-assembly crucially depends on the control of the morphology of vicinal substrates, which is a central focus of the present review. Another promising approach is to combine vicinal surfaces which provide periodicity in one direction, and surface reconstruction on terraces, which provides a periodicity in the direction parallel to steps. This method has been used successfully for the growth of magnetic dot assemblies (Repain *et al.*, 2002).

A more refined understanding of the various essential physical ingredients of the meandering and bunching instabilities and their interplay with stress and reconstruction is necessary before reaching a mature level toward applications.

In conclusion, this review has presented the main questions, problems, and solutions related to equilibrium and out-of-equilibrium vicinal surfaces. While significant progress has been made during the past two decades, there is still a myriad of unresolved questions at both fundamental and practical levels. We believe that this field merits a higher level of research activity.

LIST OF SYMBOLS AND ACRONYMS

a	atomic length scale
$A=\Omega\mathcal{A}/k_BT$	elastic interaction volume
$\mathcal{A}$	elastic interaction constant
ATG	Asaro-Tiller-Grinfeld
BCF	Burton-Cabrera-Frank step model
c	adatom concentration on terraces
c_{eq}	equilibrium concentration
$d_{\pm}=D/\nu_{\pm}$	kinetic attachment lengths
$d_0=D/\nu_0$	transparency length
D	diffusion constant on terraces
D_L	macroscopic line diffusion constant
$D_S=\Omega c_{\mathrm{eq}}D$	macroscopic terrace diffusion constant
DAKS	discrete advective Kuramoto-Sivashinsky equation
DNV	Duport-Nozieres-Villain
ES	Erhlich-Schwoebel effect
$f=zeE$	electromigration force
F	deposition flux on terraces
$\mathcal{F}$	free energy
F_c	critical flux
$F_{\mathrm{eq}}=c_{\mathrm{eq}}/\tau$	equilibrium deposition flux
FT	Fourier transform
$G(t)$	temporal step autocorrelation
h	surface height
J	flux
J_L	flux along the step
k	wave vector (FT space variable x)
k_B	Boltzmann's constant
k_c	critical wave vector
$k_m=k_c/\sqrt{2}$	most unstable wave vector
KdV	Korteweg–de Vries
KMC	kinetic Monte Carlo simulations
KPZ	Kardar-Parisi-Zhang equation
KS	Kuramoto-Sivashinsky equation
ℓ	step separation, terrace width
$\mathcal{L}_c$	cutoff length
L_k	distance between kinks
m	step index
$m=\partial_x\zeta$	step slope
M	mobility
MBE	molecular beam epitaxy
$\mathbf{n}$	normal to a step
NSNE	nonstandard nonlinear equation
REM	reflection electron microsope
s	arclength
STM	scanning tunneling microscope
V	step velocity
$\bar{V}$	mean step velocity
w_{eq}	equilibrium step width
$w(t)$	step fluctuation width
X,Y,Z,T	slow variables
$x_s=(D\tau)^{1/2}$	desorption length
$\Gamma=\Omega\tilde{\gamma}/k_BT$	step capillary length
γ	step line tension
$\tilde{\gamma}=\gamma+\gamma''$	step stiffness
ϵ	small parameter
ζ	step meander
η	thermal noise
θ	step orientation
κ	curvature
λ_m	wavelength of the fastest growing mode
μ	chemical potential
$\nu_{\pm}$	attachment-detachment step kinetic coefficients
ν_0	transparency kinetic coefficient
$\xi=k_BT/f$	migration length
ρ	step density
τ	desorption time on terraces
ϕ	phase shift (FT step index variable m)
Ω	atomic area
ω	pulsation (FT time variable t)
$i\omega$	complex amplification rate
∂_x	partial derivative with respect to x

ACKNOWLEDGMENTS

We are indebted to Paolo Politi for a critical reading of the paper and to Ted Einstein for his valuable comments.

REFERENCES

Akutsu, Y., N. Akutsu, and T. Yamamoto, 1988, Phys. Rev. Lett. **61**, 424.

Akutsu, Y., N. Akutsu, and T. Yamamoto, 1989, Phys. Rev. Lett. **62**, 2637.

Aleiner, I., and R. Suris, 1992, Sov. Phys. Solid State **34**, 809.

Alerhand, O. L., A. N. Berker, J. D. Joannopoulos, D. Vanderbilt, R. J. Hamers, and J. E. Demuth, 1990, Phys. Rev. Lett. **64**, 2406.

Alerhand, O. L., D. Vanderbilt, R. D. Meade, and J. D. Joannopoulos, 1988, Phys. Rev. Lett. **61**, 1973.

Alfonso, C., J. Bermond, J. Heyraud, and J. Métois, 1992, Surf. Sci. **262**, 371.

Asaro, R., and W. Tiller, 1972, Metall. Trans. **3**, 1789.

Bales, G. S., and A. Zangwill, 1990, Phys. Rev. B **41**, 5500.

Balibar, S., H. Alles, and A. Parshin, 2005, Rev. Mod. Phys. **77**, 317.

Barabàsi, A. L., and H. E. Stanley, 1995, *Fractal Concepts in Surface Growth* (Cambridge University, Cambridge).

Barbier, L., L. Masson, J. Cousty, and B. Salanon, 1996, Surf. Sci. **345**, 197.

Bartelt, N., T. Einstein, and E. Williams, 1994, Surf. Sci. **312**, 411.

Bartelt, N., J. Goldberg, T. Einstein, and E. Williams, 1992, Surf. Sci. **273**, 252.

Bartelt, N. C., T. Einstein, and E. D. Williams, 1992, Surf. Sci. **276**, 308.

Bartelt, N. C., T. L. Einstein, and E. D. Williams, 1990, Surf. Sci. Lett. **240**, L591.

Bartelt, N. C., J. L. Goldberg, T. L. Einstein, E. D. Williams, J. C. Heyraud, and J. J. Métois, 1993, Phys. Rev. B **48**, 15453.

Bena, I., C. Misbah, and A. Valance, 1993, Phys. Rev. B **47**, 7408.

Bennema, P., and G. H. Gilmer, 1973, *Crystal Growth: An Introduction* (North-Holland, Amsterdam).

Benney, D. J., 1966, J. Math. Phys. **45**, 150.

Blech, I. A., 1976, J. Appl. Phys. **47**, 1203.

Bogicevic, A., S. Liu, J. Jacobsen, B. Lundqvist, and H. Metiu, 1998, Phys. Rev. B **57**, R9459.

Bonzel, H., and W. Mullins, 1996, Surf. Sci. **350**, 285.

Bosvieux, C., and J. Friedel, 1962, J. Phys. Chem. Solids **23**, 123.

Burgers, J. M., 1974, *The Nonlinear Diffusion Equation* (Reidel, Boston).

Burton, W. K., N. Cabrera, and F. C. Frank, 1951, Philos. Trans. R. Soc. London, Ser. A **243**, 299.

Chame, A., S. Rousset, H. Bonzel, and J. Villain, 1996, Bulg. Chem. Commun. **29**, 398.

Chang, J., O. Pierre-Louis, and C. Misbah, 2006, Phys. Rev. Lett. **96**, 195901.

Chernov, A. A., 2003, J. Struct. Biol. **142**, 3.

Chernov, A. A., and T. Nishinaga, 1987, in *Growth Shapes and their Stability at Anisotropic Interface Kinetics*, edited by I. Sunagawa (Terra Scientific, Tokyo), pp. 207–266.

Combe, N., and H. Larralde, 2000, Phys. Rev. B **62**, 16074.

Conrad, E., 1996, in *Handbook of Surface Science*, edited by W. N. Unertl (North-Holland, Amsterdam), Vol. 1.

Csahók, Z., C. Misbah, F. Rioual, and A. Valance, 2000, Eur. Phys. J. E **3**, 71.

Csahók, Z., C. Misbah, and A. Valance, 1999, Physica D **128**, 87.

Danker, G., 2005, Ph.D. thesis (University Otto-von Guericke).

Danker, G., 2007, unpublished.

Danker, G., O. Pierre-Louis, K. Kassner, and C. Misbah, 2003, Phys. Rev. E **68**, 020601.

Danker, G., O. Pierre-Louis, K. Kassner, and C. Misbah, 2004, Phys. Rev. Lett. **93**, 185504.

Degawa, M., H. Minoda, Y. Tanishiro, and K. Yagi, 2000, Surf. Sci. Lett. **461**, L528.

Degawa, M., H. Minoda, Y. Tanishiro, and K. Yagi, 2001, J. Phys. Soc. Jpn. **70**, 1026.

Degawa, M., H. Nishimura, Y. Tanishiro, H. Minoda, and K. Yagi, 1999, Jpn. J. Appl. Phys., Part 2 **38**, L308.

Derényi, I., C. Lee, and A.-L. Barabási, 1998, Phys. Rev. Lett. **80**, 1473.

Duport, C., P. Nozières, and J. Villain, 1995, Phys. Rev. Lett. **74**, 134.

Edwards, S. F., and D. R. Wilkinson, 1982, Proc. R. Soc. London, Ser. A **381**, 17.

Ehrlich, G., and F. G. Hudda, 1957, J. Chem. Phys. **44**, 1039.

Einstein, T., and O. Pierre-Louis, 1999, Surf. Sci. **424**, L299.

Elkinani, I., and J. Villain, 1993, Solid State Commun. **87**, 105.

Feynman, R. P., 1972, *Statistical Mechanics*, 2nd ed. (Perseus, New York).

Fiks, V. B., 1959, Sov. Phys. Solid State **1**, 14.

Fisher, M. E., and D. S. Fisher, 1982, Phys. Rev. B **25**, 3192.

Fisher, M. P. A., D. S. Fisher, and J. D. Weeks, 1982, Phys. Rev. Lett. **48**, 368.

Flynn, C. P., 2002, Phys. Rev. B **66**, 155405.

Frank, F., 1958, in *Growth and Perfection of Crystals*, edited by R. Doremus, B. Roberts, and D. Turnbull (Wiley, New York), p. 411.

Frisch, T., and A. Verga, 2005, Phys. Rev. Lett. **94**, 226102.

Frisch, T., and A. Verga, 2006, Phys. Rev. Lett. **96**, 166104.

Fujita, K., M. Ichikawa, and S. S. Stoyanov, 1999, Phys. Rev. B **60**, 16006.

Gai, Z., G. A. Farnan, J. P. Pierce, and J. Shen, 2002, Appl. Phys. Lett. **81**, 742.

Gambardella, P., M. Blanc, H. Brune, K. Kuhnke, and K. Kern, 2000, Phys. Rev. B **61**, 2254.

Garcia, S. P., H. Bao, and M. A. Hines, 2004, Phys. Rev. Lett. **93**, 166102.

Giesen, M., 1997, Surf. Sci. **370**, 55.

Giesen, M., 2001, Prog. Surf. Sci. **68**, 1.

Giesen-Seibert, M., R. Jentjens, M. Poensgen, and H. Ibach, 1993, Phys. Rev. Lett. **71**, 3521.

Giesen-Seibert, M., F. Schmitz, R. Jentjens, and H. Ibach, 1995, Surf. Sci. **329**, 47.

Gillet, F., 2000, Ph.D. thesis (Université Grenoble I, Grenoble).

Gillet, F., Z. Csahók, and C. Misbah, 2001, Phys. Rev. B **63**, 241401.

Gillet, F., O. Pierre-Louis, and C. Misbah, 2000, Eur. Phys. J. B **18**, 519.

Gliko, O., I. Reviakine, and P. G. Vekilov, 2003, Phys. Rev. Lett. **90**, 225503.

Goldfarb, I., 2007, Nanotechnology **18**, 335304.

Grinfeld, M., 1986, Sov. Phys. Dokl. **31**, 831.

Gruber, E., and W. Mullins, 1967, J. Phys. Chem. Solids **28**, 875.

Guhr, T., A. Müller-Groeling, and H. Weidenmüller, 1998, Phys. Rep. **299**, 189.

Haselwandter, C. A., and D. D. Vvedensky, 2008, Phys. Rev. E **77**, 061129.

Heyraud, J. C., and J. J. Métois, 1987, J. Cryst. Growth **84**, 503.

Hibino, H., Y. Homma, M. Uwaha, and T. Ogino, 2003, Surf. Sci. **527**, L222.
Himpsel, F. J., A. Kirakosian, J. N. Crain, J. L. Lin, and D. Y. Petrovykh, 2001, Solid State Commun. **117**, 149.
Houchmandzadeh, B., and C. Misbah, 1995, J. Phys. I **5**, 685.
Houchmandzadeh, B., C. Misbah, and A. Pimpinelli, 1994, J. Phys. I **4**, 1843.
Ichikawa, M., and T. Doi, 1992, Appl. Phys. Lett. **60**, 1082.
Ihle, T., C. Misbah, and O. Pierre-Louis, 1998, Phys. Rev. B **58**, 2289.
Jackson, K. A., 2004, *Kinetic Processes: Crystal Growth, Diffusion, and Phase Transformations in Materials* (Wiley, New York).
Jayaprakash, C., C. Rottman, and W. F. Saam, 1984, Phys. Rev. B **30**, 6549.
Jeong, H.-C., and E. D. Williams, 1999, Surf. Sci. Rep. **34**, 171.
Joós, B., T. L. Einstein, and N. C. Bartelt, 1991, Phys. Rev. B **43**, 8153.
Kallunki, J., and J. Krug, 2004, Europhys. Lett. **E66**, 749.
Kallunki, J., J. Krug, and M. Kotrla, 2002, Phys. Rev. B **65**, 205411.
Kandel, D., and E. Kaxiras, 1996, Phys. Rev. Lett. **76**, 1114.
Kandel, D., and J. D. Weeks, 1992, Phys. Rev. Lett. **69**, 3758.
Kandel, D., and J. D. Weeks, 1995, Phys. Rev. Lett. **74**, 3632.
Kardar, M., G. Parisi, and Y.-C. Zhang, 1986, Phys. Rev. Lett. **56**, 889.
Karma, A., and C. Misbah, 1993, Phys. Rev. Lett. **71**, 3810.
Kassner, K., and C. Misbah, 2002, Phys. Rev. E **66**, 026102.
Kato, R., M. Uwaha, Y. Saito, and H. Hibino, 2003, Surf. Sci. **522**, 64.
Keller, J. B., H. G. Cohen, and G. J. Merchant, 1993, J. Appl. Phys. **73**, 3694.
Kessler, D. A., J. Koplik, and H. Levine, 1988, Adv. Phys. **37**, 255.
Khare, S. V., N. C. Bartelt, and T. L. Einstein, 1995, Phys. Rev. Lett. **75**, 2148.
Khare, S. V., and T. L. Einstein, 1996, Phys. Rev. B **54**, 11752.
Kosterlitz, J. M., and D. J. Thouless, 1973, J. Phys. C **6**, 1181.
Krug, J., 1997, J. Stat. Phys. **87**, 505.
Krug, J., V. Tonchev, S. Stoyanov, and A. Pimpinelli, 2005, Phys. Rev. B **71**, 045412.
Kuramoto, Y., and T. Tsuzuki, 1976, Prog. Theor. Phys. **55**, 356.
Latyshev, A., A. Aseev, A. Krasilnikov, and S. Stenin, 1989, Surf. Sci. **213**, 157.
Latyshev, A., L. Litvin, and A. Aseev, 1998, Appl. Surf. Sci. **130-132**, 139.
Leonard, F., and J. Tersoff, 2003, Appl. Phys. Lett. **83**, 72.
Li, A., F. Liu, D. Y. Petrovykh, J.-L. Lin, J. Viernow, F. J. Himpsel, and M. G. Lagally, 2000, Phys. Rev. Lett. **85**, 5380.
Litvin, L., A. Krasilnikov, and A. Latyshev, 1991, Surf. Sci. **244**, L121.
Liu, D.-J., and J. W. Evans, 2002, Phys. Rev. B **66**, 165407.
Liu, F., J. Tersoff, and M. G. Lagally, 1998, Phys. Rev. Lett. **80**, 1268.
Lodder, A., 1989, Physica A **158**, 723.
Marchenko, V. I., 1981, Sov. Phys. JETP **54**, 605.
Marchenko, V. I., and A. Y. Parshin, 1980, Sov. Phys. JETP **52**, 129.
Maroutian, T., L. Douillard, and H.-J. Ernst, 2001, Phys. Rev. B **64**, 165401.
Métois, J.-J., and M. Audiffren, 1997, Int. J. Mod. Phys. B **11**, 3691.
Métois, J. J., and S. Stoyanov, 1999, Surf. Sci. **440**, 407.
Michely, T., and J. Krug, 2004, *Islands, Mounds, and Atoms*, Springer Series in Surface Sciences Vol. 42 (Springer, Berlin).
Misbah, C., and O. Pierre-Louis, 1996, Phys. Rev. E **53**, R4318.
Misbah, C., O. Pierre-Louis, and A. Pimpinelli, 1995, Phys. Rev. B **51**, 17283.
Misbah, C., O. Pierre-Louis, and Y. Saito, 2008, unpublished.
Misbah, C., and A. Valance, 1994, Phys. Rev. E **49**, 166.
Müller, P., and J. J. Métois, 2005, Surf. Sci. **599**, 187.
Müller, P., and A. Saul, 2004, Surf. Sci. Rep. **54**, 157.
Mullins, W. W., 1957, J. Appl. Phys. **28**, 333.
Mullins, W. W., 1959, J. Appl. Phys. **30**, 77.
Mullins, W. W., 1963, *Solid Surface Morphologies Governed by Capillarity*, Metal Surfaces: Structure, Energetics and Kinetics (ASM, Cleveland, OH).
Mullins, W. W., and R. F. Sekerka, 1964, J. Appl. Phys. **35**, 444.
Murty, M. V. R., and B. H. Cooper, 1999, Phys. Rev. Lett. **83**, 352.
Myslivecek, J., C. Schelling, F. Schaffler, G. Springholz, P. Smilauer, J. Krug, and B. Voigtlander, 2002, Surf. Sci. **520**, 193.
Néel, N., T. Maroutian, L. Douillard, and H.-J. Ernst, 2003, Phys. Rev. Lett. **91**, 226103.
Nepomnyashchii, A., 1974, Fluid Dyn. **9**, 354.
Nielsen, J. F., M. S. Pettersen, and J. P. Pelz, 2001, Surf. Sci. **480**, 84.
Nita, F., and A. Pimpinelli, 2005, Phys. Rev. Lett. **95**, 106104.
Omi, H., and T. Ogino, 2000, Thin Solid Films **380**, 15.
Ondrejcek, M., M. Rajappan, W. Swiech, and C. P. Flynn, 2006, Phys. Rev. B **73**, 035418.
Ondrejcek, M., W. Swiech, M. Rajappan, and C. P. Flynn, 2005, Phys. Rev. B **72**, 085422.
Pai, W. W., A. K. Swan, Z. Zhang, and J. F. Wendelken, 1997, Phys. Rev. Lett. **79**, 3210.
Paulin, S., F. Gillet, O. Pierre-Louis, and C. Misbah, 2001, Phys. Rev. Lett. **86**, 5538.
Pehlke, E., and J. Tersoff, 1991a, Phys. Rev. Lett. **67**, 465.
Pehlke, E., and J. Tersoff, 1991b, Phys. Rev. Lett. **67**, 1290.
Pierre-Louis, O., 1997, Ph.D. thesis (Université Joseph Fourier Grenoble I).
Pierre-Louis, O., 2001, Phys. Rev. Lett. **87**, 106104.
Pierre-Louis, O., 2003a, Phys. Rev. E **68**, 021604.
Pierre-Louis, O., 2003b, Surf. Sci. **529**, 114.
Pierre-Louis, O., 2005, Europhys. Lett. **72**, 894.
Pierre-Louis, O., 2006, Phys. Rev. Lett. **96**, 135901.
Pierre-Louis, O., M. R. D'Orsogna, and T. L. Einstein, 1999, Phys. Rev. Lett. **82**, 3661.
Pierre-Louis, O., and H. I. Haftel, 2001, Phys. Rev. Lett. **87**, 048701.
Pierre-Louis, O., and J.-J. Métois, 2004, Phys. Rev. Lett. **93**, 165901.
Pierre-Louis, O., and C. Misbah, 1996, Phys. Rev. Lett. **76**, 4761.
Pierre-Louis, O., and C. Misbah, 1998a, Phys. Rev. B **58**, 2259.
Pierre-Louis, O., and C. Misbah, 1998b, Phys. Rev. B **58**, 2276.
Pierre-Louis, O., C. Misbah, Y. Saito, J. Krug, and P. Politi, 1998, Phys. Rev. Lett. **80**, 4221.
Pimpinelli, A., I. Elkinani, A. Karma, C. Misbah, and J. Villain, 1994, J. Phys.: Condens. Matter **6**, 2661.
Pimpinelli, A., H. Gebremariam, and T. Einstein, 2005, Phys. Rev. Lett. **95**, 246101.
Pimpinelli, A., V. Tonchev, A. Videcoq, and M. Vladimirova, 2002, Phys. Rev. Lett. **88**, 206103.
Pimpinelli, A., and J. Villain, 1998, *Physics of Crystal Growth* (Cambridge University Press, Cambridge, UK).

Pimpinelli, A., J. Villain, D. Wolf, J. Métois, J. Heyraud, and I. G. Uimin, 1993, Surf. Sci. **295**, 143.
Politi, P., 1997, J. Phys. I **7**, 797.
Politi, P., G. Grenet, A. Marty, A. Ponchet, and J. Villain, 2000, Phys. Rep. **324**, 271.
Politi, P., and J. Krug, 2000, Surf. Sci. **446**, 89.
Politi, P., and C. Misbah, 2004, Phys. Rev. Lett. **92**, 090601.
Politi, P., and C. Misbah, 2006, Phys. Rev. E **73**, 036133.
Politi, P., and J. Villain, 1996, Phys. Rev. B **54**, 5114.
Ranguelov, B., and S. Stoyanov, 2008, Phys. Rev. B **77**, 205406.
Ratsch, C., M. F. Gyure, R. E. Caflisch, F. Gibou, M. Petersen, M. Kang, J. Garcia, and D. D. Vvedensky, 2002, Phys. Rev. B **65**, 195403.
Repain, V., G. Baudot, H. Ellmer, and S. Rousset, 2002, Europhys. Lett. **58**, 730.
Ritter, G., C. Matthai, O. Takai, A. Rocher, A. Cullis, S. Ranganathan, and K. Kuroda, 1998, Eds., *Recent Developments in Thin Film Research: Epitaxial Growth and Nanostructures, Electron Microscopy and X-Ray Diffraction* (Elsevier Science, Amsterdam).
Robinson, I. K., and D. J. Tweet, 1992, Rep. Prog. Phys. **55**, 599.
Ronda, A., I. Berbezier, A. Pascale, and A. Portavoce, 2003, Mater. Sci. Eng., B **101**, 95.
Rost, M., and J. Krug, 1995, Phys. Rev. Lett. **75**, 3894.
Rost, M., P. Smilauer, and J. Krug, 1996, Surf. Sci. **369**, 393.
Rous, P. J., T. L. Einstein, and E. D. Williams, 1994, Surf. Sci. **315**, L995.
Rousset, S., S. Gauthier, O. Siboulet, J. Girard, S. de Cheveigné, M. Huerta-Garnica, W. Sacks, M. Belin, and J. Klein, 1992, Ultramicroscopy **42-44**, 515.
Rusanen, M., I. T. Koponen, T. Ala-Nissila, C. Ghosh, and T. S. Rahman, 2002, Phys. Rev. B **65**, 041404.
Rusanen, M., I. T. Koponen, J. Heinonen, and T. Ala-Nissila, 2001, Phys. Rev. Lett. **86**, 5317.
Saam, W. F., 1989, Phys. Rev. Lett. **62**, 2636.
Saffman, P. G., and G. I. Taylor, 1958, Proc. R. Soc. London, Ser. A **245**, 312.
Saito, Y., 1996, *Statistical Physics of Crystal Growth* (World Scientific, Singapore).
Saito, Y., 1999, J. Phys. Soc. Jpn. **68**, 3320.
Saito, Y., and M. Uwaha, 1994, Phys. Rev. B **49**, 10677.
Saito, Y., and M. Uwaha, 1996, J. Phys. Soc. Jpn. **65**, 3576.
Sato, M., and M. Uwaha, 1995, Europhys. Lett. **32**, 639.
Sato, M., and M. Uwaha, 1998, J. Phys. Soc. Jpn. **67**, 3675.
Sato, M., and M. Uwaha, 1999, Surf. Sci. **442**, 318.
Sato, M., M. Uwaha, and Y. Saito, 1998, Phys. Rev. Lett. **80**, 4233.
Sato, M., M. Uwaha, and Y. Saito, 2000, Phys. Rev. B **62**, 8452.
Sato, M., M. Uwaha, and Y. Saito, 2005, J. Cryst. Growth **275**, e129.
Sato, M., M. Uwaha, Y. Saito, and Y. Hirose, 2002, Phys. Rev. B **65**, 245427.
Sato, M., M. Uwaha, Y. Saito, and Y. Hirose, 2003, Phys. Rev. B **67**, 125408.
Schelling, C., G. Springholz, and F. Schäffler, 1999, Phys. Rev. Lett. **83**, 995.
Schwenger, L., R. L. Folkerts, and H.-J. Ernst, 1997, Phys. Rev. B **55**, R7406.
Schwoebel, R., 1969, J. Appl. Phys. **40**, 614.
Schwoebel, R. L., and E. J. Shipley, 1966, J. Appl. Phys. **37**, 3682.
Shao, H., P. C. Weakliem, and H. Metiu, 1996, Phys. Rev. B **53**, 16041.
Sivashinsky, G., 1977, Acta Astronaut. **4**, 1177.
Stoyanov, S., 1990, Jpn. J. Appl. Phys., Part 2 **29**, L659.
Stoyanov, S., and V. Tonchev, 1998, Phys. Rev. B **58**, 1590.
Sutherland, B., 1971, J. Math. Phys. **12**, 246.
Tanaka, S., N. C. Bartelt, C. C. Umbach, R. M. Tromp, and J. M. Blakely, 1997, Phys. Rev. Lett. **78**, 3342.
Tersoff, J., 1996, Phys. Rev. Lett. **77**, 2017.
Tersoff, J., Y. H. Phang, Z. Zhang, and M. G. Lagally, 1995, Phys. Rev. Lett. **75**, 2730.
Thürmer, K., D.-J. Liu, E. D. Williams, and J. D. Weeks, 1999, Phys. Rev. Lett. **83**, 5531.
Tiller, W. A., 1991, *The Science of Crystallization, Macroscopic Phenomena and Defect Generation* (Cambridge University Press, Cambridge, UK).
Tung, R. T., and F. Schrey, 1989, Phys. Rev. Lett. **63**, 1277.
Turban, L., P. Nozières, and M. Gerl, 1976, J. Phys. (Paris) **37**, 159.
van den Eerden, J. P., and H. Müller-Krumbhaar, 1986, Phys. Rev. Lett. **57**, 2431.
van der Vegt, H. A., H. M. van Pinxteren, M. Lohmeier, E. Vlieg, and J. M. C. Thornton, 1992, Phys. Rev. Lett. **68**, 3335.
Vekilov, P. G., and J. I. D. Alexander, 2000, Chem. Rev. (Washington, D.C.) **100**, 2061.
Villain, J., 1991, J. Phys. I **1**, 19.
Villain, J., and P. Bak, 1981, J. Phys. (France) **42**, 657.
Vilone, D., C. Castellano, and P. Politi, 2005, Phys. Rev. B **72**, 245414.
Vladimirova, M., A. De Vita, and A. Pimpinelli, 2001, Phys. Rev. B **64**, 245420.
Vlieg, E., A. W. D. van der Gon, J. F. van der Veen, J. E. Macdonald, and C. Norris, 1988, Phys. Rev. Lett. **61**, 2241.
Wang, X.-S., J. L. Goldberg, N. C. Bartelt, T. L. Einstein, and E. D. Williams, 1990, Phys. Rev. Lett. **65**, 2430.
Wheeler, A. A., C. Ratsch, A. Morales, H. M. Cox, and A. Zangwill, 1992, Phys. Rev. B **46**, 2428.
Whitham, G. B., 1976, *Linear and Nonlinear Waves* (Wiley, New York).
Williams, E. D., O. Bondarchuk, C. Tao, W. Yan, W. Cullen, P. Rous, and T. Bole, 2007, New J. Phys. **9**, 387.
Xiang, Y., 2002, SIAM J. Appl. Math. **63**, 241.
Yagi, K., H. Minoda, and M. Degawa, 2001, Surf. Sci. Rep. **43**, 45.
Yamamoto, T., Y. Akutsu, and N. Akutsu, 1994, J. Phys. Soc. Jpn. **63**, 915.
Yang, Y. N., E. S. Fu, and E. D. Williams, 1996, Surf. Sci. **356**, 101.
Yip, C. M., M. Brader, M. DeFelippis, and M. Ward, 1998, Biophys. J. **74**, 2199.
Zhao, T., J. D. Weeks, and D. Kandel, 2004, Phys. Rev. B **70**, 161303.
Zhao, T., J. D. Weeks, and D. Kandel, 2005, Phys. Rev. B **71**, 155326.